August 2017

Improved Partial Charge Models in Siliceous Zeolites for the Simulation of Adsorption and Identification of Catalytic Sites

Jarod J. Wolffis
University of Nevada, Las Vegas

IMPROVED PARTIAL CHARGE MODELS IN SILICEOUS ZEOLITES FOR THE SIMULATION OF ADSORPTION AND IDENTIFICATION OF CATALYTIC SITES

By

Jarod J. Wolffis

Bachelor of Science – Chemistry
University of Nevada Las Vegas
2013

A thesis submitted in partial fulfillment
of the requirements for the

Master of Science – Chemistry

Department of Chemistry and Biochemistry
College of Sciences
The Graduate College

University of Nevada, Las Vegas
August 2017

UNLV | GRADUATE COLLEGE

Thesis Approval

The Graduate College
The University of Nevada, Las Vegas

July 27, 2017

This thesis prepared by

Jarod J. Wolffis

entitled

Improved Partial Charge Models in Siliceous Zeolites for the Simulation of Adsorption and Identification of Catalytic Sites

is approved in partial fulfillment of the requirements for the degree of

Master of Science – Chemistry
Department of Chemistry and Biochemistry

Paul Forster, Ph.D.
Examination Committee Chair

Kathryn Hausbeck Korgan, Ph.D.
Graduate College Interim Dean

Kathleen Robins, Ph.D.
Examination Committee Member

Keith Lawler, Ph.D.
Examination Committee Member

Carryn Warren, Ph.D.
Graduate College Faculty Representative

Abstract

Utilization of computational modelling and simulation is expanding as computer processing power has increased and as new tools have been developed. This thesis focuses on efforts to improve the accuracy of simulations in aluminosilicate zeolites, an industrially important category of materials for catalysis and separations. For these sorbents, partial atomic charge represents a critical parameter in molecular mechanics simulations, determining the Coulombic non-bonding interaction. Partial charges may also be used as a measure of important physical parameters of the system such as the degree of covalency or the relative acidity of catalytic sites. We compare several common methods for predicting partial atomic charges in siliceous (pure silica) zeolites, analyze the geometric dependence of these charges, and we test if that data can be used to predict the site for tetrahedral atom substitution in the synthesis of catalytically active zeolites. In addition, we test the partial atomic charges for their ability to predict N_2 and O_2 adsorption with common dispersion-repulsion parameterizations.

A second project is also described where detailed first-principles analysis of a pentanuclear technetium iodide structure was conducted in the solid state. We utilized spin polarization in DFT to test the average magnetic moment and sought further explanation using the structures density of states and electronic band structures.

Acknowledgements

This thesis is dedicated to my family and friends, I wouldn't be here if not for you.

Thank you.

I would like to express my deepest gratitude to my supervisors Keith Lawler and Professor Paul Forster for their unwavering support, collegiality, and mentorship throughout this project.

I would like to extend additional thanks to those who offered collegial guidance and support over the years: Professor Kathleen Robins, Professor David Hatchett, Professor MaryKay Orgill, Professor Larry Tirri, and Professor Jennifer Guerra.

To those who continue to struggle to reach their goals,

may you find success in what inspires you,

may you reach for the unreachable,

may you bear the unbearable.

Table of Contents

List of Tables

Table of Figures

Chapter 1: Introduction

Section 1.1: Density Functional Theory

1.1.1: Schrodinger Equation

Quantum mechanics was introduced in the 1920's as a way of explaining phenomena that could not be explained with classical mechanics. In general, quantum mechanics is important when the length scale of the phenomena is on the same order as Planck's constant, as dictated by the Heisenberg uncertainty principle. Through the concept of wave-particle duality, quantum particles exhibit characteristics of both waves and particles, allowing us to describe the particles as waves using wave functions analogous to those found in classical wave mechanics. Following similar principles to wave mechanics, Erwin Schrödinger defined a way of describing the quantum state of a wave function in both its time-dependent, and (more relevant to this discussion) time-independent form:

$$\widehat{H}\Psi = E\Psi \qquad \text{(Equation 1)}$$

where $\widehat{H}$ is the differential many-body Hamiltonian operator, which, when acted on a trial state of the system, Ψ, returns the total (kinetic and potential) energy, E, of that state. Ψ is the wave function containing all information that can be known about the quantum system currently at hand. The stationary state with the lowest energy is dubbed the ground state of the system, and it is in this state the system will typically be found to exist. Equation 2 shows the terms of the expanded Hamiltonian operator in atomic units.

$$\widehat{H} = -\frac{1}{2}\sum_{i=1}^{N}\nabla_i^2 - \frac{1}{2M_A}\sum_{A=1}^{N}\nabla_A^2 - \sum_{i=1}^{N}\sum_{A=1}^{M}\frac{Z_A}{r_{iA}} + \sum_{i=1}^{N}\sum_{j>1}^{N}\frac{1}{r_{ij}} + \sum_{A=1}^{M}\sum_{A\neq B}^{M}\frac{Z_A Z_B}{R_{AB}}$$

(Equation 2)

Here N is the number of number of electrons, M is the number of nuclei, i and j represent electrons, A and B represent nuclei, Z represents the atomic number of a nuclei, and r and R represent the distance between the indicated particles. The combination of the first two terms represent the kinetic energy (momentum squared over twice the mass) of the system coming from both the electrons and nuclei as determined by the differential Laplacian, ∇^2, operator. The remaining three terms, which describe the potential energy, include the attractive electrostatic interactions between the nucleus and electrons, the repulsion between the electrons, and the repulsive interaction between the nuclei. Under the Born-Oppenheimer approximation, it can be assumed due to the separation in the orders of magnitude of time for the relative motion of electrons and nuclei that their contributions to the Hamiltonian may be separated. This paves the way for a simpler means of solving an electronic Hamiltonian where the nuclei act as fixed point charges - creating a stationary, attractive, Coulomb interaction potential for the electrons. Rewriting the above equation under the Born-Oppenheimer approximation yields Equation 3, where the remaining nuclear-nuclear potential is a constant scalar for fixed atomic configurations:

$$H_e = -\frac{1}{2}\sum_{i=1}^{N}\nabla^2 - \sum_{i=1}^{N}\sum_{A=1}^{M}\frac{Z_A}{r_{iA}} + \sum_{i=1}^{N}\sum_{j>1}^{N}\frac{1}{r_{ij}}$$

(Equation 3)

This simplified electronic Hamiltonian represents more clearly an electronic wave function dependent directly on the electronic coordinates (parametrically on nuclear coordinates), while the total energy of the system becomes the summation of the new electronic Schrödinger equation with a nuclear constant component of the constant nuclear repulsive term:

$$H_e\Psi_e = E_e\Psi_e \quad \text{(Equation 4)}$$

$$E_T = E_N + E_e \quad \text{(Equation 5)}$$

$$E_N = \sum_{A=1}^{M} \sum_{B>A}^{M} \frac{Z_A Z_B}{R_{AB}}$$

As in all wave phenomena problems, these wave functions are required to obey certain boundary conditions which ostensibly give rise to the quantized stationary states of the system we seek. The wave function itself is not observable, so any property must be inferred from the electronic probability density derived from the wave function. Thus the modulus square of the wave function is taken to yield that probability density. The integral over all space of the probability density must be equal to one, which indicates a 100% chance of finding the electrons, as shown below.

$$\int \ldots \int |\Psi(r_1, r_2, r_3, \ldots, r_N)|^2 dr_1 dr_2 dr_3 \ldots dr_N = 1$$

$$\int \ldots \int |\Psi(r_1, r_2, r_3, \ldots, r_N)|^2 dr_1 dr_2 dr_3 \ldots dr_N = \rho(r) \qquad \text{(Equation 6)}$$

By scaling the wave functions to produce the value of 1 upon integration, the wave functions are said to be *normalized,* describing the state of the N electrons. Furthermore, we have yet to describe the process in which we achieve the ground state of the system for the time–independent Schrödinger equation in terms of the many-body electron wave functional. To do so, we evaluate a new trial wave function using the *variational principle*. In short, the variational principle takes a trial wave function and computes a trial energy based on the given N and given external potential V_{ext}. By definition, the true ground-state of the system, Ψ_0, is the state with the lowest energy, E_0 represented by the following equation:

$$E_0 = \Psi \overset{Min}{\rightarrow} N\langle \Psi | \tilde{T} + \tilde{V}_{Ne} + \tilde{V}_{ee} | \Psi \rangle \qquad \text{(Equation 7)}$$

Once N and V_{ext} are established, the ground state of the system can be determined by constructing the Hamiltonian, formulating a trial wave function, and evaluating it by the right-hand side of the above equation. This process is continued throughout all acceptable N-electron wave functions to minimize the ε_0 expression, and repeated until the lowest numerical value for E is found, thus giving us the closest estimate (if not the actual) for the ground-state of the system.

For simple systems like a harmonic oscillator, a rigid rotor, or the central force (aka. Hydrogen atom) problem, there are known analytic functional forms of the wave function. Although the Schrödinger equation hypothetically allows for complete evaluation of any quantum system, when extended to systems with many bodies (nuclei or electrons), there is no longer a simple analytic form of the wave function. To utilize quantum mechanics with many-bodies, a numeric solution to the problem has to be solved. There are two main approaches to solving the many-body problem as it pertains to the electronic structure of atoms, molecules, and more complicated chemical entities: a wave function based and a charge density based approach.(1-4) Wave function based calculations happen to be extremely computationally expensive in order to accurately evaluate the system. Thus their use is limited to only small or medium-sized molecular systems. In comparison, the evaluation of the charge density approach aka. density functional theory (DFT) is a more efficient computational method for mapping the ground-state and thus determining the physical properties of a microscopic electronic system. DFT is the more popular of the two approaches for solving quantum chemistry problems, and it has been shown in numerous texts(5-7) that this approach is far more practical in describing large molecular systems and condensed phases.

1.1.2: Hohenberg – Kohn Theorem

The work conducted by Hohenberg and Kohn(8) lays the theoretical pillars upon which DFT has been erected, and defines the ability to solve for the ground state of a system using the density based approach. Their first theorem focused on how all properties of the system (including the Hamiltonian) can be determined by the overall electron density. This is an extension of what we describe above as the external potential, except for a constant c, which fixes the Hamiltonian since it is a unique function of the charge density, $\rho(r)$, therefore causing the many-body ground state to become a function of the overall density, $\rho(r)$. The question remains: Can we have two external potentials that yield the same ground state electron density? We can answer this using the following proof which follows the presentation in Koch *et al*.(7) by firstly defining two separate Hamiltonians that differ only by their external potentials:

$$\hat{H} = \hat{T} + \hat{V}_{ee} + \hat{V}_{ext} \qquad \text{(Equation 8)}$$

$$\hat{H}' = \hat{T} + \hat{V}_{ee} + \hat{V}'_{ext} \qquad \text{(Equation 9)}$$

where each Hamiltonian corresponds to a separate ground-state wave function, Ψ and Ψ', and with respective ground-state energies E_0 and E'_0. Assuming each comes from the same $\rho(r)$, we can apply the variation principle while making sure to account for the additional constant of the external potential,

$$E_0 < \langle \Psi' | \hat{H} | \Psi' \rangle = \langle \Psi' | \hat{H}' | \Psi' \rangle + \left(\Psi' | \hat{H} - \hat{H}' | \Psi' \right)$$

$$E_0 < E'_0 + \langle \Psi' | \hat{T} + \hat{V}_{ee} + \hat{V}_{ext} - \hat{T} - \hat{V}_{ee} - \hat{V}'_{ext} | \Psi' \rangle$$

$$E_0 < E'_0 + \langle \Psi' | \hat{V}_{ext} - \hat{V}'_{ext} | \Psi' \rangle$$

$$E_0 < E'_0 + \int \rho(\vec{r}) \{ V_{ext} - V'_{ext} \} \, d\vec{r}$$

by switching primed indices, (Proof 1)

$$E'_0 < \langle \Psi | \widehat{H'} | \Psi \rangle = \langle \Psi | \hat{H} | \Psi \rangle + \langle \Psi | \widehat{H'} - \hat{H} | \Psi \rangle$$

$$E_0' < E_0 + \int \rho(\vec{r})\{V_{ext}' - V_{ext}\}\, d\vec{r}$$

$$E_0' < E_0 - \int \rho(\vec{r})\{V_{ext} - V_{ext}'\}\, d\vec{r}$$

and by combining the two expressions:

$$E_0 + E_0' < E_0' + E_0$$

$$0 < 0$$

Since zero cannot be less than zero, we conclude that the two external potentials not only yield the same ground-state electron density, but also the ground-state energy as a functional of the ground-state electron density. This relationship is expanded in their second theorem, where for any external potential there exists a density functional E[n], whose global minimum is the exact ground state energy. Thus, the total energy expression may be rewritten as a functional of the electron density:

$$E[\rho] = T[\rho] + E_{ee}[\rho] + E_{Ne}[\rho] \qquad \text{(Equation 10)}$$

We can again separate the above expression as done previously into systematic dependencies to the kinetic energy, electronic potential, and external potential contributions. If the exact functional were known, then the Schrödinger equation would be solvable as a whole requiring no further methodological development. What has thus far been dubbed the electron-electron interaction potential may be separated into a few physically relevant terms: the classical Coulomb (Hartree) term, the electron exchange term arising from the Fermionic nature of electrons, V_X, and the electron-electron correlation term, V_C. DFT method development has long been focused on evaluating and accurately representing the complicated electron–electron exchange and correlation terms will be discussed in the following sections. Theoretically, this does start the foundations for what we today call DFT, but since the form of the universal function is unknown, our discussion continues away from general descriptions and to the considerations of major technical breakthroughs that have achieved practical solutions with DFT.

1.1.3: Kohn Sham

The seminal 1965 paper of Kohn and Sham (9) gave birth to an idea similar to the Thomas – Fermi method,(10) that direct functionals of the electron density fail in their ability to evaluate the kinetic energy terms effectively beyond the description of a free-electron gas. Thus, Kohn and Sham introduced the concept of non-interacting reference systems built from sets of one electron functions, allowing for a means to calculate the electronic kinetic energy with improved accuracy. Doing so requires a way to calculate as much information as possible from these one-electron functions while applying the remaining portions of the energy to be determined by the chosen approximate functional. This may be achieved by rewriting the Hohenberg – Kohn theorem universal functional for the energy of the ground state as:

$$E_0 = p \overset{Min}{\rightarrow} N^{\left(F[p_0]+\int \rho(\vec{r})V_N\, d\vec{r}\right)} \qquad \text{(Equation 11)}$$

$$F[\rho(\vec{r})] = T[\rho(\vec{r})] + J[p(\vec{r})] + E_{ncl}[\rho(\vec{r})] \qquad \text{(Equation 12)}$$

where from left to right, Eqn. 12 includes the functionals for the kinetic, Hartree (classical Coulombic repulsion), and non-classical electronic energies. The non-classical terms come from self-interaction, electron exchange, and other electron correlation effects. All terms present in the above expression and those in the Thomas – Fermi – Dirac Model are explicit functionals of the electron density. Unfortunately, those methods based on Thomas – Fermi and more recent models (11; 12) fail in comparison to more quantitative trends targeted to describe the electronic kinetic energy. This stems from an inaccuracy of approaches defined by real-space densities to correctly describe the doubly differential aspect of the Laplacian operator. Thus, Kohn and Sham devised a way to describe the kinetic energy with better accuracy through the mechanisms employed to solve the Hartree-Fock wave function based approach.(13) They found that Slater determinants represent the exact wave functions of non-interacting fermions, and that they also represent a ground-state wave function. By choosing a reasonable effective potential and

determining its resultant electron density, the one-electron wave functions may be determined as vectors which diagonalize that density in a respective one-electron basis:

$$\rho(\vec{r}) = \sum_i^N \sum_s |\varphi_i(\vec{r})|^2 \qquad \text{(Equation 13)}$$

where *s* is the spin of the Kohn-Sham orbitals. To calculate the true kinetic energy of the system, they defined expressions for both the kinetic energy contributions to the non-interacting and interacting reference systems. Unfortunately, even if these systems shared the same density, both contributions would not account for the total true kinetic energy. The Kohn-Sham approach thus allows us to separate the universal functional and add the residual portions of the non-classical electrostatic contributions not covered by the true kinetic energy into the exchange-correlation functional. With these additions we can rewrite our overall energy expression as follows (including a more general functional representation of the contribution of the external potential '*Ne*'):

$$E[\rho(\vec{r})] = T_s[\rho(\vec{r})] + J[\rho(\vec{r})] + E_{xc}[\rho(\vec{r})] + E_{Ne}[\rho(\vec{r})] \qquad \text{(Equation 14)}$$

In principle, the Kohn-Sham approach is exact, and the only fully unknown variable at this point is exchange-correlation functional. The exchange-correlation functional contains not only the contributions to the potential energy, but now also the kinetic energy with respect to the external potentials. Unfortunately, as in the universal functional, the true exchange-correlation functional is unknown. Any further extension to the Kohn-Sham approach makes the exchange-correlation functional more accurate for the system at hand. To clarify, the quality of DFT depends on how accurately the exchange-correlation functional is calculated. To provide the most accurate solution, we will see in the next section not only the drawbacks of DFT but its evolution through the issues of self-interaction of the charge density and the behavior of the corresponding exchange-correlation potentials in the long range asymptotic region.

1.1.4: LDA's, GGA's, Meta GGA's, Hybrids, and Dispersion Corrections

We have discussed the Hohenberg-Kohn theorem and Kohn-Sham method as the basis of DFT. Now we move in to establishing why the local density and local spin-density approximations are the model systems from which every other functional is derived. The core idea of this methodology is the concept of a uniform electron gas in which the system is effectively charge neutral, since each electron moves in a positive background of uniform charge distribution. We use the uniform electron gas because it is the only model where the exchange energy is known analytically and the correlation energy can be determined with very high accuracy.

$$E_{xc}^{LDA}[\rho] = \int \rho(\vec{r})\varepsilon_{xc}\big(\rho(\vec{r})\big)\, d\vec{r} \qquad \text{(Equation 15)}$$

$$\varepsilon_{xc}\big(\rho(\vec{r})\big) = \varepsilon_x\big(\rho(\vec{r})\big) + \varepsilon_C\big(p(\vec{r})\big) \qquad \text{(Equation 16)}$$

As can be seen from the above expression, under the local density approximation, the exchange and correlation functional energies are able to be separated and evaluated independently. This allows us to define the exchange, E_X, functional as that of an electron gas of uniform particle density, which is also known as the Slater exchange functional. The correlation, E_C, functional lacks a definite expression, but has been formulated in multiple studies including the most widely accepted form of Perdew and Wang in their 1992 publication.(14) The above expression is presented in the spin-restricted formulation, but it can be extended to account for the electron densities of a specific electron spin, ie. the local-spin density approximation:

$$E_{xc}^{LDA}\big[\rho_\alpha, \rho_\beta\big] = \int \rho(\vec{r})\varepsilon_{xc}\left(\rho_\alpha(\vec{r}), \rho_\beta(\vec{p})\right) d\vec{r} \qquad \text{(Equation 17)}$$

Obviously, this approximation relies on the overall assumption that the exchange-correlation potentials depend only on the values of ρ_α and ρ_β. This is not optimal, considering that the actual densities of our system are certainty anything but constant, and do not resemble the uniform electron gas. Still, this method overall describes many chemical (especially metallic) systems rather well and can be made more computationally efficient than the wave function based Hartree-Fock methodology.

The first step to improve the local density approximation is the use of not only the information of the electron densities but also the gradient of the charge density, which should account for the Local Density Approximation's (LDA) problem of non-homogeneity. This can be done by extending the exchange – correlation function with a Taylor expansion of the initial interpretation of the local density approximation, yielding the following:

$$E_{xc}^{GGA}[\rho_\alpha, \rho_\beta] = \int \rho(\vec{r}) \varepsilon_{xc}\left(\rho_\alpha(\vec{\rho}), \rho_\beta(\vec{p})\right) d\vec{r} + \sum_{\sigma,\sigma'} C_{xc}^{\sigma,\sigma'}(\rho_\alpha, \rho_\beta) \frac{\nabla\rho^\sigma}{\rho^{2/3}} \frac{\nabla\rho^{\sigma'}}{\rho^{2/3}} d\vec{r} + \cdots$$

(Equation 18)

The above equation defines the gradient expansion approximation, which should provide more accurate solutions to chemical problems. Unfortunately, this approximation falls short of the desired accuracy, because by extending the gradient, the sum rules no longer apply and the electron hole functions are no longer required to be negative for a pair r_1 and r_2. Due to this side-effect, LDA produces better electron hole functions. In efforts to restore the portions of the gradient where the hole constraints were removed, one arrives at what is known as the generalized gradient approximation(15-17):

$$E_{xc}^{GGA}[\rho_\alpha, \rho_\beta] = \int f\left(\rho_\alpha, \rho_\beta, \nabla\rho_\alpha, \nabla\rho_\beta\right) d\vec{r} \qquad \text{(Equation 19)}$$

As shown in equation 20, the exchange portion is an extension of LDA as described. Above, f is the reduced density gradient for spin, either based on the above generalized gradient approximation (GGA) exchange functional, ie Becke 88,(16) or a rational functional of the reduced gradient, ie. PBE.(18) An example of a rational functional is shown below, where S_σ is the local inhomogeneity parameter.

$$E_{xc}^{GGA} = E_{xc}^{LDA} - \sum_{\sigma} F(S_\sigma)\rho_\sigma^{4/3}(\vec{r})\, d\vec{r} \qquad \text{(Equation 20)}$$

$$S_\sigma = \frac{|\nabla\rho(\vec{r})|}{\rho_\sigma^{4/3}(\vec{r})}$$

Of all the variations of these two types of GGA's, in theory each exchange function could be combined with any correlation functional. In practice, only a few of these combinations are used in computations. BP86(19) and BLYP(16; 20) for example, BP86 is a combination of Becke's exchange functional with Perdew's 86(21) correlation functional, while BLYP is Beck's 88 exchange with Lee-Yang-Parr correlation function.(20) Overall, these GGA functionals are coined as nonlocal in the literature, which can often be misleading. All GGA functionals are mathematically local and are defined to be nonlocal because they extend beyond the boundaries of LDAs. The idea of meta-GGA functionals includes either incorporating higher derivatives of the electron density, or the kinetic energy density within the exchange-correlation functional. All of the mentioned functionals depend on the Kohn-Sham orbitals, which describe the spin-up and spin-down kinetic energy densities.

At this point, we've expressed multiple ways of evaluating an accurate expression for the exchange functional in order to determine more meaningful results from DFT. Hybrid functions allow us to take an additional step by again extending the exchange-correlation functional, but this time by combining the Hartree-Fock exact exchange energy with a DFT approximation to the exchange energy

which includes some other electron-electron correlation. The first step was taken by Becke in his 1993(22) functional which utilizes his 1988(16) exchange functional with Perdew and Wang's 1991 correlation functional.(23) This approach introduced a couple of error functionals to correct for the exact exchange in the overall functional. These adiabatic connection methods or ACM's, extend to the very popular B3LYP(24) functional, which has been used in many chemical applications including those of open-shell transition-metal chemistry. With the introduction of Becke's 1996(25) function, the previous method's three error parameters are limited to one, allowing us to show the adaptation of the exchange with respect to hybrid functionals as follows:

$$E_x = \alpha E_x^{DFT} + (1 - \alpha) E_x^{HF} \qquad \text{(Equation 21)}$$

All hybrid functionals follow this general formulation, where improvements to predicted chemistry are made by combining several different DFT exchange functionals in a similar manner, ie. the B3 of B3LYP is 8% Slater LDA exchange, 72% Becke88 GGA exchange, and 20% exact Hartree-Fock exchange. It has been proven that a long-range correction for exchange functionals allows solutions to various problems through DFT that are computationally intractable or incorrect by other functionals or methodologies. The exact exchange employed for hybrid functionals at least partially accounts for this long-range effect. As with the PBE0(26; 27) functional, which uses 25% Hartree-Fock exchange at all length scales and 75% PBE exchange at all length scales. Hybrid functionals provide significantly more accurate predictions when compared to other functionals, but like other DFT function, they do have short-comings.

Dispersive interactions are attractive forces that appear due to instantaneous induced dipoles and higher-order multipoles. These forces are termed the van der Waals interactions, or more specifically London dispersion, and are a medium-to-long range electron correlation effect. Coincidentally, the regions where these interactions are important are where there is little or no overlap of localized electron densities. A downside with LDA, GGA, and hybrid functionals is their inability to accurately describe

these interactions. In fact, wave function based methods need additional correlation terms beyond those of Hartree-Fock to correctly describe these interactions. A popular solution to this problem is to add a semi-empirical correction term to an already existing DFT functional.(28; 29) The correction basically acts as an additional constant for attractive nuclear-nuclear potential energies, and they do not directly alter the electronic structure for a given arrangement of nuclei. The corrections also provide a significant improvement to descriptions of the intermolecular chemistry of a system with a miniscule increase in computational cost. The added dispersion term allows for adjustments for different atom types and parent functionals with adjustable parameters. There are considerations that arise with this technique if the system is not well-behaved and the atoms become infinitesimally close to each other. As these corrections are purely attractive, this leads to energy and forces becoming infinite, leading to unfavorable energetics and optimized geometries. If this is accounted for with a damping function or if the system is reasonably well-behaved, this technique performs rather well in comparison to experiment and other DFT models. The corrections aren't a new type of functional, but in recent years there has been development of correlation functions that intrinsically include dispersion interactions spearheaded by the work of Langreth *et al*.(30-33)

We have described multiple types of functionals up to this point, and have briefly covered the ways in which each type was derived. The main point in discussing these functionals is to define in what scenario each of the above expressions are applicable and why. We conclude this topical review with a summary.(34) LDAs are optimal for electron band structures of "sea of electron" metals. They tend to overestimate lattice parameters, overestimate binding energies, and show incorrect phase stabilities. GGAs greatly reduce the bond dissociation energy error, improve transition-state barriers, and generally provide a better description than LDAs of the chemistry (ie. bonding) of a system. GGAs are good for equilibrium geometries, vibrational frequencies, multipole moments, and accurate molecular atomization energies. Hybrid functionals describe intra- and intermolecular charge transfer phenomena much better than LDAs and GGAs and are therefore superior at predicting excitation spectra using time-dependent

DFT (TD-DFT). Hybrid functionals are also typically the best choice for a model chemistry black box for compounds and reactions chemistry. One drawback to hybrid functionals is that in periodic systems they become quite computationally expensive, limiting their use in condensed phase simulations.(35) Lastly, dispersion corrections and functionals are necessary for accurate predictions of binding/cohesive energies, lattice parameters, and geometries of molecular compounds of solid-state molecular compounds.

Section 1.2: Partial Charges Methods

1.2.1: Semi-Empirical Techniques

There are many techniques for computing the partial charges of a system, and the most commonly used techniques in classical mechanics simulations are the semi-empirical methods that do not require *ab initio* simulations. The electronegativity-equalization method (EEM) was the first of such methods developed by Mortier *et al*.(36) EEM stems from the postulate that when atoms join together to form a molecule, their electronegativites become equalized.(37) By expanding the internal energy of an N-electron system as a second order Taylor series with respect to the number of electrons in the system, an expression for the chemical potential of an atom ($\partial E/\partial N$) can be readily obtained. The electronegativity of a species is the negative of that chemical potential. Equating each atom's chemical potential expression equalizes the electronegativity and provides a readily solvable system of linear equations that yield the partial atomic charges of the system. EEM is parameterized by the values of the electronegativity and hardness for the neutral atoms of the system.(37; 38) The EEM method is advantageous over fixed generic charges for each atom since it provides a geometry and connectivity dependent description of the partial atomic charges and allows for simulations to adjust to the electrostatic environment of the system.

Seeking an improved description of partial charges, particularly for modeling biological systems, Rappe and Goddard introduced the charge equilibration (QEq) method.(39) QEq utilizes a similar Taylor expansion to EEM, but instead of the atomic hardness, QEq relates the derivatives of the energy with respect to the number of electrons to the ionization potential and electron affinity of the atoms. The difference between the functions of these terms is a damped Coulomb term, evaluated by the Coulomb integral of s-type orbitals centered on each atom. At short bond distances the charge distribution arises not from interacting point charges, but from overlapping atomic electron densities, and the damped Coulomb term acts to shield the nuclei improving the underlying physics of the QEq model - as opposed to EEM, which uses the full 1/R Coulomb term between the nuclei. Overall, QEq has been shown to perform quite well for inorganic, organic, and biological systems, and it is by far the most ubiquitous semi-empirical charge determination method in the academic literature. The general utility lattice program (GULP)

software package has even built in the derivatives of the QEq model to allow the charges of the system to fluctuate correctly as part of the dynamics.(40)

To improve the QEq model for describing the partial charges in metal-organic frameworks (MOFs) with regards to modern electronic structure calculations, Wilmer *et al*. introduced the extended charge equilibration method (EQEq).(41) The major change between QEq and EQEq is that in EQEq, each atom can have a different and unique value for the charge the Taylor expansion is centered on, and choosing a value of zero should return the original QEq values. EQEq also expands the internal energy of the whole system, not just the individual atoms, and includes two additional terms beyond those included in QEq. The first term accounts for the interaction of the charge on an atom with those of all other atoms in the system and the second is a familiar short-ranged damping term to prevent infinite charge separation between arbitrarily close atoms. The author's tests of EQEq demonstrated a marked improvement over QEq in predicting charges on MOFs when compared to the REPEAT and ChelpG methods that will be discussed later.

Also seeking to improve on the QEq method, Chan and Martinez developed the charge transfer of polarization current equalization (QTPIE) method.(42) QTPIE was developed to include polarization and charge transfer effects and to represent correct behavioral effects as bonds are broken, like in a reactive force field simulation. Instead of using a Taylor expansion for terms of atomic charges, QTPIE uses charge transfer variables and introduces a term to penalize long-range charge transfer, thus reducing unphysical finite charges between separate atoms. In general, QTPIE performs similarly to QEq given that its parameters are optimized for QEq. However, QTPIE is much better at describing polarization currents, which are potentially important to zeolites, given the prevalence of the core-shell model in many zeolite structural force fields.

1.2.2: Ab Initio Techniques

The previously described methods are semi-empirical and require no other input than their parameter set and the structure of the framework. While they are regarded as less accurate than a full *ab initio* simulation (ie. DFT), they are advantageous in that the charges can be evaluated in a matter of seconds instead of the minutes, hours, or days time scale required for a complete DFT simulation and post-processing. Charges derived from DFT simulations are regarded as more accurate than their semi-empirical counterparts. The simplest technique is Mulliken population analysis,(43) which for each atom, sums the one-particle density matrix contracted with the overlap matrix represented in the atomic orbital basis over just the orbitals centered on that atom. Mulliken population analysis is a computationally cheap post-processing method and is typically included by default in most *ab initio* simulations. An atomic orbital basis set is required, prohibiting performance of Mulliken population analysis in plane-wave basis simulations, especially because Mulliken population analysis also suffers from a heavy basis set dependence. Another computationally inexpensive technique is Löwdin population analysis,(44) which symmetrically orthogonalizes the one-particle density matrix, and then computes the charges on each atom by summing over the individual atom's atomic basis functions. The Löwdin symmetrically orthogonalized basis functions are the orbitals that most closely resemble the underlying non-orthogonal atomic basis. Löwdin population analysis suffers less of a basis set dependence than Mulliken population analysis, but it still requires an underlying atomic orbital basis set prohibiting its use in plane-wave simulations. Atom-specific projections from Fourier-space to real-space enable some similar integrations of atomic charge density, but they are not as robust as rigorous Mulliken or Löwdin analysis.

An alternative to population analysis is the fitting of partial atomic charges directly from the electrostatic potential (ESP) of the system. The ESP is comprised of the one-electron potential energy and the Hartree potential, ie. DFT. ESP encompasses all of the potential energy ansatz except the exchange-correlation potential. The CHarges from ELectrostatic Potentials (CHELP) method computes the partial atomic charges from the electrostatic potential by performing a linear least squares fit between the quantum ESP and the classical ESP created by the partial atomic charges, $E=\sum_{i,j} q_j/r_{ij}$, with a Lagrange

constraint that the partial atomic charges must sum to a defined total value.(45) CHELP represents the electrostatic potentials on a radial grid of points emanating from each atomic center to determine the fit, and includes the constraint that the radial grid points within the van der Waals radius of any atom are discarded from the fit. The CHELP method does not exhibit the desired property of rotational invariance owing to the sparse placement of grid points that depend on the molecular geometry. The sparse placement of grid points around the exterior of the molecule also leads to an inadequate representation of the more internal atoms of the system. The CHarges from ELectrostatic Potentials on a Grid (CHELPG) method instead defines a headspace around the system and places a regular series of grid points within that volume to fit the ESP.(46) This denser, more evenly spaced grid, does a better job of representing the ESP and effectively removes the rotational variance of CHELP. The main drawback to the CHELPG is that it does not include any concept of periodicity and requires an effective vacuum of headspace grid points around the system, which confines its usage to molecular clusters. The Repeating Electrostatic Potential Extracted ATomic charges (REPEAT) method enables analysis of fully periodic systems by employing a full Ewald sum of the classical electrostatic potential.(47) In addition, REPEAT uses a modified form of the RESP error function to improve the description of buried atoms without a large grid density around them because of the removal of grid points by the van der Waals radii constraint.(48) REPEAT interfaces well with many of the leading periodic DFT packages, and is becoming widely used for MOFs.(49-54)

The Quantum Theory of Atoms in Molecules (QTAIM or AIM) is a model pioneered by Richard Bader that strives to describe the properties of atoms and bonds in a system through a partitioning of the electron density distribution function (aka the charge density).(55) The partitioned charge density divides the whole simulation volume into smaller volumes that directly correspond to the atoms of the system and may or may not include a vacuum volume unassociated with any particular atom. The partitioning of the charge density can be accomplished by defining zero flux surfaces between the atoms in the system, and these zero flux surfaces are defined as locations where the charge density, with respect to the surface, is at

a minimum.(56) In bonded systems, there are shared electron densities between the atoms, yet the charge density of the core electrons is much larger, allowing for zero flux surfaces to be drawn through bonds and the magnitude of charges included on each atom can be used to describe the covalency of that bond. The charge density is typically represented along a regular real space grid spanning the whole system as in CHELPG and REPEAT. The total number of electrons associated with an atom (and thus the partial atomic charge) can be found by summing the charge density for all the grid points within an atom's Bader volume. Bader's AIM approach has been implemented for the analysis of the charge densities of periodic systems, including many algorithmic advances that prevent the tendencies of Bader surfaces to align along the grid directions.(57-59) The iterative Hirshfeld (HI) method is another AIM model that seeks to parse the electronic charge density onto individual atoms.(60) The non-iterative Hirshfeld scheme parses the total charge density by weights determined from the isolated charge densities on a reference state of the atom of interest (the neutral atom in Hirshfeld's original paper), divided by the sum of the isolated charge density on all atoms. The superior iterative approach refines these weights, and thus the on-atom charge densities, under a constraint that the weights remain normalized.(61) One comment on Hirshfeld charges is their inability to correctly reproduce the electrostatic potential of the system, which a reference - free methodology known as the iterative stockholder (ISA) method seeks to correct.(62) Density Derived Electrostatic and Chemical method (DDEC) is an iterative AIM method that combines the ISA method with the reference charge densities used in Hirschfield analyses to reproduce reliable electrostatic potentials and partial atomic charges.(63) The DDEC/c6 version is the best of the options due to its enhanced performance in the determination of net atomic charges.

Section 1.3: Sampling Thermodynamic Properties with Monte Carlo

By defining a partition function, all thermodynamic quantities of a system of interest can be computed. In only a few cases can the multidimensional integrals needed to compute thermodynamic properties be computed analytically, so the integration needs to be done numerically. Monte Carlo methods (MC) are computational algorithms that numerically integrate an expression by randomly sampling the possible states of the system. Purely random sampling is the first choice of all MC methods, but it can lead to incorrect property determinations due to over-sampling of regions where the contributions to the value of interest are negligible, ie. where it is systematically improbable for the system to exist. Increasing the number of states sampled or using importance sampling can fix this concern. Importance sampling uses a predetermined range of system conditions to sample where the effective probabilities of the value of interest will be at their peak. Unfortunately, importance sampling too can run into difficulties from both under-sampling and the impossibility of extension to describe multidimensional integrals that generate points with a probability density exactly proportional to those of the function of interest.

In chemistry, the partition function is sampled with MC and then processed with statistical mechanics to predict the expectation values of relevant thermodynamic properties. The focus is on the evaluation of the Boltzmann distribution and thus the partition function. The Boltzmann distribution is the probability that a system is in certain states at given conditions. Often the configurational portion of the partition function is not of particular interest - just the averages of microscopically determinable quantities A(r^N) are (whose expectation values are defined in the following equation using the partition function):

$$\langle A \rangle = \frac{\int dr^N e^{-\beta U(r^N)} A(r^N)}{\int dr^N e^{-\beta U(r^N)}} = \int dr^N \frac{e^{-\beta U(r^N)}}{Z} A(r^N) \qquad \text{(Equation 22)}$$

This formulation allows us to solve thermodynamic integrals using the efficient sampling scheme described by Metropolis *et al.*(64) Metropolis explained that instead of choosing states at random and determining their Boltzmann factor $e^{-\beta U}$, one could with more efficiency choose configurations with that are connected to other probable nearby states and weigh them evenly. Therefore, the Metropolis algorithm generates sequences of random states that in the end reach a significant probability per the equilibrium distribution of the appropriate statistical ensemble. This is done by solving directly for the thermodynamic average of the observable A. By rewriting it in terms of a summation, this allows us to solve for the average without determining the partition function.

$$\langle A \rangle = \frac{1}{N\_samples} \sum_{i=1}^{N\_samples} A_i(r^N) \qquad \text{(Equation 23)}$$

Another fundamental part of the Metropolis algorithm is what is known as a Markov chain: a sequence of trials that yields one set of states dependent only on their preceding state. There is a transition probability which connects the Boltzmann probability,

$$\rho(r^N) \equiv \frac{e^{-\beta U(r^N)}}{z} \qquad \text{(Equation 24)}$$

in the current, M, state through the transition to the next, N, state:

$$\rho_M \pi_{M \to N} = \rho_N \pi_{N \to M} \qquad \text{(Equation 25)}$$

Here, π is a dimensionless square matrix that satisfies the condition of microscopic reversibility. Connecting the states M and N are what Metropolis called "trial" moves, which simultaneously move multiple atoms across multiple directions in phase space and relates the energy differences between the

final and initial configuration to determine the probability of the transition. The trial move is accepted with the following probability:

$$P_{acc}(r^m \to r^n) = min\left(1, \frac{\rho_{boltz}(r^n)}{\rho_{boltz}(r^m)}\right) = \min\left(1, e^{-\beta \Delta U}\right) \quad \text{(Equation 26)}$$

If the determination of the probability from initial M to final N state is found to be less than a randomly generated number between [0,1] then the move becomes rejected outright. If the trial move lowers the energy of the system, then the probability is greater than 1, and the move is always accepted.

The benefits of Monte Carlo simulations are that they can be performed on various statistical ensembles. The simplest type of ensemble is the microcanonical ensemble, which fixes the number of particles in the system, the volume, and the energy of the system. The Boltzmann distribution for this ensemble directly relates to the entropy of the system.

$$\rho = \frac{1}{\Omega};\ S = kB \ln \Omega \quad \text{(Equation 27)}$$

The canonical ensemble builds on this, allowing the energy to fluctuate while holding the volume, temperature and the number of particles fixed. Its partition function is represented as Q(N,V,T), ie. the NVT ensemble, and has the Boltzmann probability of a microscopic configuration:

$$\rho_{Boltz} = \frac{\frac{V^N}{N! \Lambda^{3N}} e^{-\beta U}}{Q_{NVT}} \quad \text{(Equation 27)}$$

where U is the potential energy, V the volume, Λ is the de Broglie's thermal wavelength, β is the Boltzmann distribution, and N is the number of particles. The pre-factor is the connection between the

non-interacting ideal and interacting microcanonical states of the system. The free energy associated with the canonical ensemble is the Helmholtz free energy:

$$-\beta A = \ln(Q) \qquad \text{(Equation 28)}$$

The grand canonical ensemble allows the number of particles within the system to fluctuate while it holds the chemical potential μ, volume, and temperature fixed. The number of particles is allowed to fluctuate by equating the chemical potentials for the species of interest with a reservoir of molecules that can be moved into and out of the system. This canonical Boltzmann distribution can be modified in terms of the grand canonical ensemble:

$$P_{Boltz} = \frac{\frac{V^N}{N!\Lambda^{3N}} e^{-\beta(U-\mu N)}}{\Xi_{\mu VT}} \qquad \text{(Equation 29)}$$

The Monte Carlo method, specifically in the grand canonical ensemble, is the leading means for simulating gas adsorption using statistical thermodynamics of the interacting system of interest. Grand canonical Monte Carlo is the most advantageous methodology for adsorption studies because of the direct relationship between the chemical potential of the adsorbed fluid and the desired pressure of the system made with an equation of state. With zeolites and other porous materials, the phase space available to adsorbed gases within the framework is sampled by defining how the particles move within the system and the energetic interactions that define how the gas interacts with the framework. The trial moves include molecule translation and rotation (canonical moves) as well as the creation and destruction of the molecules within the framework. Using the previously outlined details, a very accurate picture of gas adsorption can be obtained using only simple classical dispersion and electrostatic interactions.

Section 1.4: Zeolites, a Brief Introduction

Since the mid-eighteenth century, zeolites have been a topic of considerable interest of study, thanks to a Swedish geologist by the name of Axel Cronstedt. During an experiment, he rapidly heated a stone noting the adsorptive properties of the mineral as it released water vapor.(65) Therefore, he coined the term "zeolite", from "zeo," – (to boil) and "lithos" – (stone). A few hundred years later, and the name represents almost two hundred and fifty structurally different materials, some of which we use every day. Naturally occurring zeolites such as volcanic and sedimentary rocks are often what comes to mind to those familiar with the word. So far, there have been about forty naturally occurring zeolites discovered. The most commercially and academically sought after naturally occurring zeolites include mordenite, chabazite, and clinoptilite. Due to their ready availability and cheap manufacture, zeolites have found uses in countless adsorption and catalytic industrial processes. Mining naturally occurring zeolites is still the most economical approach to zeolite material obtainment. However, synthetic zeolites have garnered considerable attention in various industrial applications within the last 40 years such as in the manufacture of consumer products (laundry detergent, zeolite Linde Type A) and oil-processing (faujastite, zeolite X and Y). Both natural and synthetic zeolites have their uses, but what makes each structure unique and useful are their individual molecular geometries.

Basic zeolite topology is a network of corner-sharing tetrahedra with an overall framework stoichiometry of TO_2, where T are metal/metalloid atoms (typically Si), connected through two-coordinate oxygen. The tetrahedra link together to form several composite building units, which together form many different topology patterns with regular pore structures that vary in shape, size, and accessible pockets. The International Zeolite Association (IZA) currently recognizes 232 unique zeolite topologies that occur naturally or have been synthesized in laboratories in its structural database, each denoted with a 3-letter code.(14) The simplest zeolites are networks of tetrahedra of silicon and oxygen atoms (SiO_4) only, and are named the siliceous zeolites. The majority of the IZA recognized frameworks may be

synthesized over a range of Si/Al ratios and may contain additional T-site substitutions, creating far more than just 232 zeolite frameworks. While the number of zeolite structure types appears small compared to the large number of metal-organic frameworks (MOFs) that have been reported, many of the topologies have been synthesized with several different T-atoms that create an overall framework charge (like Al). These may be ion-exchanged to contain a wide range of cations to balance that charge and each different ratio and cation lends different properties to the framework. The inclusion of extra-framework cations may further modify the effective pore size and surface chemistry, which in turn affects the performance of specific zeolite in specific applications. Zeolites are attractive materials for investigation into new processes and problems since several structures are commercially produced, widely available and inexpensive, they exhibit a low toxicity (as they are made from earth-abundant elements), and they are stable in non-ambient environments required for catalysis and practical separations.

The porous in nature of zeolites allows for physical separations of many different fluids. Where the absorbed fluid physisorbs or chemisorbs to a site within the framework, strong framework-guest interaction occurs and the fluid separates. The most attractive site for most fluids of interest is the accessible extra-framework cations, which attract through strong electrostatic interactions. These sites are often blocked with water following zeolite synthesis or exposure to air, but that water may be removed by heating and placing in a vacuum to create more accessible sites for adsorption. Of course, there are several factors affecting the adsorption capacity of a framework such as: available cations in the framework, pore sizes of the cages, the type of fluid being adsorbed, and intrinsic structural properties of the zeolite such as the effective charge at particular atomic sites which we will explore in the next chapter. The average pore size in zeolites ranges from 4-5 angstroms, and can essentially deter some fluids from certain regions or sections of the framework based on the size of the fluid molecules. Changing the size of the cations in the framework directly affects the size of the channels of a zeolite, and therefore which fluids can access certain regions in the interior of zeolites. Systematically, we can predict

adsorption and separation processes in zeolites using statistical mechanics, ie. grand canonical Monte Carlo, as described in the previous section.

The primary interest of our groups regarding zeolites is for their adsorption and separation properties, but it is worth noting that another key use for zeolites is in catalysis. The ability to adjust size-selectivity of the material as mentioned above is certainly key to their importance in industrial catalysis alongside their overall availability. T-atom substitution with elements such as Sn and Ti provides Lewis acid sites in the framework, which enables acid catalysis. An additional route for creating a zeolite catalyst is to ion exchange monovalent cations with those of higher valency. This leaves framework sites with a higher concentration of negative charge that are a long distance from their balancing counter-cation. These sites also act as acid catalysis sites, often through the destruction and re-formation of silanol groups that have been created due to an abundance of framework charge at these sites. There has been a large effort in the literature to determine *a priori* which sites will be the acidic sites, and in the next chapter we discuss how we used several different classical and *ab initio* (ie. DFT) partial atomic charge determination methods to predict the acidic sites using just siliceous forms of the zeolite frameworks, and how these determined charges affect the simulated adsorption for two commonly separated gases - N_2 and O_2.

Chapter 2: Predicting Partial Atomic Charges in Siliceous Zeolites

Section 2.1: Introduction

Zeolites represent the most commercially important class of crystalline nanoporous materials, finding application in catalysis, adsorption, molecular sieving, ion exchange, and electronics.(66-78) While the International Zeolite Association (IZA) currently recognizes only 232 unique zeolite topologies.(79) the majority of these may be synthesized over a range of Si/Al ratios, may contain additional T-site substitution (ie., Ge, Sn, Ti, P), and may be ion-exchanged to contain a range of cations. All these substitutions modify effective pore size and surface chemistry which in turn affects a specific zeolites performance for specific applications. Considering the diversity of potential zeolites and their potential for applications, appreciable development has occurred towards developing simulation approaches to aid in understanding and predicting zeolite behavior.(80) The majority of these studies have focused on force field-based molecular mechanics approaches.

Simulations frequently aim to accurately describe a zeolite's structure or to provide an accurate description of the framework atoms' interaction with guest species. The chief commonality between force fields developed for these purposes is the inclusion of a Coulomb term utilizing partial charges located on the framework atom centers. Following the work of Catlow et al.,(81) many popular structural force fields use formal ionic charges at each atom center (+4 for Si and -2 for O) with a core-shell term on the oxygen atoms.(82) As on-site ion polarization and charge transfer between ions are nearly indistinguishable, the core-shell term can be thought of as describing either the polarizability of the oxygen or the covalency between the framework atoms.(83) Other force fields geared towards modeling structure instead use no core-shell term and smaller partial atomic charges, accounting for covalency with dispersion-repulsion terms or conventional harmonic bonding potentials.(84-89) Force fields developed expressly for separation and sieving applications (such as adsorption and diffusion) do not typically include core-shell terms. If partial charges have been parameterized for the framework, they are often much smaller than

those used in a structural force field.(90; 91) If no partial charges have been specified, then they must be determined through various approaches, as detailed in the following sections.

For adsorption and diffusion problems, the simplest and most widely used method is to treat the framework atoms as rigid (ie. fixed positions) as this greatly reduces the computational complexity of the simulation.(92) However, it is known that zeolites can exhibit appreciable flexibility, in part due to the small energetic penalty associated with changing the T-O-T angle.(68; 84) Recent experiments and simulations have shown that flexibility must be addressed in at least some instances, such as the important commercial zeolite MFI (ZSM-5), in order to obtain reasonable accuracy.(93-95) Many of the better simulations currently being published address this flexibility,(96-98) however the simulation force field now needs to describe both the framework structure and interaction with guest species well. Therefore, the question remains - what is the correct description of the partial charges of a zeolite framework?

Another key industrial use of zeolites is as solid acid catalysts where confinement within nanopores allows for size and shape selectivity. Coupled with the possibility of high acidity, tunability in the number of (and, consequently, spacing between) acid sites, zeolites make nearly ideal acid catalysts. The catalytic site in aluminosilicates may arise from the exchange of higher valence charge-balancing cations (ie. Na^{+} exchanged for La^{3+}), creating strong local fields near the framework Al. The distance between a high valence cation site and the framework Al sites favors water disassociation by stabilizing hydroxyl species associated with the cation and H^{+} associated with an Al^{3+} site, and a trivalent cation (such as La^{+3}) can create two catalytic Brønsted acid sites per cation in an aluminosilicate.(99) Since strong local fields create the Brønsted acid site, it follows that the high valent cations are likely to be located at the least electropositive Al. In other words, the Al sites with the highest partial charges will likely function as the primary acid sites. Alternatively, the substitution of heavier metals like Sn or Ti for Si has been shown to greatly increase the catalytic capabilities of a zeolite.(100) These heavier metals are strong Lewis acid sites and can catalyze reactions such as petroleum refining, isomerization, methanol conversion, esterification, etc.(101) Although pure SiO_2 zeolites themselves are not important catalysts, many commercial catalysts have sufficiently high Si/Al ratios that they are nearly siliceous in overall

composition. Even for zeolites with smaller Si/Al ratios, insights generated from the pure SiO_2 framework often provide useful information, predicating catalytic sites and behavior.

Recently Hamad *et al*. gave an overview of many common methods and demonstrated their performance in predicting partial atomic charges for some representative metal-organic frameworks (MOFs).(102) They tested methods that require *ab initio* quantum mechanical simulations as well as those that only use a crystal structure. Their results showed a surprisingly high degree of variability in the predicted partial atomic changes depending on methodology. Not surprisingly, these differences impact separation, adsorption, and diffusion simulations. In addition, they demonstrated that the choice of partial atomic charge had a large impact on the predicted structural properties when framework flexibility was introduced into the simulation.

Here, we present a study similar in spirit to that of Hamad *et al*. focused on understanding the predicted partial atomic charges of siliceous zeolite frameworks. Unlike MOFs, it is more difficult to break down zeolites into simple molecular clusters as the same composite building units (CBUs) appear in many zeolite frameworks and the partial charges for one CBU may vary greatly depending on which other CBUs are connected to it. There are several different methodologies that have been created to determine the partial atomic charges on atoms in a structure from structural and quantum chemical information. These methods can be applied to single molecules or periodic systems, and as our goal is to analyze their performance in zeolites the focus will be only on methods that can be applied to extended periodic systems. As many of these methods have been thoroughly discussed in the literature, we only offer a brief summary of the methods we use in Table 1 (a fuller review is in the previous introductory chapter). In this work, we will compare the predicted partial atomic charges from each method, consider the effect of the local geometry on the charges, and we will assess if these charges can be used to identify known acidic or catalytic T-sites in select zeolites. Lastly, we will analyze the effect of compression on the predicted partial charges, and the effect the partial atomic charges from the different methodologies has on predicted gas adsorption behavior.

Table 1. A summary of the partial atomic charge determination methods used in this work.

Method	Type	Description	Ref.
EEM	semi-empirical	Charges determined through equalization of electronegativity	(36)
QEq	semi-empirical	Like EEM but uses screened Coulomb repulsions in lieu of atomic hardness	(39)
EQEq	semi-empirical	QEq which allows the Taylor series to be expanded around non-zero charges	(41)
QTPIE	semi-empirical	QEq but in terms of charge transfer variables that penalize long-range charge transfer	(42)
Iterative Hirshfeld (HI)	*ab initio*	Parses the charge density by fitting it to a superposition of reference atomic states.	(60; 61)
DDEC	*ab initio*	Atoms-in-Molecule (AIM) decomposition of charge density coupled with an iterative stockholder approach using the reference atomic charge densities	(63)
Bader	*ab initio*	Atoms-in-Molecule (AIM) decomposition of charge density	(57-59)
REPEAT	*ab initio*	Charges fit to reproduce the electrostatic potential	(47)

Section 2.2: Methods

2.2.1: Simulation

The crystal structures for the zeolites studied were taken directly from the Structure Commission of the IZA's (IZA-SC) database of structures.(79) The IZA-SC's structures, optimized with DLS76 using only bond length and bond angles, provides fully self-consistent idealized structures appropriate as starting points for our analysis. Atomic connectivity and geometry were evaluated using the zeoTsites package, and verified with structure visualization.(103; 104) The EEM and QEq partial atomic charges were determined using the General Utility Lattice Program (GULP).(40) The EQEq partial atomic charges were determined with the stand-alone program provided as a supplement to the work of Wilmer *et al*.(41) The QTPIE partial atomic charges were determined with GULP.

Periodic plane-wave DFT calculations were performed with version 5.4.1 of the Vienna *ab-initio* Simulations Package (VASP).(105-107) The generalized gradient approximation (GGA) exchange-correlation functional of Perdew, Burke and Ernzerhof (PBE) was utilized.(18) As it has been previously demonstrated that long-range dispersion is necessary for accurately predicting zeolite frameworks,(108) Grimme's -D3 semi-empirical dispersion correction was included during structural optimizations.(29) The plane augmented wave (PAW)(109; 110) pseudopotentials for PBE which represent the valance configurations of $2s^2 2p^4$ for O and $3s^2 3p^2$ for Si were employed. Optimized cell volumes were obtained through a fit to the Vinet equation of state(111) from a series of constant volume conjugate-gradient optimizations of the cell shape and atomic positions that spanned at least ±5% of the IZA-SC listed unit cell volumes. Constant volume optimizations were performed as two subsequent optimizations of the cell shape and lattice positions, and a final single point energy evaluation was performed to minimize Pulay stress. For the optimizations only the gamma point was used to represent the first Brillouin zone. The first Brillouin zone was represented with an automatically generated Γ-centered mesh with grid points spaced evenly at ~0.03 $2\pi Å^{-1}$ increments along the reciprocal axes for the single point simulations used to compute the charge density and electrostatic potential. The k-space integration in the first Brillouin zone

was done with the tetrahedron method with Blöchl corrections.(112) The plane wave basis was cut off at 520 eV. The Kohn-Sham (9) expressions were solved via the RMM-DIIS algorithm with blocked Davidson pre-convergence steps. The tolerance for energies is 10^{-5} eV. The convergence tolerance for forces was 10^{-2} eV/Å. REPEAT partial atomic charge analysis was performed using the stand-alone package of Campañá *et al*.(47) Bader partial atomic charge analysis was performed using the 0.95a version of the Bader Charge Analysis package distributed by Henkelman *et al*.(56) Iterative Hirshfeld (HI) charges were determined using the HIVE program.(61) DDEC charges were found with the 'DDEC6' algorithm in the DDEC package distributed by Manz and Sholl.(113)

Gas adsorption was simulated with Monte Carlo in the grand canonical ensemble (GCMC) with our own in-house modified version of the MuSiC package using the Peng-Robinson equation of state for fugacities.(64; 114-117) Each simulation employed 200,000 equilibration cycles and 300,000 production cycles. A cycle here consists of N moves, where N is the number of adsorbed particles (minimum 20). 2x2x2 unit cells were used to represent the zeolite framework, and the framework was held as rigid during the simulations. The adsorbed particles could fluctuate with random translations, rotations, insertions, and deletions with equal weight. The adsorbate-framework Coulomb interactions were computed using Ewald sums, and on-the-fly adsorbate-adsorbate Coulomb interactions were computed using the damped, shifted potential and force method of Fennell and Gezelter cutoff at 12 Å.(118) All Coulomb interactions used a damping parameter, α, of 0.2 $Å^{-1}$. The van der Waals interactions were computed with 12-6 Lennard-Jones (LJ) potentials with cutoff at 12 Å. The Lorentz-Berthelot mixing rules were used to obtain the pair-wise LJ parameters from the atomistic force fields. A potential energy map for adsorbate-framework interactions was made prior to the GCMC simulation. The framework LJ parameters were taken from the TraPPe-zeo force field.(91) The atomistic LJ parameters for N_2 and O_2 were taken from the all atom TraPPe-small force field.(119; 120) The inaccessible volumes in the zeolite framework were blocked using our recently develop energy based pore mapping program with Ar as a probe (ε=120K, σ=3.4Å).(92) The simulated adsorption isotherms were excess corrected using the pore volumes produced

by our energy based pore mapping program. Simulated heats of adsorption were obtained with fluctuation theory.

2.2.2: Experimental

Siliceous sodalite (SOD) was synthesized according to the procedure outlined in Qisheng *et al*. (121) The organic structure directing agent was pyrolyzed and the material converted to its final rhombohedral (R-3) state following procedures suggested by King *et al*.(122) The SOD was compressed in a diamond anvil cell with Fluorinert-70 as a non-penetrating pressure transmitting medium. *In situ* X-ray diffraction was performed at beamline 16 BMD of the High-Pressure Collaboration Access Team HP-CAT, Advanced Photon Source APS, Argonne National Laboratory ANL. Ruby was used as a pressure calibrant. Diffraction images were integrated using Fit2d and unit cell parameters were determined using GSAS.

A sample of the zeolite FAU was obtained from Joesph Hriljac.(123) 100 mg of the sample was activated under dynamic vacuum at 300°C for 18 hours followed by a N_2 surface area measurement at 77K. Adsorption isotherms were measured using a Micromeritics ASAP 2020 adsorption analyzer fitted with a He cryostat with a stability of 0.01K. All the isotherms were collected up to ~750 mmHg with incremental doses of 5 cm^3/g and sufficiently long equilibration times. Desorption measurements were also taken at the end of each isotherms. Prior to each measurement, the sample was reactivated at 250°C under dynamic vacuum for an hour followed by an hour of equilibration in the cryostat at the target temperature. N_2 and O_2 isotherms were measured at 130K, 140K and 150K. Isosteric heats of adsorption were calculated by using the Clausius-Clapeyron relation.

Section 2.3: Results and Discussion

2.3.1: Comparing Charge Methodologies

To compare the magnitudes of the charges produced by the various methods for determining partial charges, we will focus first look at the IZA-SC structure for zeolite-β (BEA) (data tables for the IZA-SC structures of the other known siliceous zeolites are in the SI). BEA is an important zeolite in that it has been demonstrated in the literature to be highly site-selective with regards to acid catalysis and tetrahedral atom substitution.(124) Structurally, BEA consists of three intersecting twelve membered rings (12MR) with 17 unique oxygen atoms and 9 T atoms. Table 2 shows the different partial charges determined for BEA by both semi-empirical and *ab initio* techniques broken down by its crystallographically unique atoms. Looking first at the semi-empirical techniques, we see the methods produce an increasingly ionic description of the frameworks following the order: QTPIE < QEq < EEM < EQEq. The QTPIE charges are markedly low compared to the rest of the methods. We believe they are so low because the polarization correction, although implemented for periodic boundary conditions, does not work well for extended systems. The EEM and QEq methods both produce charges that would describe a polar covalent system (ie. less than 50% ionic q_{Si}=+2), and that are in line with zeolite force fields such as that of Nicholas and TraPPe-ZEO where q_{Si} is 1.1.e and 1.5e respectively.(86; 91)

The EQEq charges are much larger than any of the other semi-empirical methods for all the zeolites studied. The EQEq charges are in line with very strong polar covalent bonds, which is the best description of the bonding in zeolite frameworks.(125) The reason the EQEq charges are much larger than the regular QEq charges is the re-centering of the Taylor expansion. Centering the charges on zero did in fact return the same charge values as QEq. Here the Taylor sum was centered around the fully ionic charges: +4 for Si and -2 for O. We found that it didn't matter what value was picked for oxygen (0, -1, -2); EQEq returned the same charges so long as the Taylor series for Si was centered at +4.

Table 2. A comparison of the partial charges determined with several methodologies for the IZA-SC structure of BEA. The site 'Label' is the one used in the IZA-SC database. The average value for each atom type and the RMS deviation from that average are shown at the bottom of the table.

Label	*EEM*	*QEq*	*EQEq*	*QTPIE*	*HI*	*DDEC*	*Bader*	*REPEAT*
O1	-0.8066	-0.6043	-1.2013	-0.0322	-1.2786	-1.1327	-1.5984	-0.5807
O2	-0.8426	-0.6315	-1.1570	-0.0352	-1.3155	-1.0665	-1.6150	-0.6439
O3	-0.8046	-0.6007	-1.2053	-0.0321	-1.2827	-1.0985	-1.5967	-0.5770
O4	-0.8857	-0.6562	-1.2921	-0.0375	-1.3539	-0.9411	-1.5885	-0.7248
O5	-0.8857	-0.6042	-1.2038	-0.0322	-1.2778	-1.0508	-1.5977	-0.5674
O6	-0.8452	-0.6328	-1.1638	-0.0353	-1.3169	-1.0971	-1.6153	-0.6277
O7	-0.8073	-0.6026	-1.2110	-0.0322	-1.2853	-1.2864	-1.5991	-0.5650
O8	-0.7980	-0.5977	-1.2103	-0.0316	-1.2742	-1.6345	-1.5942	-0.5810
O9	-0.8646	-0.6408	-1.2880	-0.0363	-1.3355	-0.9970	-1.6090	-0.6664
O10	-0.8429	-0.6355	-1.3070	-0.0372	-1.3150	-1.0361	-1.6020	-0.6565
O11	-0.7974	-0.5989	-1.2089	-0.0316	-1.2757	-1.7678	-1.5952	-0.5741
O12	-0.8420	-0.6356	-1.3043	-0.0372	-1.3148	-1.0232	-1.6008	-0.6263
O13	-0.8413	-0.6271	-1.3101	-0.0369	-1.3171	-1.6368	-1.6031	-0.6000
O14	-0.8840	-0.6505	-1.3959	-0.0415	-1.3500	-0.9747	-1.6128	-0.7772
O15	-0.8527	-0.6361	-1.3265	-0.0375	-1.3229	-1.6380	-1.6013	-0.6490
O16	-0.8394	-0.6282	-1.3046	-0.0367	-1.3133	-1.3367	-1.6031	-0.5900
O17	-0.8493	-0.6354	-1.3199	-0.0371	-1.3190	-1.7086	-1.6036	-0.6295
T1	1.6672	1.2405	2.4059	0.0677	2.6149	2.1571	3.1964	1.2500
T2	1.6680	1.2366	2.4130	0.0678	2.6153	2.2334	3.1977	1.2272
T3	1.6649	1.2535	2.4939	0.0670	2.6061	2.5754	3.2078	1.2656
T4	1.6652	1.2528	2.4973	0.0672	2.6054	2.6140	3.2092	1.2289
T5	1.6708	1.2411	2.6745	0.0808	2.6295	2.7166	3.1985	1.3045
T6	1.6679	1.2439	2.6615	0.0804	2.6259	2.5198	3.1988	1.2647
T7	1.6821	1.2584	2.5541	0.0670	2.6188	2.9355	3.2077	1.2233
T8	1.6819	1.2655	2.5498	0.0666	2.6166	2.7506	3.2078	1.2090
T9	1.6789	1.2530	2.5483	0.0677	2.6184	2.4350	3.2010	1.2636
Avg. qO	-0.8406	-0.6246	-1.2594	-0.0353	-1.3087	-1.2604	-1.6021	-0.6257
RMSD	0.0287	0.0185	0.0659	0.0028	0.0247	0.2869	0.0072	0.0566
Avg. qT	1.6719	1.2495	2.5331	0.0703	2.6168	2.5486	3.2028	1.2485
RMSD	0.0067	0.0090	0.0887	0.0055	0.0075	0.2334	0.0049	0.0278

Turning to the *ab initio* methods, we see that the REPEAT charges are the lowest of the survey and all the other methods provide a more ionic description of the system. The HI and DDEC methods produce very similar charges that like EQEq describe the strongly polar covalent bonding in the system that core-shell potentials are built to mimic. Bader analysis produces the most ionic description of the system, which arises from the atoms-in-molecules produced atomic volumes for Si having an unphysical nearly zero value. This appears to be a buried atom problem, wherein an atom is contained within the

diffuse valence shell of several other atoms making it appear that the atom has no valence charge density. Tetrahedral atoms in strongly polar covalent systems will be particularly susceptible to this problem. HI and DDEC are less prone to buried atom issues as they both use iterative comparisons to reference atomic states (neutral and ionic). The DDEC3 algorithm relies more heavily on Bader atoms-in-molecule decomposition for charge determination, and the DDEC3 charges were much more ionic than even the Bader charges with some being too ionic: ie. $q_{Si} > 4$, $q_O < -2$. Because of this, we believe that the Bader charges are an over-estimation caused by an unphysical parsing of the charge density. Interestingly, the non-Bader *ab initio* methods are replicated quite well by a semi-empirical method: QEq for REPEAT and EQEq centered on the ionic charges for HI and to a lesser extent DDEC. This good agreement is the case for all the zeolites studied as there is a high uniformity in the magnitude of the charges predicted by a method across all the zeolites studied. Each charge determination method produced charges that vary from site-to-site on the order of 0.01e, with the variations on the O atoms being greater than those of the Si atoms. These variations represent the different chemical environments around each unique T-site, and these site-to-site charge variations can be used to gain physical insight into the zeolite framework. Each charge determination method produced charges that vary from site-to-site on the order of 0.01e, with the variations on the O atoms being greater than those of the Si atoms. These variations represent the different chemical environments around each unique T-site, and these site-to-site charge variations can be used to gain physical insight into the zeolite framework.

2.3.2: The Relationship Between Acidic/Catalytic Sites and Partial Atomic Charges

The determination of a zeolite's catalytic site experimentally has been a heavily investigated topic over the past few decades. A leading hypothesis is that the T-site with the largest T-O-T angle should be the acidic site going along with the concepts of strain in the framework and the ionic character of a metal-oxygen-metal bond increasing with an increased bond angle.(126) However, Sastre *et al*. (and others) have shown little to no direct correlation between local structure and the acidic site and instead conjectured that the acidity arises from the long-range electrostatics.(127; 128) In a different study, Gale

showed the classical- and cluster-based models often mis-predicted the site of interest because of a neglect of long-range electrostatics, and that full periodic super cell simulations are more likely to make correct predictions.(129) Contrarily, Yang *et al*. asserted that distortions away from a regular TO_4 tetrahedron (in terms of the RMS deviation of the O-T-O angles at a site) are what cause a T-site to be more acidic.(108) As zeolites are acid catalysts, one hypothesis is that the catalytic site will be the most acidic and therefore have the most positive charge in the system from its Lewis acidity. An aluminosilicate has Brønsted acidity from the presence of a hydroxyl associated with an oxygen bound to an Al. It is reasonable to expect the hydroxyl to associate with an oxygen atom having the most negative charge and where neighboring T-atoms will likely bear a higher positive charge. The charge determination methodologies readily predict the most positive site in a zeolite, so we will test this hypothesis by analyzing a few well-studied commercially relevant zeolite frameworks: BEA, BEC, MFI, MWW, and TON. Using only siliceous frameworks, this will also determine if the acidic sites can be predicted *a priori* treating each T-site equivalently from a parameterization/pseudo-potential point of view.

Table 3: A comparison of the partial charges determined for the DFT optimized structure of BEA. The site 'Label' is the one used in the IZA-SC database. Literature identified T-sites of interest are in grey.

Label	*EEM*	*QEq*	*EQEq*	*QTPIE*	*HI*	*DDEC*	*Bader*	*REPEAT*
T1	1.6045	1.2446	2.1724	0.0669	2.5908	3.6562	2.2824	1.3139
T2	1.6049	1.2378	2.1808	0.0669	2.5938	2.7429	2.9094	1.3151
T3	1.6003	1.2580	2.2366	0.0662	2.5812	2.5536	2.7367	1.2516
T4	1.5996	1.2566	2.2355	0.0664	2.5824	2.1657	2.9270	1.2395
T5	1.6084	1.2351	2.3960	0.0782	2.6091	2.6920	2.9683	1.3201
T6	1.5968	1.2379	2.3589	0.0778	2.5996	2.3176	3.1222	1.2508
T7	1.6179	1.2712	2.2849	0.0669	2.5945	2.8284	2.9523	1.2579
T8	1.6136	1.2827	2.2673	0.0672	2.5890	1.9532	3.1693	1.1923
T9	1.6131	1.2644	2.2770	0.0672	2.5928	2.7103	3.1828	1.3604

Since experimentally measured structures rely on data of variable quality (most are determined by powder PXRD) and the refinements use different approaches (especially with respect to the level of

restraints/constraints), we were concerned that experimental structures would not be sufficiently self-consistent for our purposes. We have already analyzed the DLS76 structures, but these structures are highly idealized and can often be off from the experiment either in terms of unit cell volume or a specific structural feature. To determine if these small changes to the framework can have noticeable effect on the predicted partial atomic charges in the previous section, we re-optimized the DLS76 structures of our commercially relevant zeolite frameworks using periodic plane-wave DFT. Table 3 shows the partial atomic charges for each method charges for the T-sites for optimized BEA. When compared to the values shown in Table 2, it can be readily seen that the charge for each site changed following the DFT optimization. However, the predicted magnitudes of the charges do not change significantly (>0.3e). The EQEq and Bader charges experienced the greatest change in magnitude with the average T-site charges dropping to 2.267e and 2.916e, respectively. On the other hand, the HI and REPEAT charges for the optimized structures are much closer (> 0.03e) to the DLS76 structures charges: 2.593e and 1.278e respectively. In addition to changing values at each site, the ordering of sites by charge magnitude also changed with optimization for each method. For example, the site T5 has the greatest REPEAT charge for the DLS76 structure, yet the site T9 has the greatest REPEAT charge for the DFT optimized structure. This demonstrates just how sensitive these charge determinations are to structure, as upon optimization there was only a 1.4% increase in volume chiefly from an elongation of the crystallographic *c*-axis, which had the consequence of increasing the eccentricity of the elliptical 12MR channels of BEA. Because of the sensitivity of the charges to structure, the comparison with the literature for determining acidic sites will be done with the likely higher quality DFT optimized structures.

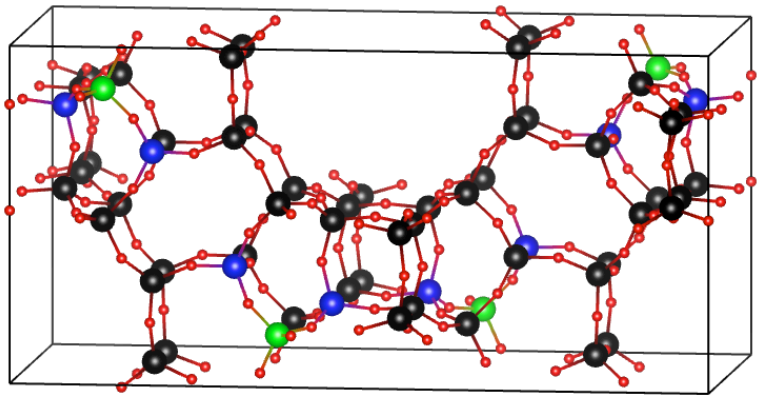

Figure 1: The crystal structure of BEA along [100]. Site T5 is highlighted in blue, site T9 is highlighted in green, oxygens are in red, and the remaining T-sites are black.

The literature provides several different (often inconsistent) accounts of which site is the acid site or the most favorable for substitution for each zeolite depending on how the problem was approached and the experimental conditions. There is also not much literature devoted to the determination of site acidity, instead the focus has been on determining the preferred T-atom (T=Sn, Ge, Ti, etc) substitution site as that site will act as the catalytic site post-substitution. It is worth noting that frequently the IZA-SC and experimental structures have different site labels, so for consistency we will use the IZA-SC site notation. Extended X-ray adsorption fine structure spectroscopy and periodic DFT simulations comparing HOMO-LUMO gaps of substituted frameworks have identified the T5/T6 site of BEA as the primary substitution site, consistent with the large T-O-T angle between sites T5 and T6. (100; 130) These studies also indicated that the T5/T6 site should be the most acidic. The later work of Yang *et al*. argues that, while T6 is the most favorable substitution site, T9 as the least stable substitution site should be the most acidic site based on simulated water adsorption.(108) The T5 and T9 sites of BEA are illustrated in Figure 1, and similar cartoons for the other materials are available in the Appendix B. For BEC (the pure polymorph C of BEA with higher crystallographic order), the primary substitution site for metal atoms was determined to be at T1 in the D4R unit. However, T3 was shown to become the most favorable with increasing Ge concentration.(131-133) The description of MFI is the most varied, and a recent review of the preferred

substitution sites concluded that most sites were identified as a preferred substitution site by at least one study, but sites T8 and T10 are implicated most frequently.(134) Part of the difficulty may arise from the high flexibility in MFI, with at least two distinct monoclinic and orthorhombic phases that have been shown to distort with heating or guest molecules loaded into the framework.(93; 94; 135-137) Later simulation studies have identified the acidic site as T11, T7, or T12 as the most acidic site.(138-141) Gale's study into MFI that expressed the need for correct-long range electrostatics identified T4 as the primary substitution site, which was corroborated with Ti and Fe substitution studies.(129; 142-144) Hydroxyl IR studies ranked sites T1, T3, and T5 as the most acidic in MWW, with T6 as the most stable substitution site and T8 the least.(127; 128) A later experimental and QM/MM study indicated that Al substitution prefers sites: T6 > T3 > T8, and the acidity went as T8 > T3 > T6 in the presence of acetone and T6 > T8 > T3 in the presence of TMPO.(127; 128) Early cluster simulations indicate that T1 and T4 are the most favorable Al substitution sites in TON.(145) However, a later NMR and simulation study indicated T4 would be the most favorable and almost no substitution should occur at T1.(146) Cluster simulations mark T2 as the most acidic site,(147) a later cluster study selected T1 as the most stable, accessible Brønsted acid site (although the other sites surpassed it yet were dubbed inaccessible),(138) and a more recent *ab initio* molecular dynamics employed T3 as the Brønsted acid site to good effect in elucidating the mechanism of propene methylation in TON.(148)

The different charge determination methods provide identify different sites as the most positive (Tables like table 4 for the other zeolites are in the Appendix B). EQEq, QTPIE, and HI all predict T5 and T6 as the first and second most positive sites in BEA, whereas Bader and REPEAT identify T9 as the most positive site. The charge difference between the first and second most positive sites in BEA is large enough (~34% of the total for HI) to suggest chemically significant distinctions between the sites. Somewhat surprisingly, DDEC has a large distribution of charges (1.95e-3.65e) in BEA and the other zeolites, and it picks T1 as the most positive site in BEA. The other charge determination methods all predict that T3 is the most positive site of BEC. The literature BEC studies used force field and cluster

simulations, both of which were noted by Gale as prone to incorrect predictions,(129) which casts enough of a shadow of doubt that the charge determination results cannot be instantly ruled out. REPEAT is the only method that predicts site T4 as the most acidic in MFI, following Gale's prediction. Considering the other methods, we see that Bader predicts T8 and DDEC T1 for MFI. HI, EQEq, and EEM all agree on site T3 for MFI, with REPEAT indicating that should be the second most acidic site. No method agreed with the substitution literature on MWW, placing T6 or T1 as the most positive site. QEq and REPEAT agreed with the QM/MM study identifying T8 as the most positive site, and DDEC was the sole method that selected T3 as the most acidic site. Similar to BEC, most of the charge determination methods agree that site T4 is be the most positive site in TON, with DDEC as the only *ab initio* method to predict T1 as the most positive. The margins between the charges at different sites are the lowest for TON, making it seem that T2 and T4 should have comparable acidity according to Bader and HI.

Overall, the REPEAT method appears to yield the best agreement for the most electropositive T-site compared with the most reliable literature. An exception is the case of BEC, and to a lesser extent TON, where REPEAT agrees with most of the other methods. DDEC is the only *ab initio* method that agrees with the literature determination of T1 for BEC and TON. Both these charge determination methods use the DFT periodic electrostatic potential (and thus long-range electrostatics) to determine the charges, so it is sensible they are the most adept at predicting acidic sites. HI also does a reasonable job of predicting the literature-identified substitution sites. A unique aspect of our approach compared to other investigations is that we used DFT-optimized structures while most other investigators performed simulations on the experimental structure. Considering the differences noted above, this is likely a major reason why we reach slightly different conclusions in some cases, especially compared with cluster and QM/MM studies. An additional point is that, in the optimization of MFI, we discovered two different solutions in the same range of unit cell volumes, and the lower energy solution reported more closely resembles the high temperature, evacuated phase of MFI.

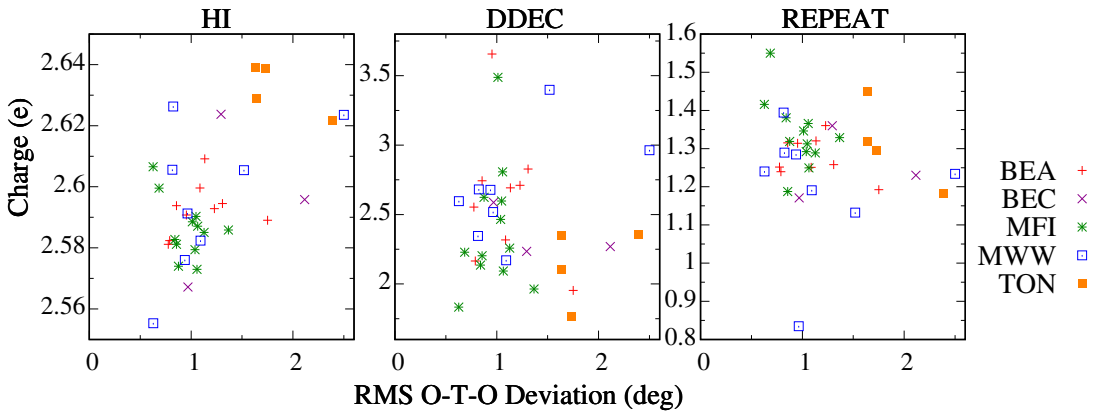

Figure 2: A comparison of the RMS deviation of the O-T-O angles to the HI, DDEC, and REPEAT charges for each crystallographically unique T-site in the 5 zeolites.

To see if there is any connection between partial atomic charge for a T-site and its local structure, we analyzed the dependence on the local bond angles for the leading *ab initio* charge determination methods. Following Yang's assertion, the T-sites with the greatest RMS deviation of O-T-O angles should be the most acidic,(108) and Figure 2 illustrates those deviations for the 5 zeolites using three different sets of charges. The average O-T-O angle in each case is the anticipated ~109.47°. In each of the structures with each of the tested partial charge determination methods, the site with the largest RMS O-T-O deviation was not the site with the highest charge. The data show no clear correlation between predicted charge RMS O-T-O deviation. The scatter evident in Figure 2 clearly shows that, for the most promising methods investigated here, O-T-O deviations have at best a secondary affect partial charge. There is however some evidence of correlation between the T-O-T angles and predicted partial charges (Figure 3). Specifically, for the HI method, charges track the average T-O-T angles quite well, although not quantitatively. By its design, the HI method should do the best job of predicting the iconic character of a bond. Considering that more linear metal-oxygen-metal bond angles are expected to be more ionic, the observed correlation is expected. In TON, there are several linear T-O-T bonds in the system. We interpret that those large angles strain the tetrahedra, leading to the higher than average RMS deviations of the O-T-O and T-O-T angles. Since all these sites show higher simulated charges in HI, there is likely a

relationship although far from perfect. For example, site T2 is connected via two linear T-O-T angles (giving the second highest average T-O-T angle in the cell), but the average O-T-O angle at T2 is the closest to the anticipated value with an RMSD of 1.73°.

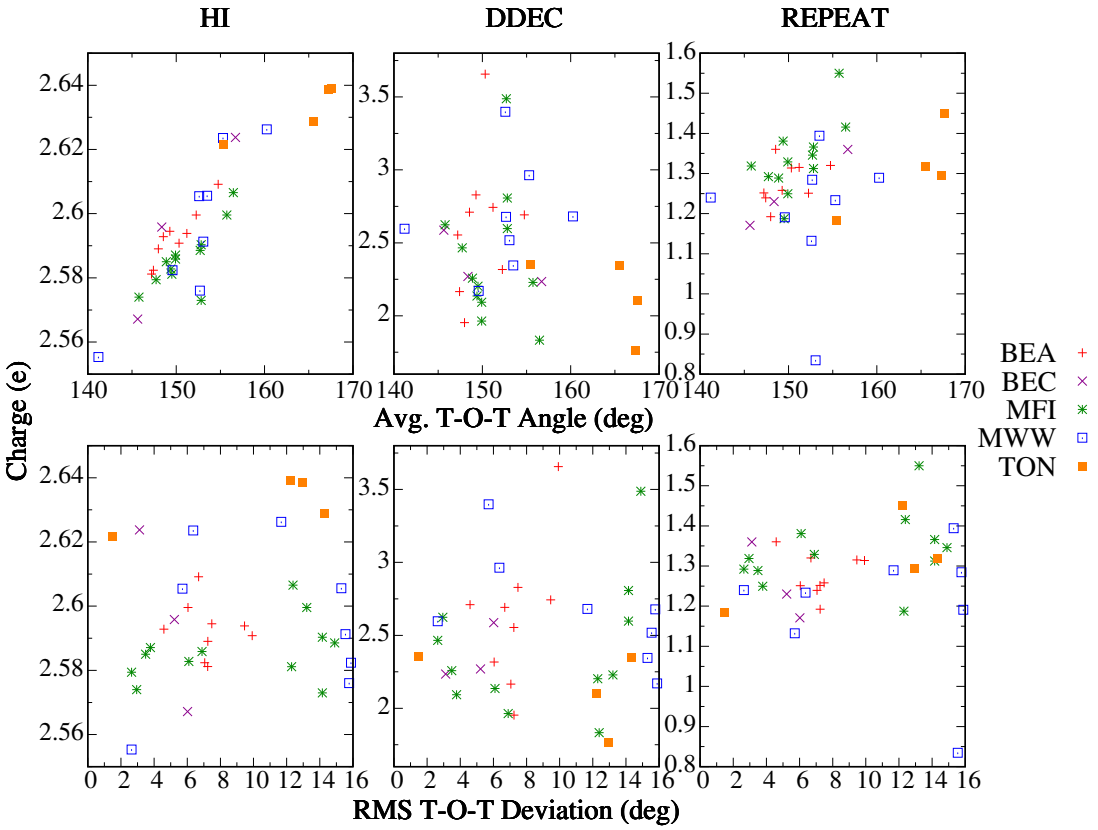

Figure 3: A comparison of the average (top) and RMS deviation (bottom) of the T-O-T angles to the HI, DDEC, and REPEAT charges for each crystallographically unique T-site in the 5 zeolites.

The correlation between RMS deviations of the T-O-T angles and partial charge is about as poor as the correlation between the partial charges and the RMS O-T-O deviations, ie. the HI and DDEC plots just look like scatter plots. The REPEAT method appears to have a weak dependence on the RMS T-O-T deviations, but again it is not significant enough to be quantitative. We cannot exclude the possibility that stronger correlations might emerge when considering multiple, coupled geometric factors, but such analysis is beyond the scope of this project. However, as summarized at the start of this section, other

teams have attempted to extract similar relationships from local geometry without success. Our results are consistent with their conclusions that long range correlations are at least as important as local geometry.

2.3.3: The Effect of Compression on Partial Atomic Charges

Compressing a zeolite under high pressure is one of the best ways to experimentally manipulate and change a zeolite's structure, and it is one of the best tests for predicting zeolite structures using force field simulations. Since we have shown that changes in structure lead to changes in the predicted partial atomic charges, we endeavored to explore how the partial atomic charges of a zeolite changed in response to compression. We have synthesized and compressed samples of rhombohedral (R-3) siliceous sodalite (SOD) in fluorinert-loaded diamond anvil cells. Fluorinert has previously served as a quasihydrostatic non-penetration pressure transmitting medium in other zeolite studies.

Table 4: The structural parameters for the ambient and three compressed unit cells of R-3 SOD.

Pressure (kbar)	*a* (Å)	*c* (Å)	Volume (Å^3)	Avg. Si-O Length (Å)	Average Si-O-Si Angle
0	12.46	7.21	969.40	1.601	149.97°
4	12.34	6.86	904.66	1.564	150.29°
14	12.11	6.32	802.27	1.504	150.78°
22.2	11.92	6.21	764.14	1.480	150.79°

The lattice vectors of the compressed SOD sample were determined with synchrotron powder X-ray diffraction (Table 4) at ambient conditions and at 4, 14, and 22.2 kbar. Over this pressure range, it was found that R-3 symmetry was maintained. As *in-situ* high pressure diffraction studies of powder samples do not typically provide sufficiently reliable atomic positions, we used *ab initio* simulations to predict reasonable atom coordinates (optimized structures in the SI). We started using the atomic positions from King *et al.*'s single crystal X-ray diffraction study and relaxed the atom positions, keeping the lattice parameters fixed to our experimentally determined values.(122) The optimization process reduced

internal stress from the original guessed structure that used our lattice vectors and King's atomic crystal coordinates by homogenizing the Si-O bond lengths and a reducing/homogenizing the Si-O-Si bending angles. The cell maintained the nearly rectangularly elongated 6MRs which differentiate rhombohedral SOD from the icosahedral form found in the IZA-SC. The Si-O bond lengths initially varied between 1.57-1.64 Å, and optimized to all be around 1.62 Å at 0 kbar. The Si-O-Si bending angles also became closer in value going from 147-152° to all being around 146°. These median structural values are quite similar to the potential parameters of typical zeolite force fields, ie. 1.61 Å and 149.5° for the Nicholas Force Field.(86) The primary mechanism for compression is an increase Si-O-Si bend (ie. a lower Si-O-Si angle). The regular 6MR's Si-O-Si angles went from 146.0°, 139.6°, 132.2°, to 129.6° at 0, 4, 14, and 22.2 kbar respectively; whereas the elongated 6MR's Si-O-Si angles not shared with a regular 6MR compress slower going from 146.0°, 142.1°, 135.9°, to 133.6° upon compression. Upon compression, the bond lengths also acquire more alternation while still staying ~1.62 Å. The difference increases from 0.004 Å, 0.006 Å, 0.012 Å, to 0.0016 Å as pressure is increased. The elongated 6MR is the stiffest feature of the cell with its' nearly rectangular shape only becoming more pronounced with compression (the largest Si-Si-Si angle in the elongated 6MR increases from 138.7° to 153.3° with compression).

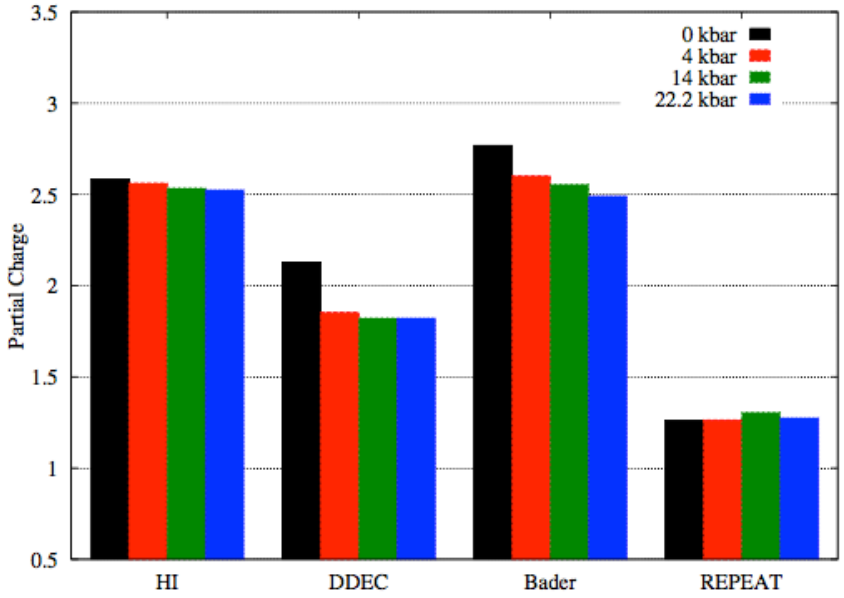

Figure 4: A comparison of partial charge methods for the ambient and compressed structures of R-3 SOD.

The compression caused noticeable changes to the SOD structure, so we decided to investigate the effect of those structural changes on the partial atomic charges. Figure 4 shows the charges for the single crystallographically unique Si atom of each of the four optimized SOD structures predicted by the *ab initio* methods. The magnitudes of the charges on the uncompressed structures are close to those predicted for the IZA-SC structures (Table 2 and SI), providing confidence in the results of the optimization. The HI, DDEC, and Bader methods all exhibited a monotonic decrease in charge on the Si atom with increased pressure. This effect was more pronounced for the DDEC and Bader methods, where the initial drop in charge is far larger than for any subsequent compression. The more apparent decrease is because the atoms-in-molecules parsing will be the most sensitive to the subtle changes in geometry, and the difference between the Si-O-Si angles in the two different 6MRs had the biggest change between 0 and 4 kbar. The HI charges do not change significantly, indicating that the valence state and ionic character of the Si-O bonds did not change during this amount of compression. The ionic character of the Si-O bonds, while not changing much, decreased with increasing pressure as is evident by the decrease in HI, DDEC, and Bader charges. Previous studies have shown that, for inorganic compounds, lower metal-

oxygen-metal bending angles tend to be more covalent.(149; 150) The Si charges predicted by REPEAT do not appear to change appreciably with compression. The nearly identical charges up to 2.22 kbar show that the electrostatic potential is scaling relative to the change in the size of the void volumes. We take these REPEAT charges to imply that there is a reasonably constant environment for physisorbed guest species within the pores of this zeolite during compression.

2.3.4: Performance in Predicting Gas Adsorption

One of the most common applications of partial atomic charges is to perform force field gas simulations to model gas adsorption capacity, the heat of adsorption, and a material's ability to separate gases. We have previously studied the ability of the siliceous zeolite frameworks to separate Kr and Xe gas mixtures.(92) Kr and Xe have no partial atomic charges and cannot be used to test the applicability of our determined partial charges, so we will model N_2 and O_2 which have partial atomic charges to replicate their standing molecular quadrupole moments. The adsorption of N_2 and O_2 into the FAU (faujasite) framework was simulated with GCMC using the same TraPPe-ZEO dispersion-repulsion parameters employed in our previous study, and is compared to in-house obtained experimental adsorption data. As in the previous sections, we used a DFT optimized structure with charges determined from the *ab initio* methods. In the high symmetry Fd-3m FAU structure, there is only one crystallographically unique tetrahedral atom and four unique oxygen atoms in the unit cell, and the partial charges on the tetrahedral atom are $1.140 < 1.500 < 2.357 < 2.556 < 2.953$ for REPEAT, TraPPe-ZEO (force field, denoted TZ), HI, DDEC, and Bader methods respectively. As may be seen in Figure 5, the simulated isotherms and heats of adsorption increase with higher partial charges on the T-sites with differences in magnitude (roughly) proportional to differences in partial charge. The large difference in partial charge magnitude between REPEAT and TraPPE-ZEO compared with HI, DDEC, and Bader is quite apparent in the simulated N_2 isotherms and HOA; a similar split is also present for O_2 but with a much smaller magnitude due primarily to oxygen's much smaller quadrupole moment (and partial atomic charges). The different

partial charges do make a significant difference in predicted adsorption, for both the isotherm and predicted heat of adsorption.

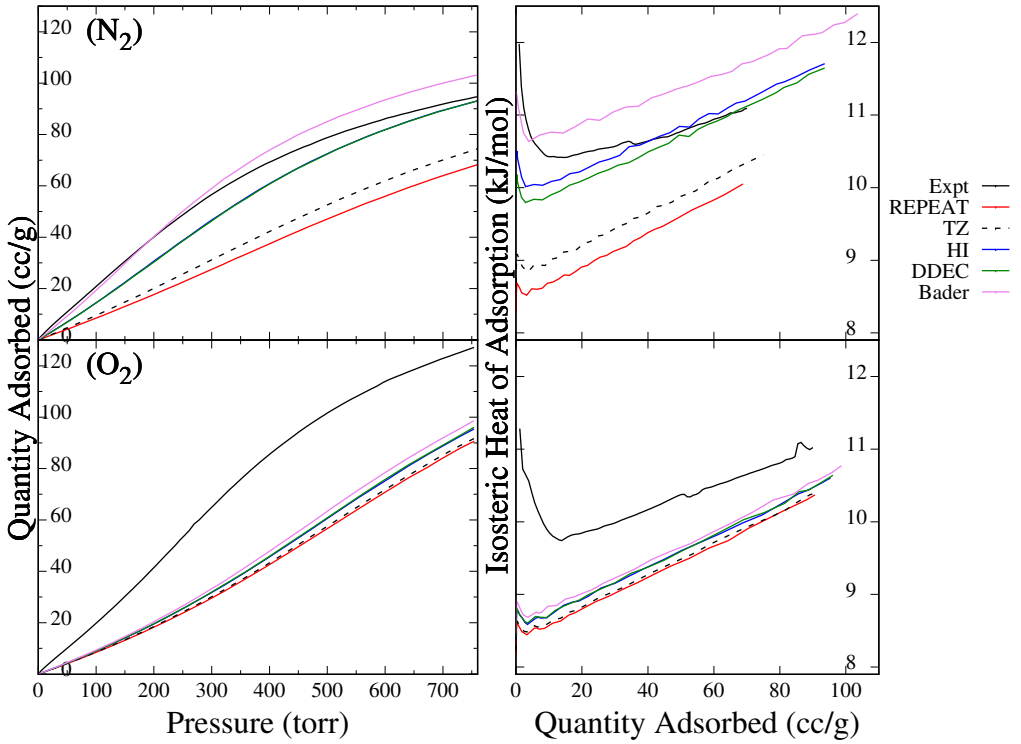

Figure 5: Simulated and experimental (Expt) N_2 (top) and O_2 (bottom) adsorption isotherms (left) and heats of adsorption (right) for FAU at 140K. The TraPPe-ZEO dispersion-repulsion parameters were used in all simulations.

The most eye-catching detail is how most of these combinations, including the defined charges for TraPPe-ZEO, under-predicts the experimental adsorption by upwards of 25%. In our previous investigations, we noted that just a 12-6 Lennard-Jones dispersion-repulsion for the adsorbate species did lead to an under-prediction at high loadings, especially for relatively low temperatures near the critical temperature in large pore materials like HKUST-1 and FAU.(151) The remedy was to utilize a 9-6 Lennard-Jones potential that was parameterized for the liquid state for the fluid-fluid interactions.(152) Even then, the predicted isotherms for Kr and Xe into a sample of FAU from the same batch under-predicted experimental adsorption by 5-15% at various temperatures. Using 10% as a reasonable margin of error for these results, the HI and DDEC charges are the best at reproducing the experimental

adsorption. However, it is unreasonable to conclude that a simple substitution of charges into an existing force field would produce perfect agreement as many common zeolite force fields are fit for different purposes and with their own respective charge models. To further demonstrate that we performed additional GCMC simulations combining the iterative Hirshfeld charges with the dispersion-repulsion parameters of several other common force fields (Figures in SI), and as should be expected there was no significant improvement. A better next generation force field for simulating zeolites could be constructed by refining the dispersion-repulsion and bonding parameters for the zeolite framework with the better determined partial atomic charges produced by the iterative Hirshfeld or the similarly valued EQEq method.

To see if the site-to-site variations in charges mattered for predicting adsorption compared to a "one-charge fits all" type approach, we created a hypothetical set of partial atomic charges that featured site-to-site variations yet had the same average values as the base TraPPe-ZEO charges which uses only a single charge for Si and O. The REPEAT charges are the closest in value to the TraPPe-ZEO charges, so they were scaled so that their average values matched the TraPPe-ZEO charges. While FAU with its fairly uniform internal surface (compared to other zeolites like BEA and MFI) may not be the best example to show the differences from using site-specific charges, Figure 6 clearly shows a difference in the GCMC predicted adsorption for N_2 and O_2 using the REPEAT, scaled REPEAT, and TraPPe-ZEO charges. Increasing the magnitude of the REPEAT charges did increase the overall predicted adsorption, but it is still not equivalent to the adsorption predicted using the single valued TraPPe-ZEO charges. The scaled REPEAT charges do exhibit a smaller predicted adsorption than the TraPPe-ZEO charges, and this

is most likely because the oxygens in the adsorption site at the 6MR window into the β-cage have lower than average charges (-0.728e and -0.686e) compared to the other oxygens (-0.768e and -0.817e). This

inhomogeneity in charge clearly leads to a lower electrostatic potential at the solid-fluid interface in FAU compared to just using -0.75e for each oxygen, which directly affects the predicted adsorption.

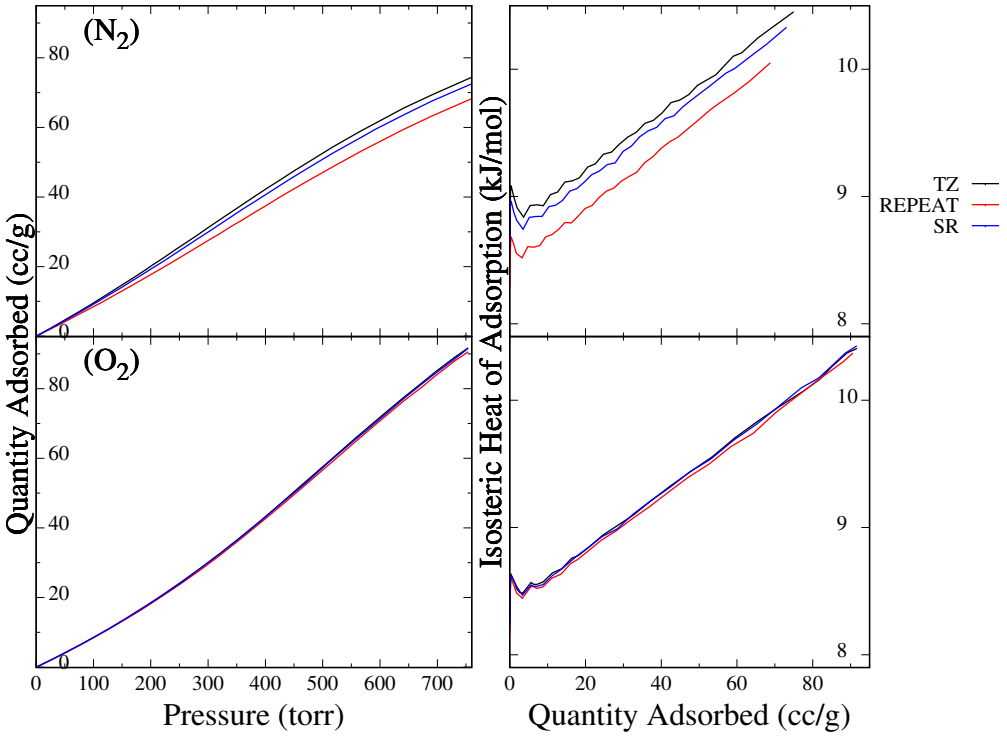

Figure 6: Simulated N_2 (top) and O_2 (bottom) adsorption isotherms (left) and heats of adsorption (right) for FAU at 140K using the TraPPe-ZEO (TZ), REPEAT, and scaled REPEAT (SR) charges.

Section 2.4: Conclusions

We have shown that the different methodologies to compute partial atomic charges produce significantly different solutions when applied to the known pure silica zeolites. Atoms-in-molecule partitioning of the DFT charge density predicted the system to be the most ironically charged whereas all the other different methodologies predicted charges that better reflected the known covalency of the Si-O bond. All the methodologies showed at least some difference in charge between the different crystallographically unique sites with the RMS differences of the Bader charges being the least pronounced of all the methods. That these differences are physical and meaningful is evident from inspection of the zeolites' internal geometry where the chemical environment around each T-site is unique. Partial atomic charge analysis on the full periodic structure is a simple way to *a priori* predict the most catalytically active sites or sites most likely to undergo substitution in zeotype frameworks, especially since none of the simple local geometric metrics from the literature were found to correlate with the partial atomic charges. The closest connection to local geometry and partial atomic charge is the correlation between the average T-O-T angle at a T-site and the iterative Hirshfeld charges, but it is too weak to build a simplified, analytic algebraic model. Slight changes in the zeolite structure through structural optimization or compression experiments also had a noticeable impact on the predicted partial atomic charges and their variation between crystallographically unique atomic sites. This serves to emphasize the need for high quality, reliable structures for zeolite simulations. Framework-to-framework and site-to-site variations in partial charge represent subtle, yet important, features that will cannot be captured by fixed charge force fields, although they may be accounted for by core-shell potentials to at least some extent. Given the large amount of site-to-site charge variation observed within this work, we recommended using partial charges that account for these differing chemical environments rather than a fixed value for atoms of the same type.

The lingering question is which choice of partial atomic charges is the most appropriate appears to depend on the specifics of the problem to be addressed. The iterative Hirshfeld charges described the

strongly polar covalent nature of the bonding within the framework and tended to better predict substitution sites, whereas the REPEAT charges were better overall at predicting the acidic/catalytic site within a zeolite. Given their agreement with *ab initio* methods in both magnitude and variance between T-sites, the QEq/EQEq methods are likely to prove the best overall approach to predicting partial atomic charges once they have been tweaked to better reproduce the values and site-to-site variations of the REPEAT/iterative Hirshfeld charges. This is especially true for molecular dynamics where the charges should be recomputed "on-the-fly" to reflect the new bonding environment and where full *ab initio* methods are prohibitively computationally expensive. The EQEq approach is likely better for zeolites because centering the Taylor expansion on the fully ionic states returns partial charges closely resembling the HI charges. As we have shown the choice of partial atomic charge has an impact on the prediction of gas adsorption, and merely substituting 'better' partial atomic charges is not a sufficient solution as in many cases the van der Waals parameters are co-fit with the partial atomic charges. For flexible framework simulations with zeolites, a better force field of sufficiently high quality that can describe the zeolite structure and interaction with guest species needs to be parameterized around the iterative Hirshfeld or tweaked EQEq charges.

Acknowledgements

This research was sponsored (or sponsored in part) by the National Nuclear Security Administration under the Stewardship Science Academic Alliances program through DOE Cooperative Agreement #DE-NA0001982. DEPV is a postdoctoral researcher funded by the Foundation of Scientific Research-Flanders (FWO) project no.12S3415N. Portions of this work were performed at HPCAT (Sector 16), Advanced Photon Source (APS), Argonne National Laboratory. HPCAT operations are supported by DOE-NNSA under Award No. DE-NA0001974 and DOE-BES under Award No. DE-FG02-99ER45775, with partial instrumentation funding by NSF. The Advanced Photon Source is a U.S.

Department of Energy (DOE) Office of Science User Facility operated for the DOE Office of Science by Argonne National Laboratory under Contract No. DE-AC02-06CH11357.

Appendix A

A New Binary Halide Structure Type; Pentanuclear Technetium Iodide, Tc_5I_{13}

An additional project was carried out during my work towards this Master's thesis that is summarized here, but not described in detail. The work is only summarized because the simulations complement and experimental project, and the experimental portion of the work has not yet been fully analyzed. Additionally, the project did not fit the theme of this thesis closely. This section summarizes this work which is anticipated to contribute towards two papers eventually.

The above simulations support an investigation into a new binary halide, (Tc_5I_{13}), discovered within UNLV's Radiochemistry program. The synthesis and parts of the physical analysis of this new compound were conducted by William Kerlin. Additional work on the experimental side includes Frederic Poineau, Alfred Sattelberger, Ken Czerwinski, Christos Malliakas and Mercouri Kanatzidis.

Computational analysis of the Tc_5I_{13} utilized DFT in order to verify the structures overall resistivity and magnetic susceptibility. The connectivity of the Tc_5I_{13} allowed for C_{4V} symmetry, but upon closer examination of the overall electronic structure, this cluster distorts to C_{2V}. Further analysis of the solid's band gap gave insight to the electronic behavior of this material and validation of the experimental resistivity and magnetic susceptibility measurements.

Appendix B

Site	*EEM*	*QEQ*	*EQEQ*	*QTPIE*	*HI*	*DDEC*	*Bader*	*REPEAT*
O1	-0.774202	-0.631929	-1.036083	-0.086770	-1.325206	-1.028014	-1.600983	-0.539895
O2	-0.689064	-0.632021	-1.038750	-0.085061	-1.317877	-1.864432	-1.610583	-0.557171
O3	-0.645093	-0.614842	-1.110000	-0.081369	-1.292247	-1.991698	-1.602900	-0.502692
O4	-0.704105	-0.633518	-1.160417	-0.088324	-1.334426	-1.812537	-1.616783	-0.574868
T1	1.406232	1.256155	2.172625	0.170762	2.634046	3.348341	3.215600	1.087313

Table 5: A comparison of the partial charges determined from several methodologies for the zeolite AFI. The 'site' is the atom label used in the crystal structure for the zeolite available from the IZA database.

Site	*EEM*	*QEQ*	*EQEQ*	*QTPIE*	*HI*	*DDEC*	*Bader*	*REPEAT*
O1	-0.852655	-0.628127	-0.612083	-0.215842	-1.320097	-1.547614	-1.608800	-0.642418
O2	-0.828231	-0.593643	-0.906625	-0.193609	-1.308859	-1.287266	-1.592000	-0.499565
T1	1.669785	1.226890	1.315625	0.422307	2.620639	2.949988	3.203300	1.213643
T2	1.749712	1.235773	2.036500	0.380259	2.671794	2.634797	3.207500	0.998194

Table 6: A comparison of the partial charges determined from several methodologies for the zeolite AST. The 'site' is the atom label used in the crystal structure for the zeolite available from the IZA database.

Site	*EEM*	*QEQ*	*EQEQ*	*QTPIE*	*HI*	*DDEC*	*Bader*	*REPEAT*
O1	-0.811032	-0.602777	-1.042000	-0.175670	-1.282522	-0.843682	-1.584300	-0.516477
O2	-0.838241	-0.619111	-0.944500	-0.183512	-1.312232	-1.419059	-1.599800	-0.515805
O3	-0.879443	-0.642891	-1.115000	-0.198150	-1.344200	-1.859602	-1.615250	-0.564586
O4	-0.854545	-0.628229	-0.964500	-0.190312	-1.327832	-1.387346	-1.602600	-0.606252
O5	-0.842564	-0.626453	-1.068000	-0.184073	-1.309615	-0.556544	-1.608500	-0.600894
O6	-0.808881	-0.604700	-1.034000	-0.175728	-1.277105	-2.379267	-1.596900	-0.567360
T1	1.683588	1.239911	2.017500	0.370327	2.625334	2.642443	3.203400	1.050206
T2	1.683415	1.246773	2.026500	0.371216	2.625599	2.252482	3.194100	1.157041
T3	1.678086	1.241911	2.014000	0.369276	2.618654	2.818485	3.206300	1.204407

Table 7: A comparison of the partial charges determined from several methodologies for the zeolite ATS. The 'site' is the atom label used in the crystal structure for the zeolite available from the IZA database.

Site	*EEM*	*QEQ*	*EQEQ*	*QTPIE*	*HI*	*DDEC*	*Bader*	*REPEAT*
O1	-0.866994	-0.653234	-1.112375	-0.073923	-1.337235	-1.167701	-1.593600	-0.695877
O2	-0.841764	-0.644894	-1.040750	-0.072006	-1.307554	-1.117364	-1.615800	-0.661990
O3	-0.810354	-0.613103	-1.088375	-0.065066	-1.285151	-1.311074	-1.605600	-0.593024
O4	-0.795226	-0.598660	-1.121125	-0.063240	-1.274561	-1.724300	-1.600800	-0.562299
O5	-0.840221	-0.598660	-1.166000	-0.078570	-1.324097	-1.175658	-1.588850	-0.633372
O6	-0.864830	-0.621887	-1.226250	-0.079777	-1.336629	-1.290089	-1.608100	-0.730123
O7	-0.839861	-0.631223	-1.267625	-0.073691	-1.312502	-1.415521	-1.598900	-0.603010
T1	1.642886	1.246463	2.138938	0.135606	2.596001	2.808032	3.201100	1.242549
T2	1.683695	1.255197	2.424500	0.131480	2.616078	2.886835	3.217200	1.217628
T3	1.672344	1.252268	2.512750	0.161340	2.625989	2.605755	3.193500	1.260528

Table 8: A comparison of the partial charges determined from several methodologies for the zeolite BEC. The 'site' is the atom label used in the crystal structure for the zeolite available from the IZA database.

Site	*EEM*	*QEQ*	*EQEQ*	*QTPIE*	*HI*	*DDEC*	*Bader*	*REPEAT*
O6	-0.866622	-0.636674	-1.237500	-0.147688	-1.324633	-1.641312	-1.604800	-0.629218
O7	-0.870967	-0.619082	-1.372000	-0.147338	-1.343626	-1.437304	-1.615000	-0.658488
O8	-0.878374	-0.631286	-1.408250	-0.151364	-1.345212	-1.849636	-1.596700	-0.685511
O9	-0.842189	-0.622495	-1.168000	-0.139250	-1.318434	-1.677410	-1.588500	-0.576521
O10	-0.614185	-0.449882	-0.901000	-0.098008	-1.286921	-0.982846	-1.597700	-0.535570
O11	-0.896998	-0.650790	-1.149500	-0.153982	-1.354699	-0.887756	-1.613650	-0.704838
O12	-0.827326	-0.601867	-1.245500	-0.134504	-1.297371	-1.608520	-1.595400	-0.609018
O13	-0.842351	-0.613791	-1.233375	-0.138043	-1.317615	-1.557767	-1.609675	-0.636052
T1	1.671514	1.239518	2.366000	0.277720	2.619958	2.964827	3.205650	1.146052
T2	1.707324	1.250045	2.604500	0.283127	2.638796	3.209814	3.199000	1.303286
T3	1.699361	1.241046	2.363750	0.282718	2.646101	2.887784	3.219550	1.301056
T4	1.736056	1.218917	2.914500	0.315872	2.667061	3.225984	3.212500	1.313722
T5	1.711717	1.230841	2.580250	0.270116	2.646253	2.865273	3.217750	1.248628

Table 9: A comparison of the partial charges determined from several methodologies for the zeolite CFI. The ‘site’ is the atom label used in the crystal structure for the zeolite available from the IZA database.

Site	*EEM*	*QEQ*	*EQEQ*	*QTPIE*	*HI*	*DDEC*	*Bader*	*REPEAT*
O1	-0.862213	-0.639178	-1.109500	-0.182638	-1.329609	-1.409656	-1.613150	-0.653231
O2	-0.809182	-0.599962	-1.084000	-0.164202	-1.287172	-0.947447	-1.593600	-0.549504
O3	-0.819134	-0.611151	-1.098000	-0.168816	-1.290150	-1.240758	-1.604267	-0.605897
O4	-0.850938	-0.628249	-1.024000	-0.177498	-1.322156	-2.073244	-1.614300	-0.659419
T1	1.670733	1.239270	2.157750	0.346577	2.614192	2.835551	3.212625	1.234026

Table 10: A comparison of the partial charges determined from several methodologies for the zeolite CHA. The ‘site’ is the atom label used in the crystal structure for the zeolite available from the IZA database.

Site	EEM	QEQ	EQEQ	QTPIE	HI	DDEC	Bader	REPEAT
T1	1.674579	1.273844	2.540000	0.230692	2.609022	2.647245	3.207900	1.168964
T2	1.642906	1.236277	2.484000	0.234571	2.593503	2.664387	3.203600	1.261054
T3	1.660740	1.260439	2.616000	0.256279	2.616880	3.050561	3.211300	1.289377
T4	1.644847	1.278389	2.401000	0.218773	2.586892	2.618166	3.208200	1.320613
T5	1.679611	1.287487	2.482000	0.220482	2.606778	2.062985	3.206000	1.103967
T6	1.657623	1.249025	2.445000	0.210930	2.599866	3.420922	3.203500	1.156213
T7	1.641145	1.252317	2.418000	0.217774	2.592793	2.832705	3.209500	1.155039
T8	1.654392	1.275733	2.669000	0.280969	2.617138	2.876056	3.207000	1.209192
T9	1.643478	1.247881	2.490000	0.243842	2.592941	2.844698	3.202000	1.274742
T10	1.664945	1.259854	2.597000	0.251977	2.614554	2.884195	3.202500	1.023757
O1	-0.798564	-0.612874	-1.217000	-0.111246	-1.275935	-0.938252	-1.591200	-0.550957
O2	-0.827369	-0.624955	-1.293000	-0.124687	-1.307266	-1.252664	-1.607500	-0.524664
O3	-0.846148	-0.637971	-1.296000	-0.122764	-1.320874	-1.301117	-1.612000	-0.550683
O4	-0.790552	-0.610160	-1.183000	-0.106804	-1.263218	-1.264937	-1.594800	-0.621298
O5	-0.854973	-0.647786	-1.290000	-0.125716	-1.322710	-1.354487	-1.608400	-0.693213
O6	-0.842870	-0.639492	-1.254000	-0.116887	-1.315017	-1.607290	-1.608000	-0.623269
O7	-0.846218	-0.650760	-1.306000	-0.128289	-1.312030	-1.528111	-1.604100	-0.663897
O8	-0.815240	-0.619195	-1.247000	-0.115678	-1.296174	-0.908124	-1.601100	-0.527807
O9	-0.874125	-0.657971	-1.377000	-0.138769	-1.342684	-1.719939	-1.615250	-0.735883
O10	-0.830896	-0.633011	-1.258000	-0.117564	-1.309973	-2.046153	-1.602900	-0.687133
O11	-0.850291	-0.643541	-1.241000	-0.116899	-1.319134	-1.144658	-1.610600	-0.666122
O12	-0.786676	-0.610685	-1.163000	-0.103149	-1.262924	-1.098358	-1.599500	-0.559282
O13	-0.786930	-0.599454	-1.168000	-0.101682	-1.261873	-0.830961	-1.594100	-0.551354
O14	-0.826266	-0.623698	-1.253000	-0.116771	-1.300473	-1.207713	-1.603300	-0.497400
O15	-0.803732	-0.611303	-1.204000	-0.111413	-1.276916	-0.917296	-1.592400	-0.554725
O16	-0.838842	-0.631052	-1.254000	-0.117620	-1.313282	-1.991896	-1.607200	-0.631264
O17	-0.823949	-0.631950	-1.222000	-0.110844	-1.297649	-1.828097	-1.606000	-0.543740
O18	-0.826046	-0.636691	-1.258000	-0.117077	-1.297749	-1.783639	-1.594600	-0.538683
O19	-0.847384	-0.657275	-1.324000	-0.131929	-1.317742	-1.467062	-1.606700	-0.667323
O20	-0.847195	-0.641421	-1.334000	-0.130502	-1.321873	-1.711167	-1.601600	-0.574222

Table 11: A comparison of the partial charges determined from several methodologies for the zeolite CSV. The 'site' is the atom label used in the crystal structure for the zeolite available from the IZA database.

Site	EEM	QEQ	EQEQ	QTPIE	HI	DDEC	Bader	REPEAT
O1	-0.831512	-0.621809	-1.241333	-0.057999	-1.294781	-1.528315	-1.602800	-0.723507
O2	-0.823418	-0.611832	-1.203000	-0.054626	-1.294445	-1.794144	-1.600950	-0.685155
O3	-0.861764	-0.640994	-1.233500	-0.060820	-1.317870	-1.474437	-1.612250	-0.791941
O4	-0.827219	-0.619095	-1.151000	-0.055735	-1.295582	-1.363009	-1.597725	-0.666528
O5	-0.849813	-0.631477	-1.315000	-0.059801	-1.312946	-2.081640	-1.600000	-0.774523
O6	-0.857578	-0.626990	-1.391500	-0.062278	-1.325386	-1.264227	-1.602500	-0.773669
O7	-0.842730	-0.612586	-1.281500	-0.055630	-1.308013	-1.276183	-1.596000	-0.673843
O8	-0.837851	-0.612994	-1.297000	-0.055553	-1.317875	-1.453244	-1.611250	-0.667080
O9	-0.862851	-0.620978	-1.329500	-0.057886	-1.329416	-1.723967	-1.609900	-0.812162
O10	-0.855447	-0.640329	-1.143000	-0.060159	-1.321167	-1.243158	-1.615400	-0.717672
O11	-0.858089	-0.615064	-1.407500	-0.060466	-1.332366	-1.650481	-1.603400	-0.816976
T1	1.664777	1.258364	2.400500	0.114247	2.597022	3.065633	3.203900	1.410825
T2	1.665280	1.255023	2.560500	0.123148	2.605200	3.118207	3.209600	1.525296
T3	1.699461	1.232976	2.629500	0.111563	2.637034	3.196525	3.209400	1.376136
T4	1.700920	1.240819	2.523500	0.109708	2.627813	3.409815	3.214100	1.454514
T5	1.669118	1.237299	2.207000	0.113747	2.611552	2.537699	3.210350	1.367744
T6	1.737621	1.209911	2.813500	0.117081	2.659384	3.238546	3.214100	1.650931
T7	1.724470	1.232086	2.974500	0.129955	2.659586	2.894773	3.186800	1.613836

Table 12: A comparison of the partial charges determined from several methodologies for the zeolite DDR. The 'site' is the atom label used in the crystal structure for the zeolite available from the IZA database.

Site	*EEM*	*QEQ*	*EQEQ*	*QTPIE*	*HI*	*DDEC*	*Bader*	*REPEAT*
O1	-0.852232	-0.599174	-1.297792	-0.060024	-1.324128	-1.523634	-1.604100	-0.606215
O2	-0.867533	-0.611017	-1.265167	-0.061483	-1.336541	-1.473620	-1.607700	-0.604458
O3	-0.871729	-0.611389	-1.422000	-0.062941	-1.337921	-1.337280	-1.613333	-0.665549
O4	-0.857189	-0.606500	-1.314667	-0.060474	-1.320733	-0.970779	-1.596550	-0.632217
O5	-0.884227	-0.624166	-1.358167	-0.063925	-1.344806	-1.356722	-1.616833	-0.678526
O6	-0.852657	-0.599983	-1.320333	-0.059061	-1.325878	-1.264710	-1.592533	-0.578095
O7	-0.869317	-0.605286	-1.607000	-0.062950	-1.341571	-1.212172	-1.596600	-0.704853
T1	1.584281	1.111097	2.520583	0.112152	2.664666	2.885044	2.952875	1.225565
T2	1.719660	1.218530	2.582000	0.122288	2.653506	2.729931	3.206367	1.267124
T3	1.724921	1.216128	2.444000	0.119932	2.666867	2.725138	3.198400	1.188012
T4	1.725682	1.194771	3.005000	0.126277	2.667807	2.636271	3.213700	1.372906

Table 13: A comparison of the partial charges determined from several methodologies for the zeolite DOH. The 'site' is the atom label used in the crystal structure for the zeolite available from the IZA database.

Site	*EEM*	*QEQ*	*EQEQ*	*QTPIE*	*HI*	*DDEC*	*Bader*	*REPEAT*
O1	-0.854725	-0.629615	-1.305250	-0.081092	-1.323328	-2.615678	-1.599300	-0.742028
O2	-0.797734	-0.619534	-1.182250	-0.073589	-1.265003	-1.951333	-1.578600	-0.664302
O3	-0.833591	-0.645848	-1.228000	-0.080430	-1.293440	-0.883669	-1.601900	-0.788994
O4	-0.862028	-0.632897	-1.339000	-0.078771	-1.332214	-2.055089	-1.614500	-0.713834
O5	-0.824189	-0.610708	-1.272000	-0.070520	-1.294536	-2.056188	-1.602100	-0.625216
O6	-0.844760	-0.608106	-1.298000	-0.070158	-1.319609	-2.767755	-1.601700	-0.647901
O7	-0.846654	-0.611758	-1.317000	-0.070751	-1.322250	-1.105478	-1.602400	-0.618858
O8	-0.829442	-0.632498	-1.233500	-0.076897	-1.302633	-0.869276	-1.609700	-0.681421
O9	-0.876286	-0.663245	-1.309750	-0.082275	-1.339404	-0.851118	-1.613350	-0.778498
O10	-0.811079	-0.622354	-1.227250	-0.072691	-1.280214	-0.800245	-1.589500	-0.617071
O11	-0.844565	-0.636971	-1.282000	-0.076151	-1.319030	-0.712588	-1.592400	-0.647226
O12	-0.860755	-0.648290	-1.380000	-0.083514	-1.318984	-1.185389	-1.599800	-0.779015
T1	1.646553	1.267990	2.446500	0.152441	2.590049	2.616908	3.198200	1.340110
T2	1.659476	1.250201	2.526750	0.148485	2.604219	2.080182	3.193800	1.316350
T3	1.724727	1.240802	2.653500	0.141143	2.651329	4.000000	3.219200	1.310239
T4	1.652148	1.301611	2.433500	0.159316	2.579606	3.166626	3.174200	1.495729
T5	1.696290	1.243896	2.713250	0.169259	2.640675	3.972442	3.205600	1.490152

Table 14: A comparison of the partial charges determined from several methodologies for the zeolite DON. The 'site' is the atom label used in the crystal structure for the zeolite available from the IZA database.

Site	EEM	QEQ	EQEQ	QTPIE	HI	DDEC	Bader	REPEAT
O1	-0.825136	-0.626240	-1.279000	-0.039906	-1.303483	-1.280383	-1.605500	-0.670487
O2	-0.816881	-0.607797	-1.276000	-0.038200	-1.298143	-1.461304	-1.600900	-0.649391
O3	-0.826394	-0.623688	-1.259875	-0.040135	-1.296419	-1.316382	-1.597600	-0.655736
O4	-0.881600	-0.653114	-1.350000	-0.044401	-1.354688	-0.915174	-1.618500	-0.787725
O5	-0.840177	-0.593865	-1.108250	-0.037400	-1.312569	-2.034554	-1.608000	-0.640882
O6	-0.852132	-0.609877	-1.310250	-0.038765	-1.321578	-1.558781	-1.603600	-0.623126
O7	-0.856538	-0.615203	-1.259125	-0.040733	-1.323953	-1.126658	-1.592800	-0.662632
O8	-0.854996	-0.619380	-1.307750	-0.041008	-1.328153	-1.384769	-1.607500	-0.729146
O9	-0.824973	-0.611990	-1.266875	-0.040446	-1.291944	-1.432047	-1.588100	-0.718166
O10	-0.881898	-0.647237	-1.371250	-0.044980	-1.344334	-0.902972	-1.617300	-0.820565
O11	-0.844866	-0.623460	-1.324000	-0.040492	-1.312289	-1.706465	-1.607300	-0.708119
O12	-0.821135	-0.599681	-1.287625	-0.036456	-1.300806	-0.996681	-1.595100	-0.651215
O13	-0.872572	-0.630783	-1.380250	-0.042787	-1.343199	-1.142347	-1.599100	-0.827439
O14	-0.863834	-0.628829	-1.356750	-0.043949	-1.335674	-1.382104	-1.611000	-0.888403
O15	-0.863394	-0.628958	-1.362250	-0.043152	-1.331691	-1.374775	-1.607600	-0.788010
O16	-0.864245	-0.630476	-1.251500	-0.042379	-1.344911	-1.170939	-1.619300	-0.776156
O17	-0.879596	-0.642956	-1.303500	-0.044513	-1.338898	-1.917026	-1.614000	-0.785337
O18	-0.861294	-0.621992	-1.055500	-0.042350	-1.327924	-1.779884	-1.609500	-0.640805
O19	-0.878326	-0.629531	-1.363000	-0.040626	-1.349625	-0.757525	-1.589400	-0.740959
O20	-0.429815	-0.309205	-0.663000	-0.020030	-1.321458	-2.073367	-0.804250	-0.671499
O21	-0.850070	-0.627360	-1.323000	-0.038902	-1.310957	-1.825542	-1.605600	-0.707943
T1	1.450349	1.100223	2.240625	0.070962	2.623042	2.452191	2.809800	1.386085
T2	1.735658	1.230804	2.522750	0.077378	2.657342	3.261415	3.214800	1.337524
T3	1.686718	1.250217	2.648500	0.085348	2.636266	2.775479	3.214500	1.508092
T4	1.701873	1.235793	2.668750	0.076034	2.644160	2.673185	3.215900	1.396494
T5	1.722469	1.232567	2.790250	0.091503	2.652201	2.512481	3.195000	1.694426
T6	1.685415	1.246425	2.511500	0.082450	2.631019	2.595112	3.199500	1.405180
T7	1.712534	1.229404	2.388500	0.085387	2.648478	2.803775	3.193000	1.319956
T8	1.680625	1.259615	2.509500	0.085179	2.619793	2.662392	3.188600	1.590754
T9	1.713977	1.227165	2.684500	0.079653	2.645055	2.873350	3.196200	1.290989
T10	1.693956	1.239967	2.630000	0.074922	2.640504	2.468597	3.191600	1.412813

Table 15: A comparison of the partial charges determined from several methodologies for the zeolite EUO. The 'site' is the atom label used in the crystal structure for the zeolite available from the IZA database.

Site	EEM	QEQ	EQEQ	QTPIE	HI	DDEC	Bader	REPEAT
O1	-0.823767	-0.626219	-1.081500	-0.044585	-1.294117	-1.273639	-1.602850	-0.612267
O2	-0.858252	-0.649183	-1.178500	-0.048048	-1.323336	-1.128989	-1.612375	-0.650273
O3	-0.817155	-0.621867	-1.132000	-0.044671	-1.290143	-1.235728	-1.601983	-0.581393
O4	-0.799751	-0.608974	-1.113500	-0.042726	-1.273252	-1.316394	-1.597350	-0.552511
T1	0.000000	1.253716	2.252750	0.090015	2.590189	2.477375	3.207325	1.198222

Table 16: A comparison of the partial charges determined from several methodologies for the zeolite FAU. The 'site' is the atom label used in the crystal structure for the zeolite available from the IZA database.

Site	EEM	QEQ	EQEQ	QTPIE	HI	DDEC	Bader	REPEAT
O1	-0.626819	-0.602213	-1.292750	-0.078782	-1.315479	-1.486953	-1.601375	-0.680927
O2	-0.410271	-0.600758	-1.251875	-0.078708	-1.312046	-1.032179	-1.603575	-0.627512
O3	-0.357182	-0.618917	-1.283000	-0.076647	-1.302735	-1.261086	-1.604200	-0.662972
O4	-0.644525	-0.614316	-1.300750	-0.082713	-1.358971	-0.963099	-1.622175	-0.791093
O5	-0.665670	-0.618956	-1.165250	-0.090407	-1.316895	-1.558876	-1.602700	-0.598297
O6	-0.636307	-0.612350	-1.091500	-0.084180	-1.298766	-2.505161	-1.596000	-0.529893
O7	-0.430128	-0.623695	-1.245750	-0.086931	-1.334722	-2.028943	-1.609550	-0.686679
O8	-0.358864	-0.622786	-1.297500	-0.078417	-1.309911	-1.191483	-1.606100	-0.647270
T1	1.021869	1.228825	2.585250	0.155990	2.636221	2.436892	3.214575	1.389041
T2	1.052123	1.206550	2.416500	0.165583	2.648767	3.033366	3.219200	1.192363
T3	1.031077	1.232563	logout	0.162416	2.627983	2.972018	3.200900	1.339323
T4	0.542332	0.602631	1.095500	0.092999	2.643612	3.638845	1.600450	1.269468

Table 17: A comparison of the partial charges determined from several methodologies for the zeolite FER. The 'site' is the atom label used in the crystal structure for the zeolite available from the IZA database.

Site	EEM	QEQ	EQEQ	QTPIE	HI	DDEC	Bader	REPEAT
O7	-0.800233	-0.607942	-1.011167	-0.800233	-1.315584	-1.071123	-1.529879	-0.746014
O8	-0.799119	-0.609628	-0.809667	-0.799119	-1.313565	-1.126416	-1.502003	-0.746466
O9	-0.804036	-0.611518	-0.812667	-0.804036	-1.314575	-1.106410	-1.522235	-0.735360
O10	-0.800087	-0.611079	-0.912583	-0.800087	-1.317266	-1.433493	-1.418073	-0.751676
O11	-0.801034	-0.610488	-0.912417	-0.801034	-1.317393	-1.279381	-1.480640	-0.745393
O12	-0.802092	-0.609877	-1.033667	-0.802092	-1.315439	-1.316168	-1.464198	-0.745712
O13	-0.796189	-0.593375	-1.004500	-0.796189	-1.324756	-1.109097	-1.554658	-0.776628
O14	-0.802869	-0.609426	-0.786667	-0.802869	-1.315096	-1.148241	-1.512375	-0.741400
O15	-0.799851	-0.607298	-1.051667	-0.799851	-1.315095	-1.105570	-1.512810	-0.746829
O16	-0.793458	-0.619191	-1.011500	-0.793458	-1.301840	-1.192040	-1.567725	-0.692359
O17	-0.799135	-0.608495	-0.928833	-0.799135	-1.314941	-1.534378	-1.399555	-0.742715
O18	-0.799291	-0.609971	-0.806667	-0.799291	-1.315094	-1.168078	-1.490616	-0.746144
O19	-0.800351	-0.607240	-1.045667	-0.800351	-1.315347	-1.029132	-1.551902	-0.743365
O20	-0.799661	-0.606381	-1.018667	-0.799661	-1.314549	-1.030072	-1.564689	-0.737718
O21	-0.803879	-0.607001	-0.557833	-0.803879	-1.315232	-1.085435	-1.533765	-0.733250
T1	1.601558	1.216094	2.053167	1.601558	2.629702	2.267835	3.055671	1.486183
T2	1.601423	1.216486	2.124917	1.601423	2.630037	2.483047	2.965696	1.488937
T3	1.595921	1.218994	2.039583	1.595921	2.631268	2.477671	3.024247	1.488777
T4	1.609286	1.218606	1.051833	1.609286	2.630560	2.236659	3.044655	1.473546
T5	1.596896	1.217421	1.592917	1.596896	2.629671	2.688210	2.883251	1.491086
T6	1.605616	1.221677	1.605333	1.605616	2.631360	2.376507	3.023452	1.474412

Table 18: A comparison of the partial charges determined from several methodologies for the zeolite FRA. The 'site' is the atom label used in the crystal structure for the zeolite available from the IZA database.

Site	EEM	QEQ	EQEQ	QTPIE	HI	DDEC	Bader	REPEAT
O1	-0.674470	-0.636471	-1.127000	-0.081324	-1.328522	-1.016720	-1.549865	-0.666627
O2	-0.627306	-0.604671	-0.898250	-0.074050	-1.286273	-1.505422	-1.367585	-0.562349
O3	-0.727100	-0.633104	-1.115417	-0.080061	-1.321060	-0.789817	-1.601146	-0.651736
O3	-0.609323	-0.614682	-1.079750	-0.075376	-1.289664	-0.979492	-1.512189	-0.581419
T1	1.319100	1.244464	2.110208	0.155405	2.612494	2.145726	3.019901	1.231065

Table 19: A comparison of the partial charges determined from several methodologies for the zeolite GME. The 'site' is the atom label used in the crystal structure for the zeolite available from the IZA database.

Site	EEM	QEQ	EQEQ	QTPIE	HI	DDEC	Bader	REPEAT
O1	-0.806592	-0.624963	-1.136750	-0.149615	-1.290155	-1.373616	-1.596700	-0.780510
O2	-0.806303	-0.627360	-1.142000	-0.150252	-1.286162	-1.210106	-1.597750	-0.772845
O3	-0.857176	-0.659744	-1.174500	-0.164878	-1.341587	-1.118661	-1.598500	-0.912733
O4	-0.802110	-0.619881	-1.151250	-0.146795	-1.288558	-0.750734	-1.596900	-0.745055
O5	-0.818989	-0.630258	-1.159500	-0.155840	-1.301191	-1.266483	-1.603950	-0.781634
O6	-0.793298	-0.609987	-1.143500	-0.143294	-1.287512	-1.690020	-1.601800	-0.707904
O7	-0.822984	-0.638211	-1.167750	-0.160125	-1.306152	-1.006685	-1.604100	-0.825717
O8	-0.809289	-0.630076	-1.071500	-0.160824	-1.293452	-1.256398	-1.604050	-0.782043
O9	-0.853128	-0.657004	-1.191750	-0.166154	-1.339474	-1.558453	-1.616700	-0.937074
O10	-0.794321	-0.611933	-1.021500	-0.143487	-1.280939	-1.404347	-1.602700	-0.718643
T1	1.630488	1.263494	2.314750	0.306991	2.601044	2.154207	3.199400	1.622132
T2	1.645777	1.274913	2.359750	0.298955	2.606776	2.374067	3.205900	1.530043
T3	1.632637	1.260654	2.259750	0.331510	2.607678	2.583296	3.210500	1.666255
T4	1.628247	1.254486	2.220250	0.297565	2.597266	2.789221	3.203800	1.585066

Table 20: A comparison of the partial charges determined from several methodologies for the zeolite GON. The 'site' is the atom label used in the crystal structure for the zeolite available from the IZA database.

Site	EEM	QEQ	EQEQ	QTPIE	HI	DDEC	Bader	REPEAT
O1	-0.836213	-0.633041	-1.284000	-0.158395	-1.310574	-2.096471	-1.597500	-0.608861
O2	-0.877801	-0.671574	-1.367000	-0.174161	-1.337503	-1.589057	-1.622500	-0.742519
O3	-0.806319	-0.614314	-1.223500	-0.146217	-1.283771	-0.923911	-1.593300	-0.598529
O4	-0.842586	-0.648969	-1.318000	-0.161235	-1.316504	-0.956717	-1.612100	-0.627809
O5	-0.798089	-0.613065	-1.185000	-0.143117	-1.269197	-0.764177	-1.594800	-0.580677
O6	-0.849197	-0.649707	-1.276000	-0.159550	-1.318931	-1.347797	-1.615900	-0.686673
O7	-0.842938	-0.645613	-1.252000	-0.154843	-1.310096	-1.737443	-1.604900	-0.704668
O8	-0.807000	-0.623872	-1.183000	-0.139454	-1.278993	-0.892910	-1.602400	-0.643499
O9	-0.835558	-0.637933	-1.221000	-0.149427	-1.305593	-1.149553	-1.596000	-0.664290
O10	-0.811223	-0.624516	-1.196000	-0.141595	-1.283251	-1.609953	-1.606300	-0.607446
T1	1.658680	1.285051	2.424000	0.289400	2.590611	1.903951	3.201100	1.286516
T2	1.656914	1.252425	2.600000	0.321985	2.611905	2.808414	3.213300	1.250618
T3	1.652809	1.267412	2.490000	0.313096	2.593864	2.946167	3.201700	1.278912
T4	1.648118	1.260333	2.413000	0.285240	2.589193	2.657695	3.201200	1.316701

Table 21: A comparison of the partial charges determined from several methodologies for the zeolite IFR. The 'site' is the atom label used in the crystal structure for the zeolite available from the IZA database.

Site	EEM	QEQ	EQEQ	QTPIE	HI	DDEC	Bader	REPEAT
O1	-0.855146	-0.634579	-1.271750	-0.042026	-1.318414	-1.507780	-1.608300	-0.680463
O2	-0.860894	-0.635100	-1.286000	-0.042497	-1.325956	-1.631474	-1.612100	-0.680362
O3	-0.826300	-0.613118	-1.272500	-0.039707	-1.299623	-2.052288	-1.600900	-0.632664
O4	-0.813431	-0.604849	-1.255250	-0.038980	-1.288820	-1.198531	-1.596100	-0.597249
O5	-0.821672	-0.608585	-1.282500	-0.039108	-1.289672	-2.122618	-1.597500	-0.658721
O6	-0.853707	-0.629505	-1.349500	-0.043158	-1.325215	-2.200898	-1.605100	-0.709929
O7	-0.850116	-0.641491	-1.323750	-0.045259	-1.318208	-1.616755	-1.597700	-0.732922
O8	-0.833885	-0.623525	-1.326000	-0.042835	-1.301700	-1.081793	-1.597800	-0.694741
O9	-0.882463	-0.653425	-1.411500	-0.047651	-1.352657	-1.783911	-1.614400	-0.929610
O10	-0.826462	-0.621648	-1.311000	-0.043404	-1.300335	-1.789386	-1.607800	-0.752890
O11	-0.828869	-0.618120	-1.315250	-0.041744	-1.304521	-1.729628	-1.600200	-0.729359
O12	-0.859323	-0.640119	-1.347000	-0.045799	-1.328982	-1.499731	-1.602000	-0.767892
O13	-0.843860	-0.633040	-1.362000	-0.044660	-1.314689	-0.984712	-1.606500	-0.794633
O14	-0.819412	-0.623778	-1.281000	-0.043765	-1.291916	-1.540518	-1.605700	-0.814816
O15	-0.837093	-0.643565	-1.306500	-0.047017	-1.297309	-1.207850	-1.594500	-0.911140
O16	-0.847188	-0.642809	-1.342250	-0.046626	-1.309661	-1.787291	-1.602200	-0.788826
O17	-0.855833	-0.652648	-1.317500	-0.048569	-1.315927	-1.666947	-1.604300	-0.851568
O18	-0.629591	-0.473419	-0.991250	-0.034824	-1.305943	-1.129374	-1.194375	-0.824959
T1	1.471757	1.090232	2.211625	0.070723	2.618538	3.153977	2.808838	1.274281
T2	1.694310	1.239046	2.623000	0.079610	2.627396	4.000000	3.211000	1.389851
T3	1.693471	1.258812	2.721500	0.090344	2.631680	3.653772	3.207900	1.507361
T4	1.690799	1.247591	2.627000	0.081516	2.622497	2.780518	3.213500	1.376396
T5	1.696130	1.254697	2.732250	0.087990	2.641971	2.835402	3.217600	1.640209
T6	1.670891	1.269905	2.677750	0.097506	2.617303	3.052882	3.186600	1.594712
T7	1.643515	1.296321	2.490250	0.094215	2.595681	3.063795	3.194500	1.840110
T8	1.647732	1.277499	2.606500	0.189243	2.598344	2.979120	3.181900	1.457939
T9	1.673498	1.284727	2.635500	0.090380	2.607265	3.081792	3.190300	1.645860

Table 22: A comparison of the partial charges determined from several methodologies for the zeolite IHW. The 'site' is the atom label used in the crystal structure for the zeolite available from the IZA database.

Site	EEM	QEQ	EQEQ	QTPIE	HI	DDEC	Bader	REPEAT
O6	-0.876587	-0.659578	-1.028375	-0.037640	-1.343420	-1.177388	-1.597800	-0.742134
O7	-0.827648	-0.628108	-0.811250	-0.034208	-1.296780	-1.236120	-1.611000	-0.635370
O8	-0.822043	-0.622979	-0.799875	-0.033077	-1.295282	-1.273783	-1.601800	-0.615404
O9	-0.796620	-0.598910	-1.058875	-0.031595	-1.275668	-1.710674	-1.594100	-0.591040
O10	-0.840561	-0.633506	-1.201313	-0.037095	-1.312037	-1.499378	-1.597400	-0.693801
O11	-0.842142	-0.633747	-1.259688	-0.037105	-1.313566	-1.267159	-1.599400	-0.693590
O12	-0.796518	-0.595531	-1.177938	-0.031334	-1.274766	-1.557330	-1.598000	-0.584894
O13	-0.840168	-0.640648	-1.010500	-0.039834	-1.325854	-0.993139	-1.599650	-0.804008
O14	-0.857545	-0.613914	-1.186250	-0.039668	-1.331224	-1.281713	-1.620300	-0.873615
O15	-0.856987	-0.613928	-1.305500	-0.039645	-1.331614	-1.061919	-1.586600	-0.871575
O16	-0.841375	-0.640342	-1.306500	-0.039749	-1.326142	-0.984042	-1.598750	-0.787648
O17	-0.822010	-0.618789	-1.228375	-0.032687	-1.296402	-1.095358	-1.598800	-0.597459
O18	-0.880037	-0.658649	-1.301875	-0.037389	-1.346709	-1.025409	-1.592050	-0.730648
O19	-0.832808	-0.632694	-1.242875	-0.034540	-1.300899	-1.082816	-1.609100	-0.625098
T1	1.581295	1.178617	2.259438	0.061788	2.617889	3.021761	3.007406	1.323293
T2	1.647297	1.245239	1.785438	0.067349	2.599725	2.777407	3.195900	1.271711
T3	1.651776	1.241027	2.461750	0.066874	2.603398	2.438582	3.194400	1.246986
T4	1.669252	1.257471	2.273375	0.081632	2.621583	2.431965	3.198600	1.536402
T5	1.670026	1.254212	2.605625	0.081351	2.623359	2.212898	3.195900	1.520805

Table 23: A comparison of the partial charges determined from several methodologies for the zeolite ISV. The 'site' is the atom label used in the crystal structure for the zeolite available from the IZA database.

Site	EEM	QEQ	EQEQ	QTPIE	HI	DDEC	Bader	REPEAT
O1	-0.804360	-0.629845	-1.102625	-0.069579	-1.307030	-1.465980	-1.607900	-0.672227
O2	-0.772041	-0.603466	-1.055500	-0.061864	-1.270730	-0.925862	-1.594800	-0.654613
O3	-0.777290	-0.607813	-1.070250	-0.065507	-1.274111	-1.498661	-1.585500	-0.630388
O4	-0.792425	-0.623051	-1.075000	-0.065971	-1.292542	-1.614589	-1.601800	-0.667748
O5	-0.824864	-0.645795	-1.062500	-0.072118	-1.319198	-1.546438	-1.606800	-0.790335
O6	-0.782461	-0.612800	-1.056250	-0.064175	-1.286237	-1.630242	-1.587400	-0.630168
O7	-0.779124	-0.616873	-1.046500	-0.066218	-1.274570	-1.165389	-1.594500	-0.659037
O8	-0.802346	-0.634199	-1.087250	-0.071542	-1.299570	-1.763439	-1.604100	-0.674576
O9	-0.833264	-0.654838	-1.115000	-0.075453	-1.330568	-1.759986	-1.615150	-0.786921
O10	-0.761044	-0.604142	-0.953500	-0.065280	-1.259864	-1.549491	-1.587800	-0.599381
T1	1.604727	1.254878	2.183250	0.128365	2.592228	2.678139	3.200600	1.354370
T2	1.592283	1.254382	2.126000	0.133585	2.588086	2.944266	3.197900	1.367032
T3	1.585843	1.242933	2.197750	0.145473	2.588863	3.441581	3.198600	1.345032
T4	1.576159	1.247527	2.053500	0.138564	2.577805	3.030074	3.200300	1.361711

Table 24: A comparison of the partial charges determined from several methodologies for the zeolite ITE. The 'site' is the atom label used in the crystal structure for the zeolite available from the IZA database.

Site	EEM	QEQ	EQEQ	QTPIE	HI	DDEC	Bader	REPEAT
O1	-0.844280	-0.630417	-1.092250	-0.085635	-1.315367	-1.726010	-1.603000	-0.640004
O2	-0.845964	-0.645346	-1.606500	-0.089315	-1.312235	-1.575763	-1.614000	-0.771678
O3	-0.817602	-0.614788	-1.243500	-0.079827	-1.288043	-1.409726	-1.598700	-0.654341
O4	-0.867853	-0.640333	-1.083000	-0.091259	-1.336293	-1.449644	-1.607700	-0.732353
O5	-0.838955	-0.639883	-1.084000	-0.082547	-1.305378	-1.010796	-1.619550	-0.581985
O6	-0.835992	-0.626715	-0.930000	-0.079008	-1.313566	-1.003546	-1.592750	-0.550907
O7	-0.822984	-0.623207	-1.285500	-0.082639	-1.304397	-1.075382	-1.604700	-0.678993
O8	-0.601271	-0.452286	-0.725500	-0.057405	-1.277994	-1.318417	-1.199025	-0.558128
O9	-0.814931	-0.606472	-1.225000	-0.077033	-1.290347	-1.243713	-1.600200	-0.640662
O10	-0.857063	-0.646835	-1.084000	-0.086342	-1.322430	-1.322114	-1.607800	-0.619166
O11	-0.864147	-0.645238	-1.424000	-0.090449	-1.325989	-1.043533	-1.607800	-0.777623
O12	-0.599136	-0.450672	-0.804250	-0.056034	-1.274798	-1.083320	-1.198050	-0.535650
O13	-0.826840	-0.619446	-1.225000	-0.084912	-1.295897	-1.265091	-1.595900	-0.675998
O14	-0.819696	-0.624956	-0.840000	-0.079269	-1.291396	-1.052214	-1.602900	-0.583502
O15	-0.847917	-0.619880	-1.219500	-0.084652	-1.326152	-1.172568	-1.605700	-0.630067
O16	-0.857661	-0.629738	-1.312500	-0.087169	-1.331872	-1.998385	-1.594700	-0.703286
O17	-0.862760	-0.648357	-1.181000	-0.096843	-1.325436	-0.999955	-1.610500	-0.731035
O18	-0.872284	-0.641825	-1.245000	-0.094459	-1.341372	-1.247677	-1.599000	-0.725841
O19	-0.848706	-0.643331	-1.021500	-0.085447	-1.319490	-1.348671	-1.616550	-0.597289
O20	-0.858862	-0.639702	-1.322000	-0.085354	-1.323555	-1.078801	-1.615000	-0.707967
O21	-0.884459	-0.665087	-1.321000	-0.096914	-1.338578	-1.228236	-1.620100	-0.790705
T1	1.704577	1.253971	2.497000	0.179419	2.640039	2.445900	3.196900	1.340887
T2	1.642358	1.250006	1.713500	0.162548	2.594757	2.638611	3.209100	1.161536
T3	1.697231	1.263106	2.521500	0.160493	2.628241	2.424341	3.217100	1.326781
T4	1.688574	1.234610	2.013000	0.195825	2.637506	2.396944	3.197500	1.429622
T5	1.648643	1.241359	2.055500	0.157128	2.602739	2.244246	3.205000	1.119171
T6	1.695598	1.264218	2.199500	0.158680	2.625423	2.304692	3.214600	1.252916
T7	1.664099	1.268359	2.846000	0.174743	2.606645	2.755690	3.210600	1.454783
T8	1.689405	1.252326	2.640500	0.161380	2.625777	2.719109	3.206100	1.365662
T9	1.681762	1.240074	2.706000	0.183142	2.631159	3.871303	3.203100	1.357149

Table 25: A comparison of the partial charges determined from several methodologies for the zeolite ITH. The 'site' is the atom label used in the crystal structure for the zeolite available from the IZA database.

Site	EEM	QEQ	EQEQ	QTPIE	HI	DDEC	Bader	REPEAT
O1	-0.840574	-0.611792	-0.835500	-0.180065	-1.315152	-1.236348	-1.604300	-0.741553
O2	-0.813600	-0.608390	-1.092000	-0.179054	-1.288585	-1.806717	-1.597600	-0.590049
O3	-0.820837	-0.614291	-1.097500	-0.184146	-1.293832	-1.367206	-1.596700	-0.609744
O4	-0.846110	-0.608623	-0.836000	-0.180400	-1.323135	-1.441871	-1.607200	-0.717924
O5	-0.859922	-0.643163	-1.226500	-0.201695	-1.327026	-1.577672	-1.611200	-0.625795
O6	-0.842261	-0.636955	-1.193500	-0.197349	-1.309582	-0.869510	-1.608600	-0.602452
O7	-0.831820	-0.631860	-1.197500	-0.191537	-1.301028	-1.228051	-1.607500	-0.550541
O8	-0.831311	-0.634294	-1.175000	-0.195710	-1.299568	-0.913098	-1.604900	-0.571226
T1	1.723219	1.263875	1.951000	0.367562	2.643608	2.889204	3.210800	1.409604
T2	1.645847	1.240710	2.356500	0.378506	2.597631	2.824515	3.206600	1.137202
T3	1.642460	1.241498	2.324000	0.390033	2.596262	2.317070	3.208500	1.171857

Table 26: A comparison of the partial charges determined from several methodologies for the zeolite ITW. The 'site' is the atom label used in the crystal structure for the zeolite available from the IZA database.

Site	EEM	QEQ	EQEQ	QTPIE	HI	DDEC	Bader	REPEAT
O1	-0.839118	-0.630172	-1.261750	-0.085013	-1.313027	-1.741146	-1.603600	-0.618896
O2	-0.843989	-0.614703	-1.293000	-0.086636	-1.323564	-1.444606	-1.593550	-0.673473
O3	-0.866585	-0.652382	-1.284000	-0.093278	-1.322655	-1.441895	-1.619700	-0.713836
O4	-0.827555	-0.627248	-1.186000	-0.077589	-1.301861	-1.261527	-1.600200	-0.586175
O5	-0.860975	-0.648243	-1.185500	-0.084670	-1.327446	-2.202023	-1.616700	-0.633000
O6	-0.790221	-0.600611	-1.155000	-0.073616	-1.266700	-1.679767	-1.592000	-0.536732
O7	-0.838628	-0.635739	-1.202000	-0.080632	-1.307157	-1.760690	-1.605050	-0.581273
O8	-0.841823	-0.636281	-1.232000	-0.084407	-1.311585	-1.002726	-1.602800	-0.638124
O9	-0.812811	-0.623605	-1.205000	-0.079325	-1.286171	-1.031749	-1.601050	-0.620145
O10	-0.806493	-0.625802	-1.207500	-0.081738	-1.281955	-1.310079	-1.603000	-0.586244
O11	-0.869632	-0.655646	-1.285000	-0.091112	-1.334987	-1.062766	-1.614150	-0.716356
T1	1.648874	1.245486	2.336500	0.155545	2.598546	3.634355	3.205800	1.158010
T2	1.673079	1.263014	2.448000	0.157508	2.608291	2.619011	3.207300	1.228301
T3	1.645207	1.270828	2.460500	0.171142	2.594310	2.281789	3.207400	1.273614
T4	1.692198	1.248900	2.572000	0.182027	2.628265	2.880800	3.203700	1.304648

Table 27: A comparison of the partial charges determined from several methodologies for the zeolite IWR. The 'site' is the atom label used in the crystal structure for the zeolite available from the IZA database.

Site	EEM	QEQ	EQEQ	QTPIE	HI	DDEC	Bader	REPEAT
O1	-0.842753	-0.625933	-0.836000	-0.087299	-1.315060	-0.988171	-1.610975	-0.613643
O2	-0.846730	-0.631021	-0.630375	-0.089280	-1.315597	-1.019592	-1.605050	-0.613353
O3	-0.791667	-0.588079	-0.805750	-0.079605	-1.273945	-1.075884	-1.602900	-0.499753
T1	1.663940	1.238026	1.451250	0.172733	2.609642	2.051619	3.212000	1.170051

Table 28: A comparison of the partial charges determined from several methodologies for the zeolite LTA. The 'site' is the atom label used in the crystal structure for the zeolite available from the IZA database.

Site	*EEM*	*QEQ*	*EQEQ*	*QTPIE*	*HI*	*DDEC*	*Bader*	*REPEAT*
O1	-0.843265	-0.623882	-0.641750	-0.048484	-1.315509	-1.493043	-1.608250	-0.679259
O2	-0.881753	-0.650377	-0.826625	-0.053115	-1.348495	-1.285919	-1.617425	-0.738859
O3	-0.828209	-0.616709	-0.833375	-0.047765	-1.296798	-1.584613	-1.593600	-0.620660
O4	-0.864767	-0.634869	-0.846625	-0.050175	-1.336163	-1.940847	-1.611425	-0.648694
O5	-0.813394	-0.609886	-1.025000	-0.045011	-1.287860	-1.776980	-1.599775	-0.577454
O6	-0.761917	-0.572966	-0.715250	-0.046727	-1.330011	-1.782576	-1.414488	-0.694826
O7	-0.826319	-0.618024	-1.046500	-0.046684	-1.297375	-2.193106	-1.604050	-0.650133
O8	-0.831974	-0.616434	-1.004625	-0.046636	-1.306058	-1.542452	-1.604700	-0.605671
O9	-0.809412	-0.598926	-0.779250	-0.044035	-1.281712	-1.387504	-1.587975	-0.572957
O10	-0.866089	-0.635508	-1.050500	-0.049292	-1.337218	-1.369662	-1.613475	-0.641601
O11	-0.823106	-0.613450	-0.741750	-0.047082	-1.291987	-1.504845	-1.600950	-0.595992
O12	-0.826323	-0.620063	-0.796500	-0.049435	-1.298638	-1.454432	-1.602600	-0.609375
O13	-0.820278	-0.622461	-0.620250	-0.050373	-1.290111	-2.217501	-1.601850	-0.615348
O14	-0.837859	-0.633702	-0.826250	-0.053697	-1.306608	-1.669240	-1.593875	-0.629637
O15	-0.838900	-0.620514	-0.437750	-0.046632	-1.309227	-2.120329	-1.607000	-0.711323
T1	1.699405	1.243302	1.192500	0.103246	2.642065	3.295909	3.209350	1.339780
T2	1.667732	1.256814	2.140000	0.093866	2.607773	3.554782	3.208950	1.284944
T3	1.695879	1.244356	2.001750	0.093418	2.633994	3.042785	3.209700	1.228833
T4	1.687707	1.248627	1.902750	0.096497	2.628893	2.969491	3.215475	1.271280
T5	1.663010	1.269781	1.288000	0.107195	2.605343	3.520813	3.206175	1.270592
T6	1.688653	1.255519	1.104500	0.092958	2.626607	3.479821	3.216250	1.410651
T7	1.692825	1.250891	2.087000	0.093732	2.633243	3.306192	3.215425	1.206681

Table 29: A comparison of the partial charges determined from several methodologies for the zeolite MEL. The 'site' is the atom label used in the crystal structure for the zeolite available from the IZA database.

Site	*EEM*	*QEQ*	*EQEQ*	*QTPIE*	*HI*	*DDEC*	*Bader*	*REPEAT*
O1	-0.812756	-0.612289	-1.256500	-0.023434	-1.289508	-0.813448	-1.592200	-0.629223
O2	-0.800286	-0.615808	-1.220750	-0.023331	-1.262405	-1.663786	-1.596600	-0.676732
O3	-0.830423	-0.628698	-1.301250	-0.025087	-1.302665	-1.268555	-1.605600	-0.699564
O4	-0.876707	-0.646556	-1.379750	-0.027345	-1.349651	-1.853311	-1.617100	-0.890848
O5	-0.806643	-0.621805	-1.241500	-0.024484	-1.273010	-1.121451	-1.579400	-0.685823
O6	-0.854529	-0.644379	-1.298000	-0.026966	-1.325058	-0.965921	-1.605800	-0.730051
O7	-0.839699	-0.631952	-1.282500	-0.025378	-1.308551	-1.377047	-1.605200	-0.717836
O8	-0.819606	-0.627006	-1.285750	-0.025380	-1.292602	-1.369556	-1.604100	-0.728404
O9	-0.854475	-0.649432	-1.366000	-0.027600	-1.323218	-0.945420	-1.600400	-0.866262
O10	-0.866223	-0.644069	-1.347500	-0.026720	-1.338361	-1.400093	-1.613100	-0.847244
O11	-0.839733	-0.635648	-1.338500	-0.026383	-1.310795	-1.432549	-1.609400	-0.767188
O12	-0.849428	-0.639501	-1.349750	-0.026689	-1.319395	-1.370706	-1.603700	-0.729016
O13	-0.812204	-0.609569	-1.269750	-0.023469	-1.288463	-1.330262	-1.598300	-0.594329
O14	-0.845021	-0.633968	-1.318500	-0.025698	-1.309831	-0.789448	-1.606400	-0.629697
O15	-0.828525	-0.627594	-1.287750	-0.024588	-1.304375	-1.190833	-1.605400	-0.726754
O16	-0.827681	-0.627408	-1.301000	-0.025263	-1.302036	-1.084822	-1.606900	-0.662392
O17	-0.830414	-0.629221	-1.290250	-0.025985	-1.302076	-1.764955	-1.596100	-0.703073
O18	-0.814873	-0.617956	-1.269000	-0.024557	-1.286424	-1.082974	-1.601900	-0.650095
O19	-0.815776	-0.631158	-1.263250	-0.025523	-1.278495	-1.231286	-1.595300	-0.659701
O20	-0.861544	-0.650261	-1.335250	-0.028015	-1.321613	-1.428941	-1.613000	-0.792421
O21	-0.815211	-0.617878	-1.255500	-0.024055	-1.299911	-0.953060	-1.603700	-0.638186
O22	-0.868550	-0.643586	-1.348250	-0.027174	-1.331272	-0.940178	-1.603400	-0.763142
O23	-0.831259	-0.630038	-1.324500	-0.025954	-1.310953	-1.120396	-1.604400	-0.666548
O24	-0.857511	-0.642641	-1.349000	-0.027195	-1.321742	-0.946162	-1.608200	-0.711934
O25	-0.828464	-0.626451	-1.300750	-0.025654	-1.302269	-1.285784	-1.600500	-0.688055
O26	-0.820475	-0.631643	-1.284000	-0.025934	-1.291455	-0.896089	-1.604400	-0.723836
T1	1.675872	1.261921	2.574000	0.047788	2.125496	2.506777	3.202900	1.471130
T2	1.650100	1.266461	2.464000	0.049084	2.591465	2.767898	3.193100	1.415903
T3	1.666638	1.273531	2.619000	0.052428	2.607546	2.377791	3.209900	1.570886
T4	1.682993	1.264025	2.753000	0.057283	2.631453	3.013863	3.205300	1.673518
T5	1.685525	1.256231	2.610500	0.048122	2.619111	2.221662	3.206600	1.236660
T6	1.686442	1.258634	2.633750	0.049689	2.621685	2.400224	3.213600	1.457912
T7	1.681602	1.273166	2.607250	0.049716	2.614923	2.503852	3.206400	1.406183
T8	1.650026	1.273572	2.573500	0.056042	2.598744	2.781100	3.203400	1.401748
T9	1.664775	1.254047	2.551750	0.048886	2.602924	2.248624	3.210300	1.391082
T10	1.676310	1.252315	2.655000	0.053513	2.617991	2.206401	3.204500	1.397538
T11	1.679095	1.261924	2.656000	0.052648	2.617950	2.059066	3.208900	1.319640
T12	1.667726	1.271929	2.600250	0.052412	2.609946	2.513511	3.208200	1.496823

Table 30: A comparison of the partial charges determined from several methodologies for the zeolite MFI. The 'site' is the atom label used in the crystal structure for the zeolite available from the IZA database.

Site	EEM	QEQ	EQEQ	QTPIE	HI	DDEC	Bader	REPEAT
O1	-0.838341	-0.636638	-1.264000	-0.108183	-1.303202	-1.081445	-1.605300	-0.781725
O2	-0.853597	-0.647222	-1.379500	-0.112860	-1.311945	-1.096359	-1.605900	-0.639862
O3	-0.843794	-0.616353	-1.315000	-0.098305	-1.316512	-0.838499	-1.614350	-0.564250
O4	-0.853919	-0.637194	-1.288000	-0.107383	-1.323272	-1.056646	-1.615300	-0.770893
O5	-0.856629	-0.637821	-1.323250	-0.111376	-1.319481	-1.698191	-1.601750	-0.691246
O6	-0.857910	-0.634965	-1.357125	-0.107887	-1.325573	-1.391480	-1.611875	-0.631223
O7	-0.836775	-0.611291	-1.274750	-0.096572	-1.310967	-1.679766	-1.602000	-0.570677
O8	-0.834741	-0.623153	-1.288125	-0.100829	-1.303321	-0.857429	-1.603150	-0.648135
O9	-0.856469	-0.652877	-1.256500	-0.110656	-1.317065	-1.007673	-1.612725	-0.752638
O10	-0.812865	-0.623274	-1.229875	-0.101704	-1.281293	-1.399876	-1.596175	-0.673685
T1	1.714197	1.248681	2.661250	0.196312	2.642374	2.344290	3.221925	1.200938
T2	1.665538	1.260810	2.503375	0.209716	2.605227	2.235656	3.212650	1.418501
T3	1.660901	1.288138	2.492000	0.215183	2.593384	2.646563	3.199750	1.448882
T4	1.684215	1.253133	2.708250	0.228415	2.629561	2.860793	3.205100	1.278824

Table 31: A comparison of the partial charges determined from several methodologies for the zeolite MRE. The 'site' is the atom label used in the crystal structure for the zeolite available from the IZA database.

Site	EEM	QEQ	EQEQ	QTPIE	HI	DDEC	Bader	REPEAT
O1	-0.848700	-0.631056	-1.327250	-0.119933	-1.323579	-1.505834	-1.613000	-0.628307
O2	-0.871171	-0.675947	-1.390000	-0.141823	-1.336796	-1.359423	-1.616600	-0.740782
O3	-0.834201	-0.630985	-1.351000	-0.130839	-1.313621	-1.612016	-1.606800	-0.642260
O4	-0.859589	-0.646338	-1.347500	-0.121113	-1.328096	-1.353860	-1.611300	-0.729885
O5	-0.824927	-0.602102	-1.051000	-0.102464	-1.299637	-1.665530	-1.602000	-0.627267
O6	-0.856612	-0.650917	-1.330500	-0.126715	-1.331297	-2.256836	-1.616400	-0.718222
O7	-0.830104	-0.619570	-1.204500	-0.105062	-1.300827	-1.103725	-1.602100	-0.614030
O8	-0.824618	-0.622139	-1.152500	-0.102402	-1.292809	-0.409279	-1.601900	-0.674061
O9	-0.861489	-0.641611	-1.042000	-0.113679	-1.325189	-1.308033	-1.613900	-0.708891
O10	-0.822645	-0.613500	-1.193500	-0.105622	-1.293847	-0.830946	-1.598800	-0.634168
O11	-0.803633	-0.605663	-1.270500	-0.130402	-1.278853	-1.548757	-1.588300	-0.606858
O12	-0.844122	-0.657477	-1.333500	-0.141959	-1.315498	-1.515724	-1.611900	-0.751617
O13	-0.847669	-0.671665	-1.145000	-0.143876	-1.318010	-1.129832	-1.610200	-0.673192
T1	1.250867	0.948155	1.619250	0.157981	2.605646	1.921050	2.405925	1.327315
T2	1.690302	1.254723	2.763500	0.253511	2.640442	3.030839	3.217000	1.364987
T3	1.719066	1.228096	2.465500	0.207662	2.647849	3.102625	3.221900	1.293994
T4	1.678293	1.325455	2.695500	0.283134	2.627308	3.623639	3.214300	1.378594
T5	1.653236	1.304781	2.504500	0.289336	2.609643	2.779376	3.210800	1.368627
T6	1.682819	1.245896	2.525000	0.220786	2.619989	1.771859	3.214300	1.348636

Table 32: A comparison of the partial charges determined from several methodologies for the zeolite MTF. The 'site' is the atom label used in the crystal structure for the zeolite available from the IZA database.

Site	EEM	QEQ	EQEQ	QTPIE	HI	DDEC	Bader	REPEAT
O1	-0.864901	-0.604205	-1.291667	-0.061404	-1.337452	-1.613699	-1.610275	-0.671229
O2	-0.852376	-0.598225	-1.140500	-0.059367	-1.326329	-1.279922	-1.607425	-0.625904
O3	-0.878547	-0.619615	-1.263000	-0.062411	-1.336374	-1.291006	-1.613500	-0.623130
O4	-0.869889	-0.607163	-1.330375	-0.062973	-1.340560	-1.335637	-1.598450	-0.717798
T1	1.724488	1.211406	2.398375	0.120560	2.667415	2.728300	3.221725	1.277009
T2	1.734395	1.210106	2.667375	0.125594	2.666994	3.098054	3.208550	1.355356
T3	1.726723	1.198218	2.635500	0.126521	2.663049	2.680223	3.192100	1.430032

Table 33: A comparison of the partial charges determined from several methodologies for the zeolite MTN. The 'site' is the atom label used in the crystal structure for the zeolite available from the IZA database.

Site	EEM	QEQ	EQEQ	QTPIE	HI	DDEC	Bader	REPEAT
O1	-0.837643	-0.607387	-1.063250	-0.090625	-1.309344	-1.018398	-1.603300	-0.595392
O2	-0.872476	-0.628345	-0.886750	-0.097267	-1.343401	-1.137745	-1.609000	-0.664396
O3	-0.840610	-0.611059	-1.068500	-0.092421	-1.312561	-1.087458	-1.609000	-0.616486
O4	-0.836915	-0.611925	-0.945000	-0.092670	-1.309204	-1.161684	-1.602500	-0.589599
O5	-0.870453	-0.630788	-1.144750	-0.102446	-1.341040	-1.047904	-1.609800	-0.702374
O6	-0.827124	-0.606823	-1.041250	-0.090916	-1.293338	-1.033541	-1.590100	-0.651659
O7	-0.869665	-0.633302	-1.013000	-0.102615	-1.340776	-1.201895	-1.612200	-0.747245
O8	-0.861298	-0.629084	-1.133250	-0.094480	-1.325985	-1.064819	-1.611000	-0.695423
O9	-0.848059	-0.615347	-1.084500	-0.094480	-1.323955	-1.024658	-1.613700	-0.633079
O10	-0.867742	-0.628453	-0.973250	-0.098555	-1.341630	-1.262210	-1.607000	-0.736174
T1	1.713204	1.234173	1.939500	0.186285	2.653769	2.223910	3.219400	1.260808
T2	1.705853	1.239517	2.060500	0.185741	2.644524	2.135728	3.211800	1.224855
T3	1.701563	1.233556	2.080000	0.189225	2.642312	2.231311	3.211700	1.357885
T4	1.706688	1.250073	2.176250	0.218295	2.655829	2.289642	3.209500	1.497421
T5	1.700744	1.242804	2.058750	0.189486	2.640486	2.217719	3.223200	1.236227
T6	1.725093	1.246933	2.048500	0.195410	2.665796	2.354869	3.210800	1.365363
T7	1.695933	1.248302	1.944500	0.186846	2.633045	2.256292	3.202400	1.417592

Table 34: A comparison of the partial charges determined from several methodologies for the zeolite MTT. The 'site' is the atom label used in the crystal structure for the zeolite available from the IZA database.

Site	EEM	QEQ	EQEQ	QTPIE	HI	DDEC	Bader	REPEAT
O1	-0.849199	-0.616404	-1.205000	-0.163043	-1.325883	-0.676248	-1.601350	-0.641245
O2	-0.837291	-0.623080	-1.198500	-0.167469	-1.311268	-1.182581	-1.611600	-0.666382
O3	-0.877484	-0.644385	-1.232000	-0.179441	-1.333312	-0.977803	-1.605800	-0.784285
O4	-0.826371	-0.613906	-1.135500	-0.159850	-1.297023	-1.448983	-1.603400	-0.566170
O5	-0.816799	-0.610858	-1.255500	-0.160522	-1.281168	-1.415957	-1.585300	-0.589910
O6	-0.877759	-0.637898	-1.376500	-0.184356	-1.347130	-1.203686	-1.614400	-0.820787
O7	-0.819422	-0.607468	-1.275000	-0.160418	-1.291057	-0.840995	-1.592300	-0.580517
O8	-0.869350	-0.632857	-1.357500	-0.181204	-1.343410	-1.078994	-1.625600	-0.678147
O9	-0.851427	-0.633906	-1.401000	-0.183147	-1.320284	-1.198774	-1.611300	-0.728462
O10	-0.846327	-0.625316	-1.340500	-0.171287	-1.319725	-0.976574	-1.604500	-0.526399
O11	-0.862290	-0.628504	-1.315000	-0.173797	-1.339514	-1.328559	-1.614100	-0.584433
T1	1.690363	1.220692	2.356000	0.331490	2.637172	2.037638	3.215200	1.377073
T2	1.681698	1.234244	2.165500	0.324515	2.624713	2.394601	3.201300	1.226610
T3	1.676303	1.258161	2.548000	0.336453	2.620329	2.392392	3.206900	1.364121
T4	1.691604	1.256155	2.565000	0.322933	2.627022	2.333719	3.217000	1.203818
T5	1.702706	1.271709	2.818000	0.398066	2.648471	2.285955	3.226000	1.648604
T6	1.699006	1.251021	2.741500	0.342669	2.635690	2.184563	3.213500	1.182245
T7	1.707128	1.253492	2.633000	0.338873	2.644723	2.530619	3.216000	1.125280

Table 35: A comparison of the partial charges determined from several methodologies for the zeolite MTW. The 'site' is the atom label used in the crystal structure for the zeolite available from the IZA database.

Site	*EEM*	*QEQ*	*EQEQ*	*QTPIE*	*HI*	*DDEC*	*Bader*	*REPEAT*
O1	-0.790895	-0.593532	-1.126000	-0.027279	-1.280475	-1.111715	-1.578700	-0.284796
O2	-0.833843	-0.635731	-1.227167	-0.031385	-1.310720	-1.681552	-1.600000	-0.587873
O3	-0.794107	-0.610009	-1.159292	-0.029453	-1.272090	-1.477424	-1.581617	-0.590175
O4	-0.872114	-0.668946	-1.346667	-0.037625	-1.337909	-1.763811	-1.612133	-0.698874
O5	-0.861233	-0.652418	-1.388500	-0.037239	-1.332827	-1.375796	-1.592200	-0.672322
O6	-0.857946	-0.631009	-1.301750	-0.033364	-1.335832	-1.005034	-1.592667	-0.666913
O7	-0.859944	-0.649304	-1.264500	-0.033329	-1.329857	-1.001765	-1.610967	-0.682066
O8	-0.868837	-0.643810	-1.370333	-0.034299	-1.329160	-1.466432	-1.610100	-0.711657
O9	-0.846644	-0.618428	-1.314083	-0.031451	-1.321357	-1.573025	-1.601567	-0.639914
O10	-0.834191	-0.611971	-1.324667	-0.030492	-1.304072	-1.577961	-1.599033	-0.670958
O11	-0.831718	-0.603448	-1.336333	-0.028460	-1.305594	-2.016514	-1.603300	-0.560485
O12	-0.859959	-0.622535	-1.436000	-0.029611	-1.327314	-1.339141	-1.598317	-0.618897
O13	-0.849377	-0.619100	-1.381333	-0.028896	-1.307094	-1.178213	-1.610567	-0.603327
T1	1.635292	1.270535	2.436500	0.062692	2.596112	3.378764	3.175567	1.287849
T2	1.719204	1.244694	2.720667	0.059546	2.646207	3.435430	3.213667	1.263272
T3	1.693895	1.225048	2.796167	0.057262	2.629415	2.954027	3.203333	1.190321
T4	1.667771	1.257411	2.393000	0.062048	2.614983	2.472439	3.194333	1.256426
T5	1.704724	1.241965	2.625083	0.067139	2.646182	2.763190	3.194167	1.324911
T6	1.666829	1.249534	2.422500	0.058382	2.615540	2.845413	3.202700	0.932278
T7	1.619070	1.263875	2.691000	0.083569	2.610079	2.983122	3.199300	1.279856
T8	1.689182	1.276679	2.706000	0.065888	2.627656	3.015911	3.199200	1.422358

Table 36: A comparison of the partial charges determined from several methodologies for the zeolite MWW. The 'site' is the atom label used in the crystal structure for the zeolite available from the IZA database.

Site	*EEM*	*QEQ*	*EQEQ*	*QTPIE*	*HI*	*DDEC*	*Bader*	*REPEAT*
O1	-0.857752	-0.618818	-1.343875	-0.101167	-1.327308	-1.369866	-1.609150	-0.676209
O2	-0.846183	-0.600735	-1.329500	-0.094923	-1.318217	-1.343443	-1.601475	-0.568621
O3	-0.842847	-0.594787	-1.339750	-0.094270	-1.319116	-1.060598	-1.609650	-0.586891
O4	-0.757459	-0.538898	-1.187125	-0.089121	-1.335045	-1.548463	-1.410613	-0.681239
O5	-0.864821	-0.613816	-1.211500	-0.103336	-1.330964	-1.394509	-1.607900	-0.686301
O6	-0.874883	-0.624679	-1.356250	-0.106613	-1.345186	-1.564625	-1.614650	-0.790984
O7	-0.869145	-0.621778	-1.356000	-0.100473	-1.332031	-1.389929	-1.614300	-0.583140
O8	-0.880481	-0.629840	-1.382000	-0.102451	-1.345532	-1.055091	-1.616300	-0.603715
O9	-0.835374	-0.610678	-1.289750	-0.099665	-1.300645	-1.923080	-1.601750	-0.704271
O10	-0.882478	-0.632250	-1.206000	-0.108200	-1.351881	-1.374096	-1.615100	-0.782013
T1	1.727427	1.223308	2.742125	0.192783	2.661475	2.740482	3.220200	1.244286
T2	1.297421	0.913172	2.001250	0.157455	2.666422	3.021278	2.414675	1.416120
T3	1.709944	1.221189	2.671750	0.195447	2.647841	2.476481	3.210100	1.138377
T4	1.698228	1.239423	2.537250	0.208297	2.649313	3.049589	3.219450	1.458622
T5	1.695698	1.250135	2.610500	0.208826	2.638266	3.300699	3.216500	1.520352

Table 37: A comparison of the partial charges determined from several methodologies for the zeolite NON. The 'site' is the atom label used in the crystal structure for the zeolite available from the IZA database.

Site	EEM	QEQ	EQEQ	QTPIE	HI	DDEC	Bader	REPEAT
O1	-0.853362	-0.641025	-1.267500	-0.132878	-1.326433	-1.849433	-1.607800	-0.681636
O2	-0.811640	-0.592673	-1.122500	-0.113262	-1.297132	-0.857595	-1.599400	-0.424240
O3	-0.820591	-0.620952	-1.201000	-0.123565	-1.288053	-1.389464	-1.593300	-0.649560
O4	-0.836791	-0.624147	-1.230750	-0.124716	-1.307286	-1.925440	-1.603700	-0.599563
O5	-0.878438	-0.635506	-1.289500	-0.138020	-1.356575	-1.656154	-1.610500	-0.843780
O6	-0.801737	-0.619876	-1.204500	-0.126950	-1.261059	-1.290418	-1.589700	-0.666033
O7	-0.857105	-0.642446	-1.276750	-0.136671	-1.323386	-1.514451	-1.610100	-0.714660
O8	-0.834162	-0.623293	-1.167000	-0.127119	-1.306779	-1.524386	-1.599900	-0.614775
O9	-0.812452	-0.617080	-1.211000	-0.123723	-1.286397	-1.786591	-1.603100	-0.598594
O10	-0.840731	-0.625151	-1.166000	-0.129893	-1.318958	-1.437099	-1.610200	-0.656338
T1	1.694996	1.247306	2.443500	0.237192	2.632902	2.726927	3.212600	1.135995
T2	1.660489	1.253421	2.523750	0.276681	2.608864	3.432070	3.202500	1.476154
T3	1.667413	1.253961	2.470500	0.254556	2.616137	3.616574	3.203700	1.266877
T4	1.659381	1.262970	2.426250	0.262152	2.601939	2.809005	3.201800	1.439809
T5	1.705365	1.239227	2.211500	0.255446	2.640565	2.648723	3.211600	1.237858

Table 38: A comparison of the partial charges determined from several methodologies for the zeolite RRO. The 'site' is the atom label used in the crystal structure for the zeolite available from the IZA database.

Site	EEM	QEQ	EQEQ	QTPIE	HI	DDEC	Bader	REPEAT
O1	-0.841554	-0.625491	-1.271250	-0.190201	-1.311914	-1.121425	-1.600300	-0.686080
O2	-0.852555	-0.633969	-1.304000	-0.198377	-1.320024	-1.142337	-1.610700	-0.716957
O3	-0.827210	-0.614554	-1.243500	-0.184601	-1.302685	-1.321338	-1.603300	-0.638933
O4	-0.862405	-0.642735	-1.316000	-0.203462	-1.326732	-1.058271	-1.605200	-0.724496
O5	-0.853731	-0.629434	-1.260500	-0.190881	-1.317322	-1.744066	-1.598700	-0.714854
O6	-0.833504	-0.612295	-1.230000	-0.177720	-1.307095	-1.098171	-1.594800	-0.670894
O7	-0.821019	-0.620814	-1.233500	-0.181080	-1.287606	-1.620371	-1.601900	-0.624686
O8	-0.827474	-0.612876	-1.132000	-0.178128	-1.295513	-2.230091	-1.605100	-0.663800
T1	1.671936	1.245950	2.561000	0.396450	2.617447	2.192095	3.203300	1.364818
T2	1.671222	1.244873	2.487500	0.364923	2.610263	2.669512	3.196400	1.333130
T3	1.694568	1.246149	2.449500	0.362555	2.625382	3.448927	3.208800	1.377782

Table 39: A comparison of the partial charges determined from several methodologies for the zeolite RTE. The 'site' is the atom label used in the crystal structure for the zeolite available from the IZA database.

Site	EEM	QEQ	EQEQ	QTPIE	HI	DDEC	Bader	REPEAT
O1	-0.854380	-0.629854	-1.254000	-0.129840	-1.322975	-1.479180	-1.610300	-0.683745
O2	-0.837180	-0.622934	-1.273500	-0.126961	-1.307406	-1.672850	-1.610500	-0.600501
O3	-0.837673	-0.620695	-1.247000	-0.125084	-1.310625	-1.017366	-1.608500	-0.654737
O4	-0.853339	-0.630612	-1.275000	-0.131996	-1.319904	-1.141702	-1.610900	-0.692253
O5	-0.844439	-0.637609	-1.252500	-0.132931	-1.310251	-1.162176	-1.611600	-0.718795
O6	-0.824651	-0.616479	-1.230000	-0.125152	-1.297378	-1.081904	-1.604100	-0.596843
O7	-0.833963	-0.624155	-1.208000	-0.128871	-1.296652	-1.985372	-1.596300	-0.666368
O8	-0.838963	-0.618136	-1.219000	-0.127490	-1.308448	-1.403440	-1.603000	-0.705954
O9	-0.835597	-0.635450	-1.179000	-0.130230	-1.300695	-1.157850	-1.606700	-0.663805
O10	-0.829926	-0.617739	-1.221000	-0.124549	-1.299606	-1.294131	-1.606400	-0.622075
O11	-0.825613	-0.612189	-1.116000	-0.122360	-1.290392	-1.988223	-1.594100	-0.686276
T1	1.680447	1.236351	2.553000	0.254438	2.623079	2.726566	3.218300	1.266050
T2	1.659259	1.256429	2.467500	0.263256	2.598016	2.732048	3.205600	1.346353
T3	1.666344	1.250561	2.377000	0.257795	2.605017	2.796311	3.210600	1.320090
T4	1.689390	1.242409	2.407500	0.250774	2.621313	2.908931	3.208600	1.410884
T5	1.697737	1.252022	2.519000	0.245921	2.625596	2.459578	3.215600	1.226574

Table 40: comparison of the partial charges determined from several methodologies for the zeolite RUT. The 'site' is the atom label used in the crystal structure for the zeolite available from the IZA database.

Site	EEM	QEQ	EQEQ	QTPIE	HI	DDEC	Bader	REPEAT
O1	-0.846797	-0.628028	-1.187500	-0.150236	-1.316645	-1.601582	-1.608600	-0.717407
O2	-0.827210	-0.629624	-1.176625	-0.148241	-1.291092	-1.174653	-1.600525	-0.709400
O3	-0.872791	-0.627597	-1.186250	-0.151890	-1.348735	-1.552825	-1.620425	-0.757663
O4	-0.847666	-0.618757	-1.070250	-0.146745	-1.318486	-0.954594	-1.600200	-0.661051
T1	1.723981	1.246987	2.319375	0.300184	2.657689	2.989061	3.223600	1.431369
T2	1.657052	1.261870	2.360500	0.297847	2.599870	2.642465	3.204425	1.422203

Table 41: A comparison of the partial charges determined from several methodologies for the zeolite RWR. The 'site' is the atom label used in the crystal structure for the zeolite available from the IZA database.

Site	EEM	QEQ	EQEQ	QTPIE	HI	DDEC	Bader	REPEAT
O3	-0.811093	-0.623647	-1.002000	-0.126831	-1.310551	-1.827748	-1.611500	-0.587623
O4	-0.769958	-0.593055	-0.971500	-0.116204	-1.272831	-1.105545	-1.588000	-0.564313
O5	-0.821484	-0.640406	-1.118000	-0.139171	-1.314182	-1.436051	-1.609500	-0.645829
O6	-0.793245	-0.613367	-1.059500	-0.127245	-1.294351	-1.335007	-1.602250	-0.560563
T1	1.586061	1.251435	2.066500	0.247356	2.602402	2.847595	3.207950	1.169464
T2	1.586061	1.224055	2.157250	0.267823	2.591262	2.725116	3.205775	1.173460

Table 42: A comparison of the partial charges determined from several methodologies for the zeolite SAS. The 'site' is the atom label used in the crystal structure for the zeolite available from the IZA database.

Site	EEM	QEQ	EQEQ	QTPIE	HI	DDEC	Bader	REPEAT
O1	-0.815078	-0.604771	-1.219125	-0.068938	-1.280467	-1.213927	-1.589800	-0.549952
O2	-0.862182	-0.629761	-1.301375	-0.073935	-1.330728	-0.989225	-1.618350	-0.562976
O3	-0.845409	-0.613828	-1.273750	-0.069571	-1.317101	-1.177124	-1.605300	-0.604510
O4	-0.847451	-0.636056	-1.251250	-0.074543	-1.311976	-1.210585	-1.613000	-0.703137
O5	-0.856687	-0.633620	-1.233063	-0.074105	-1.319800	-0.961670	-1.610575	-0.708105
O6	-0.836451	-0.611281	-1.225688	-0.067422	-1.305501	-0.987548	-1.608950	-0.634144
O7	-0.832902	-0.597917	-1.264500	-0.063859	-1.307560	-0.881217	-1.608100	-0.631020
T1	1.693844	1.241182	2.566125	0.145299	2.627677	2.155113	3.218100	1.107039
T2	1.656341	1.245415	2.444250	0.146991	2.600313	2.274359	3.207700	1.329895
T3	1.680486	1.228731	2.356125	0.141325	2.620307	1.790881	3.216700	1.330585
T4	1.718452	1.239822	2.603125	0.131084	2.642022	2.104259	3.220550	1.301496

Table 43: A comparison of the partial charges determined from several methodologies for the zeolite SGT. The 'site' is the atom label used in the crystal structure for the zeolite available from the IZA database.

Site	EEM	QEQ	EQEQ	QTPIE	HI	DDEC	Bader	REPEAT
O1	-0.855875	-0.609182	-0.985000	-0.340640	-1.323208	-1.291708	-1.598200	-0.692997
T1	1.711750	1.218363	1.970000	0.681280	2.646549	2.583417	3.196300	1.385995

Table 44: A comparison of the partial charges determined from several methodologies for the zeolite SOD. The 'site' is the atom label used in the crystal structure for the zeolite available from the IZA database.

Site	EEM	QEQ	EQEQ	QTPIE	HI	DDEC	Bader	REPEAT
O1	-0.848546	-0.640922	-1.376500	-0.154388	-1.316417	-0.972483	-1.595900	-0.770799
O2	-0.829409	-0.616010	-1.297500	-0.143493	-1.306423	-1.205480	-1.603700	-0.704159
O3	-0.889879	-0.654323	-1.432500	-0.167294	-1.359861	-0.964466	-1.618600	-0.905599
O4	-0.845644	-0.625682	-1.334500	-0.154786	-1.317341	-1.306200	-1.600100	-0.664490
O5	-0.809793	-0.609416	-1.234500	-0.131604	-1.278519	-0.976335	-1.597750	-0.639092
O6	-0.849456	-0.631326	-1.299000	-0.146708	-1.322944	-1.466328	-1.612300	-0.686537
O7	-0.867133	-0.640316	-1.312500	-0.147657	-1.338718	-1.420293	-1.609000	-0.775891
O8	-0.820208	-0.611539	-1.259000	-0.132877	-1.287285	-1.503686	-1.603600	-0.655708
O9	-0.815286	-0.612153	-1.241500	-0.140781	-1.281470	-1.094892	-1.594600	-0.622351
O10	-0.858857	-0.638865	-1.224000	-0.153894	-1.330812	-1.179168	-1.610300	-0.646342
T1	1.683803	1.262073	2.544000	0.307548	2.624623	2.451114	3.209800	1.292737
T2	1.686836	1.232817	2.566000	0.267311	2.622720	2.695781	3.212000	1.395290
T3	1.666007	1.270080	2.516500	0.281592	2.604347	2.390979	3.205700	1.364568
T4	1.693587	1.242060	2.734500	0.302308	2.643711	2.211890	3.201800	1.576780
T5	1.684051	1.243458	2.743500	0.323301	2.633423	2.271218	3.206800	1.481519

Table 45: A comparison of the partial charges determined from several methodologies for the zeolite STF. The 'site' is the atom label used in the crystal structure for the zeolite available from the IZA database.

Site	EEM	QEQ	EQEQ	QTPIE	HI	DDEC	Bader	REPEAT
O1	-0.792497	-0.597795	-1.170500	-0.035459	-1.258581	-1.598649	-1.589200	-0.516646
O2	-0.861932	-0.633805	-1.308500	-0.035530	-1.330981	-1.028360	-1.600100	-0.716448
O3	-0.853070	-0.640948	-1.320000	-0.038576	-1.325618	-1.273083	-1.612000	-0.733870
O4	-0.815141	-0.605042	-1.233500	-0.064095	-1.291176	-0.733442	-1.597000	-0.611392
O5	-0.826733	-0.621317	-1.210500	-0.034682	-1.301334	-2.131219	-1.600300	-0.718873
O6	-0.807380	-0.615841	-1.206500	-0.033605	-1.275098	-1.465771	-1.592900	-0.653453
O7	-0.852860	-0.644150	-1.269500	-0.038891	-1.320889	-1.610307	-1.609800	-0.745988
O8	-0.816147	-0.604862	-1.240500	-0.032141	-1.292180	-1.278869	-1.601400	-0.573552
O9	-0.806325	-0.619317	-1.202500	-0.034330	-1.281612	-1.434539	-1.599400	-0.648877
O10	-0.841328	-0.629834	-1.338500	-0.038078	-1.309762	-1.473473	-1.602500	-0.635342
O11	-0.790497	-0.608137	-1.165500	-0.033560	-1.259402	-2.245257	-1.587100	-0.684628
O12	-0.825951	-0.618623	-1.234500	-0.037022	-1.303144	-1.439996	-1.600600	-0.635851
O13	-0.798332	-0.619124	-1.175000	-0.035284	-1.260480	-1.217384	-1.592800	-0.592307
O14	-0.830829	-0.632326	-1.227000	-0.035846	-1.297222	-1.902127	-1.603400	-0.683263
O15	-0.853442	-0.650480	-1.278500	-0.038232	-1.318769	-0.950197	-1.605800	-0.763369
O16	-0.817557	-0.632039	-1.201500	-0.036819	-1.274581	-1.453051	-1.595900	-0.710584
O17	-0.852778	-0.648468	-1.312000	-0.039381	-1.323366	-1.266692	-1.615300	-0.697000
O18	-0.829470	-0.612874	-1.294500	-0.035160	-1.306235	-1.623972	-1.604400	-0.690812
O19	-0.830502	-0.616101	-1.287500	-0.034750	-1.304950	-1.386493	-1.607000	-0.659230
O20	-0.831195	-0.625179	-1.257000	-0.034666	-1.301921	-1.777956	-1.606000	-0.638988
O21	-0.869855	-0.648340	-1.260500	-0.039658	-1.334094	-1.805139	-1.609600	-0.864641
O22	-0.811838	-0.617567	-1.223500	-0.035762	-1.276533	-1.622947	-1.593800	-0.694560
O23	-0.844277	-0.633138	-1.227500	-0.038113	-1.317932	-1.815120	-1.608200	-0.673689
O24	-0.815009	-0.619808	-1.243000	-0.035893	-1.285628	-1.037567	-1.595200	-0.699130
O25	-0.847325	-0.617689	-1.297500	-0.037119	-1.323281	-1.489825	-1.606800	-0.643419
O26	-0.865334	-0.637541	-1.291000	-0.035911	-1.332585	-0.960320	-1.613600	-0.699685
O27	-0.841468	-0.639133	-1.252000	-0.035982	-1.310158	-1.452543	-1.615300	-0.701643
O28	-0.885862	-0.660075	-1.399000	-0.041932	-1.348304	-1.253214	-1.613700	-0.867754
O29	-0.851004	-0.638625	-1.339500	-0.039510	-1.324643	-1.082563	-1.615800	-0.614756
O30	-0.817596	-0.629235	-1.238000	-0.037153	-1.291000	-1.031561	-1.590000	-0.673032
O31	-0.817648	-0.614164	-1.253500	-0.034012	-1.291746	-1.387443	-1.599300	-0.605058
O32	-0.849650	-0.632277	-1.260500	-0.037163	-1.319970	-0.844720	-1.607850	-0.738582
T1	1.706483	1.235888	2.629000	0.066287	2.636546	2.723255	3.212800	1.323941
T2	1.688809	1.233518	2.531500	0.066251	2.624244	3.102450	3.201900	1.380140
T3	1.641778	1.284680	2.363500	0.074453	2.571611	3.176943	3.202700	1.237763
T4	1.653312	1.264955	2.495000	0.079084	2.593089	3.049112	3.205300	1.223465
T5	1.654799	1.244725	2.465500	0.066441	2.595973	2.762692	3.210700	1.278289
T6	1.678250	1.244952	2.529000	0.066485	2.614067	2.457232	3.209400	1.267842
T7	1.649654	1.247851	2.455500	0.072524	2.590404	2.502229	3.204300	1.356822
T8	1.644306	1.266708	2.357000	0.072163	2.583851	4.000000	3.197700	1.534274
T9	0.000000	0.000000	2.637500	0.076495	2.621403	2.371920	3.208200	1.481577
T10	0.000000	0.000000	2.461000	0.077873	2.596769	3.104586	3.190300	1.428648
T11	0.000000	0.000000	2.576000	0.076216	2.615883	2.538425	3.213600	1.341706
T12	1.673197	1.238885	2.447500	0.069814	2.591029	2.707779	3.204000	1.458679
T13	0.000000	0.000000	2.499000	0.071448	2.607115	2.675008	3.209900	1.360995
T14	0.000000	0.000000	2.630500	0.073656	2.624308	2.801543	3.207000	1.301581
T15	0.000000	0.000000	2.426000	0.071857	2.588682	2.396652	3.204000	1.448311
T16	1.654670	1.255834	2.715500	0.153078	2.635421	2.703969	3.210300	1.362391

Table 46: A comparison of the partial charges determined from several methodologies for the zeolite STT. The ‘site’ is the atom label used in the crystal structure for the zeolite available from the IZA database.

Site	EEM	QEQ	EQEQ	QTPIE	HI	DDEC	Bader	REPEAT
O1	-0.837006	-0.610553	-0.945500	-0.837006	-1.308526	-1.131120	-1.595800	-0.586424
O2	-0.865856	-0.629019	-1.137750	-0.865856	-1.334305	-0.709914	-1.600700	-0.701765
O3	-0.842158	-0.610353	-1.053000	-0.842158	-1.314922	-0.824440	-1.604300	-0.620782
O4	-0.837087	-0.608184	-1.053250	-0.837087	-1.307435	-0.466038	-1.588700	-0.638066
O5	-0.872603	-0.628130	-0.845750	-0.872603	-1.343575	-1.185252	-1.605500	-0.707800
O6	-0.871717	-0.632906	-1.020500	-0.871717	-1.342691	-1.543971	-1.606000	-0.753907
T1	1.704154	1.241687	2.053250	1.704154	2.643616	1.763262	3.209200	1.230957
T2	1.715199	1.238659	1.875750	1.715199	2.653652	1.834232	3.207000	1.339276
T3	1.704642	1.230997	2.068500	1.704642	2.645531	2.108280	3.184700	1.368202
T4	1.709504	1.246602	2.185000	1.709504	2.658925	2.418200	3.185100	1.508821

Table 47: A comparison of the partial charges determined from several methodologies for the zeolite TON. The 'site' is the atom label used in the crystal structure for the zeolite available from the IZA database.

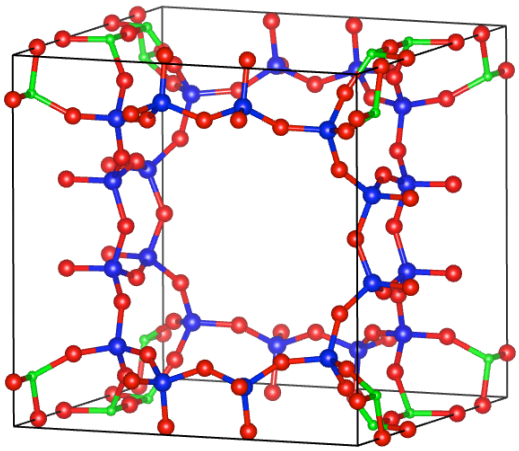

Figure 7: The structure for BEC with the acidic T-site in green, oxygen sites in red, and the remaining T-sites in blue.

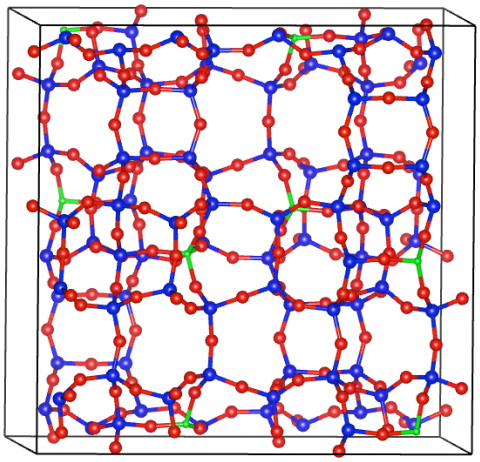

Figure 8: The structure for MFI with the acidic T-site in green, oxygen sites in red, and the remaining T-sites in blue.

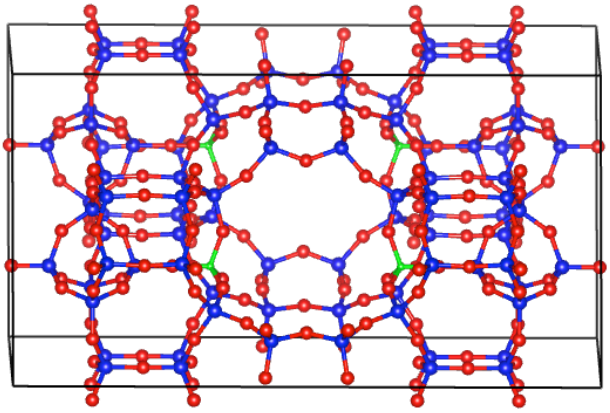

Figure 9: The structure for MWW with the acidic T-site in green, oxygen sites in red, and the remaining T-sites in blue.

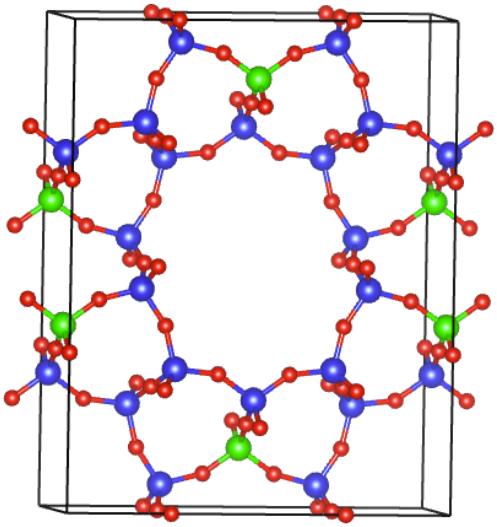

Figure 10: The structure for TON with the acidic T-site in green, oxygen sites in red, and the remaining T-sites in blue.

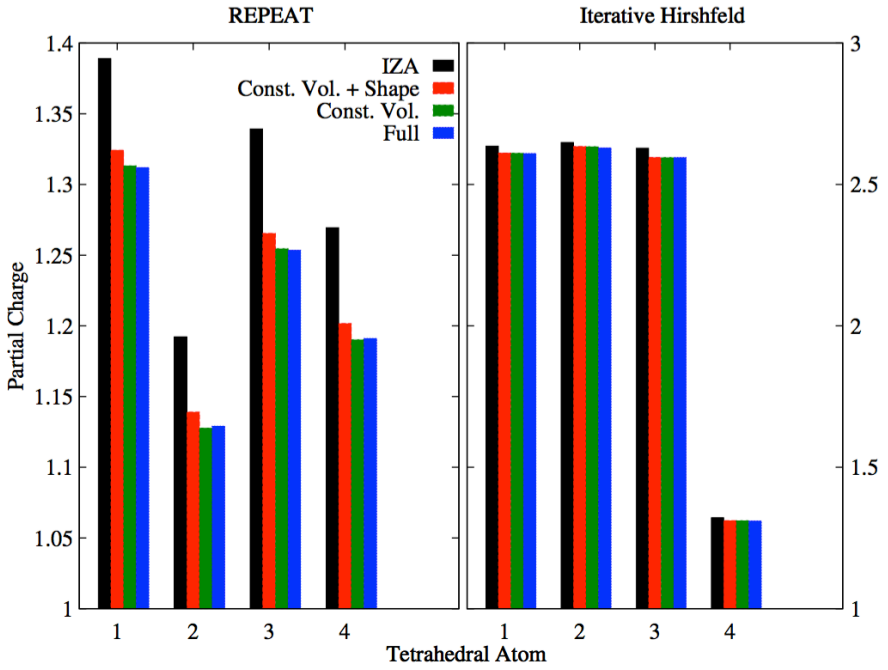

Figure 11: Comparison of partial charge for each tetrahedral atom in zeolite FER as a function of level of optimization using the REPEAT (left) and iterative Hirshfeld (right) methods.

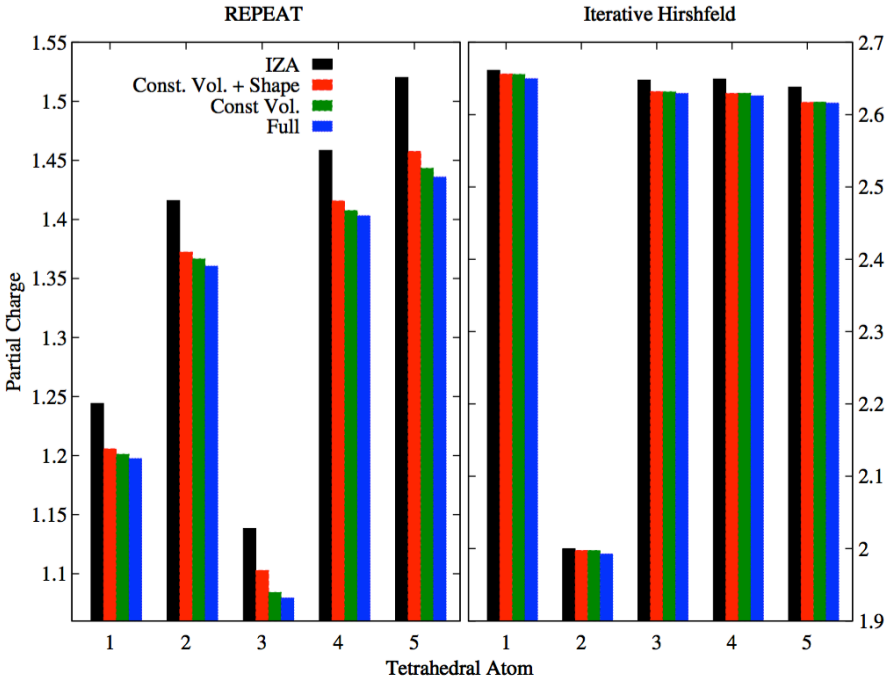

Figure 12: Comparison of partial charge for each tetrahedral atom in zeolite NON as a function of level of optimization using the REPEAT (left) and iterative Hirshfeld (right) methods.

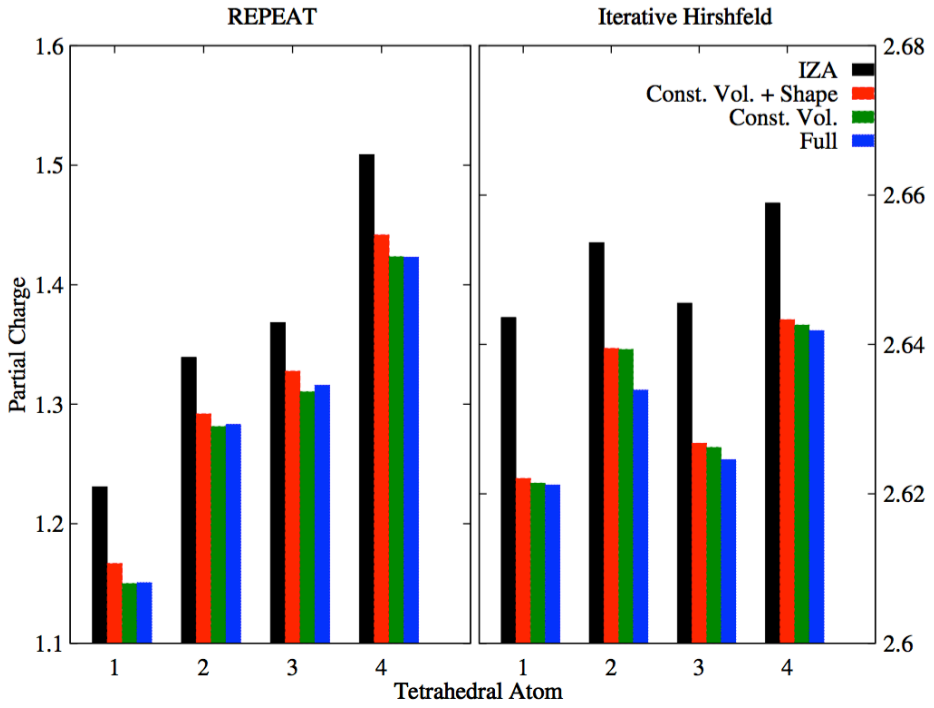

Figure 13: Comparison of partial charge for each tetrahedral atom in zeolite TON as a function of level of optimization using the REPEAT (left) and iterative Hirshfeld (right) methods.

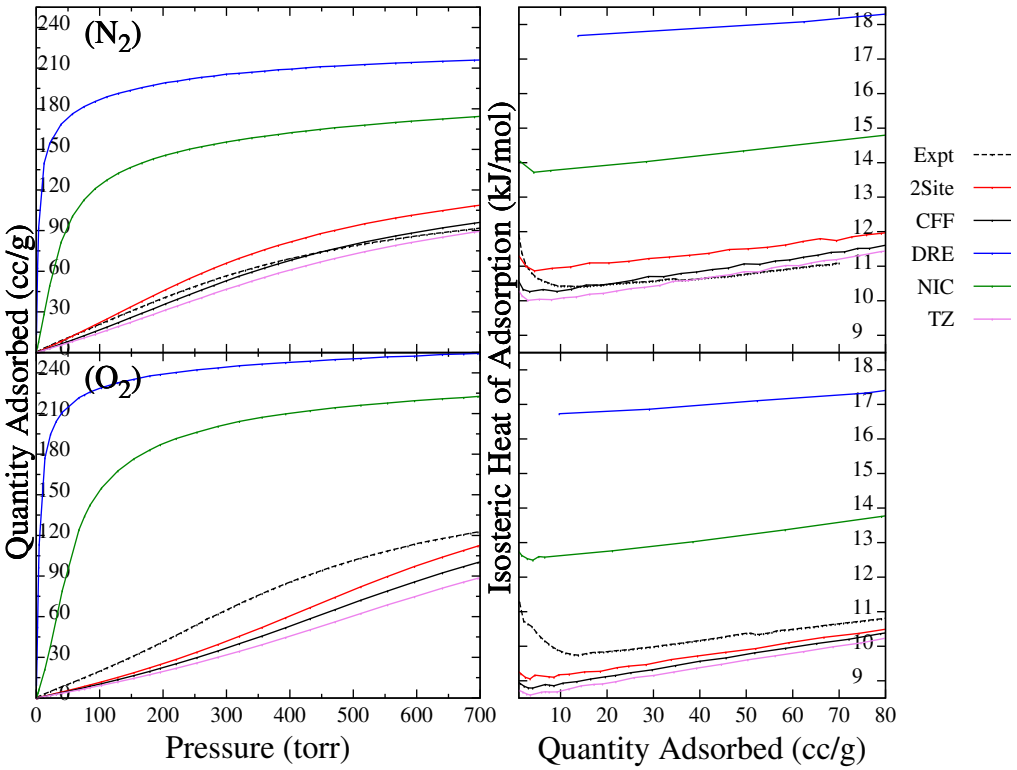

Figure 14: Simulated N_2 (top) and O_2 (bottom) adsorption isotherms (left) and heats of adsorption (right) for FAU at 140K using HI substituted partial charges on the Anne Boutin Forcefield (2-Site), Clay Forcefield (CFF), Dreiding Forcefield (DRE), Nicholas Forcefield (NIC) and TraPPe-ZEO Forcefield (TZ).

References

1. Jensen F. 1999. *Introduction to computational chemistry*. Wiley
2. McWeeny R. 1992. *Methods of Molecular Quantum Mechanics*. Academic Press
3. Szabo A, Ostlund NS. 1982. *Modern Quantum Chemistry: Introduction to Advanced Electronic Structure Theory*. Macmillan
4. Atkins PW, Friedman RS. 1997. *Molecular quantum mechanics*. Oxford University Press
5. Parr RG, Weitao Y. 1994. *Density-Functional Theory of Atoms and Molecules*. Oxford University Press
6. Schatz GC, Ratner MA. 2012. *Quantum Mechanics in Chemistry*. Dover Publications
7. Koch W, Holthausen MC. 2015. *A chemist's guide to density functional theory*. John Wiley & Sons
8. Hohenberg P, Kohn W. 1964. Inhomogeneous Electron Gas. *Physical Review* 136:B864-B71
9. Kohn W, Sham LJ. 1965. Self-Consistent Equations Including Exchange and Correlation Effects. *Physical Review* 140:A1133-A8
10. Thomas LH. 2008. The calculation of atomic fields. *Mathematical Proceedings of the Cambridge Philosophical Society* 23:542-8
11. Chen M, Jiang X-W, Zhuang H, Wang L-W, Carter EA. 2016. Petascale Orbital-Free Density Functional Theory Enabled by Small-Box Algorithms. *Journal of Chemical Theory and Computation* 12:2950-63
12. Wang YA, Carter EA. 2002. Orbital-Free Kinetic-Energy Density Functional Theory. In *Theoretical Methods in Condensed Phase Chemistry*, ed. SD Schwartz:117-84. Dordrecht: Springer Netherlands. Number of 117-84 pp.
13. Pratt GW. 1956. Unrestricted Hartree-Fock Method. *Physical Review* 102:1303-7
14. Perdew JP, Wang Y. 1992. Accurate and simple analytic representation of the electron-gas correlation energy. *Physical Review B* 45:13244-9
15. Langreth DC, Mehl MJ. 1983. Beyond the local-density approximation in calculations of ground-state electronic properties. *Physical Review B* 28:1809-34
16. Becke AD. 1988. Density-functional exchange-energy approximation with correct asymptotic behavior. *Physical Review A* 38:3098-100
17. Perdew JP, Chevary JA, Vosko SH, Jackson KA, Pederson MR, et al. 1992. Atoms, molecules, solids, and surfaces: Applications of the generalized gradient approximation for exchange and correlation. *Physical Review B* 46:6671-87
18. Perdew JP, Burke K, Ernzerhof M. 1996. Generalized Gradient Approximation Made Simple. *Physical Review Letters* 77:3865-8
19. Perdew JP. 1986. Erratum: Density-functional approximation for the correlation energy of the inhomogeneous electron gas. *Physical Review B* 34:7406-
20. Lee C, Yang W, Parr RG. 1988. Development of the Colle-Salvetti correlation-energy formula into a functional of the electron density. *Physical Review B* 37:785-9
21. Perdew JP, Yue W. 1986. Accurate and simple density functional for the electronic exchange energy: Generalized gradient approximation. *Physical Review B* 33:8800-2
22. Axel DB. 1993. Density‐functional thermochemistry. III. The role of exact exchange. *The Journal of Chemical Physics* 98:5648-52

23. Wang Y, Perdew JP. 1991. Correlation hole of the spin-polarized electron gas, with exact small-wave-vector and high-density scaling. *Physical Review B* 44:13298-307
24. Kim K, Jordan KD. 1994. Comparison of Density Functional and MP2 Calculations on the Water Monomer and Dimer. *The Journal of Physical Chemistry* 98:10089-94
25. Axel DB. 1996. Density‐functional thermochemistry. IV. A new dynamical correlation functional and implications for exact‐exchange mixing. *The Journal of Chemical Physics* 104:1040-6
26. Carlo A, Vincenzo B. 1999. Toward reliable density functional methods without adjustable parameters: The PBE0 model. *The Journal of Chemical Physics* 110:6158-70
27. John PP, Matthias E, Kieron B. 1996. Rationale for mixing exact exchange with density functional approximations. *The Journal of Chemical Physics* 105:9982-5
28. Grimme S. 2004. Accurate description of van der Waals complexes by density functional theory including empirical corrections. *J. Comput. Chem.* 25:1463-73
29. Stefan G, Jens A, Stephan E, Helge K. 2010. A consistent and accurate ab initio parametrization of density functional dispersion correction (DFT-D) for the 94 elements H-Pu. *The Journal of Chemical Physics* 132:154104
30. Dion M, Rydberg H, Schröder E, Langreth DC, Lundqvist BI. 2004. Van der Waals Density Functional for General Geometries. *Physical Review Letters* 92:246401
31. Klimes J, Bowler DR, Michaelides A. 2010. Chemical accuracy for the van der Waals density functional. *J. Phys.-Condes. Matter* 22:5
32. Klimeš J, Bowler DR, Michaelides A. 2011. Van der Waals density functionals applied to solids. *Physical Review B* 83:195131
33. Lee K, Murray ÉD, Kong L, Lundqvist BI, Langreth DC. 2010. Higher-accuracy van der Waals density functional. *Physical Review B* 82:081101
34. Levine IN. 2009. *Quantum Chemistry*. Pearson Prentice Hall
35. Joachim P, Robin H, Martijn M, Georg K. 2005. The Perdew–Burke–Ernzerhof exchange-correlation functional applied to the G2-1 test set using a plane-wave basis set. *The Journal of Chemical Physics* 122:234102
36. Mortier WJ, Ghosh SK, Shankar S. 1986. ELECTRONEGATIVITY EQUALIZATION METHOD FOR THE CALCULATION OF ATOMIC CHARGES IN MOLECULES. *Journal of the American Chemical Society* 108:4315-20
37. Sanderson RT. 1976. *Chemical bonds and bond energy*. New York: Academic Press. xii, 218 p. pp.
38. Parr RG, Pearson RG. 1983. Absolute hardness: companion parameter to absolute electronegativity. *Journal of the American Chemical Society* 105:7512-6
39. Rappe AK, Goddard WA. 1991. CHARGE EQUILIBRATION FOR MOLECULAR-DYNAMICS SIMULATIONS. *Journal of Physical Chemistry* 95:3358-63
40. Gale JD. 1997. GULP: A computer program for the symmetry-adapted simulation of solids. *J. Chem. Soc.-Faraday Trans.* 93:629-37
41. Wilmer CE, Kim KC, Snurr RQ. 2012. An Extended Charge Equilibration Method. *J. Phys. Chem. Lett.* 3:2506-11
42. Chen JH, Martinez TJ. 2007. QTPIE: Charge transfer with polarization current equalization. A fluctuating charge model with correct asymptotics. *Chemical Physics Letters* 438:315-20

43. Mulliken RS. 1955. ELECTRONIC POPULATION ANALYSIS ON LCAO-MO MOLECULAR WAVE FUNCTIONS .1. *J. Chem. Phys.* 23:1833-40
44. Löwdin P-O. 1970. On the Nonorthogonality Problem*. In *Advances in Quantum Chemistry*, ed. L Per-Olov, Volume 5:185-99: Academic Press. Number of 185-99 pp.
45. Chirlian LE, Francl MM. 1987. Atomic charges derived from electrostatic potentials: A detailed study. *J. Comput. Chem.* 8:894-905
46. Breneman CM, Wiberg KB. 1990. DETERMINING ATOM-CENTERED MONOPOLES FROM MOLECULAR ELECTROSTATIC POTENTIALS - THE NEED FOR HIGH SAMPLING DENSITY IN FORMAMIDE CONFORMATIONAL-ANALYSIS. *J. Comput. Chem.* 11:361-73
47. Campana C, Mussard B, Woo TK. 2009. Electrostatic Potential Derived Atomic Charges for Periodic Systems Using a Modified Error Functional. *Journal of Chemical Theory and Computation* 5:2866-78
48. Bayly CI, Cieplak P, Cornell W, Kollman PA. 1993. A well-behaved electrostatic potential based method using charge restraints for deriving atomic charges: the RESP model. *The Journal of Physical Chemistry* 97:10269-80
49. Erucar I, Manz TA, Keskin S. 2014. Effects of electrostatic interactions on gas adsorption and permeability of MOF membranes. *Mol. Simul.* 40:557-70
50. Ray KG, Olmsted D, He N, Houndonougbo Y, Laird BB, Asta M. 2012. van der Waals density functional study of CO${}_{2}$ binding in zeolitic imidazolate frameworks. *Physical Review B* 85:085410
51. Vaidhyanathan R, Iremonger SS, Shimizu GKH, Boyd PG, Alavi S, Woo TK. 2010. Direct Observation and Quantification of CO2 Binding Within an Amine-Functionalized Nanoporous Solid. *Science* 330:650-3
52. Morris W, Leung B, Furukawa H, Yaghi OK, He N, et al. 2010. A Combined Experimental−Computational Investigation of Carbon Dioxide Capture in a Series of Isoreticular Zeolitic Imidazolate Frameworks. *Journal of the American Chemical Society* 132:11006-8
53. Sutrisno A, Terskikh VV, Shi Q, Song Z, Dong J, et al. 2012. Characterization of Zn-Containing Metal–Organic Frameworks by Solid-State 67Zn NMR Spectroscopy and Computational Modeling. *Chemistry – A European Journal* 18:12251-9
54. Morris W, He N, Ray KG, Klonowski P, Furukawa H, et al. 2012. A Combined Experimental-Computational Study on the Effect of Topology on Carbon Dioxide Adsorption in Zeolitic Imidazolate Frameworks. *The Journal of Physical Chemistry C* 116:24084-90
55. Bader RFW. 1990. *Atoms in molecules : a quantum theory*. Oxford: Clarendon Press. xviii, 438 p. pp.
56. Henkelman G, Arnaldsson A, Jonsson H. 2006. A fast and robust algorithm for Bader decomposition of charge density. *Comput. Mater. Sci.* 36:354-60
57. Sanville E, Kenny SD, Smith R, Henkelman G. 2007. Improved grid-based algorithm for Bader charge allocation. *J. Comput. Chem.* 28:899-908
58. Tang W, Sanville E, Henkelman G. 2009. A grid-based Bader analysis algorithm without lattice bias. *J. Phys.-Condes. Matter* 21:7
59. Yu M, Trinkle DR. 2011. Accurate and efficient algorithm for Bader charge integration. *The Journal of Chemical Physics* 134:064111

60. Hirshfeld FL. 1977. BONDED-ATOM FRAGMENTS FOR DESCRIBING MOLECULAR CHARGE-DENSITIES. *Theor. Chim. Acta* 44:129-38
61. Vanpoucke DEP, Bultinck P, Van Driessche I. 2013. Extending Hirshfeld-I to bulk and periodic materials. *J. Comput. Chem.* 34:405-17
62. Manz TA, Sholl DS. 2010. Chemically Meaningful Atomic Charges That Reproduce the Electrostatic Potential in Periodic and Nonperiodic Materials. *Journal of Chemical Theory and Computation* 6:2455-68
63. Manz TA, Sholl DS. 2012. Improved Atoms-in-Molecule Charge Partitioning Functional for Simultaneously Reproducing the Electrostatic Potential and Chemical States in Periodic and Nonperiodic Materials. *Journal of Chemical Theory and Computation* 8:2844-67
64. Metropolis N, Rosenbluth AW, Rosenbluth MN, Teller AH, Teller E. 1953. Equation of State Calculations by Fast Computing Machines. *The Journal of Chemical Physics* 21:1087-92
65. Gusenius EM. 1969. Beginnings of Greatness in Swedish Chemistry (II) Axel Fredrick Cronstedt (1722-1765). *Transactions of the Kansas Academy of Science (1903-)* 72:476-85
66. Arean CO, Delgado MR, Nachtigall P, Thang HV, Rubes M, et al. 2014. Measuring the Bronsted acid strength of zeolites - does it correlate with the O-H frequency shift probed by a weak base? *Physical Chemistry Chemical Physics* 16:10129-41
67. Bao ZB, Yu L, Dou T, Gong YJ, Zhang Q, et al. 2011. Adsorption Equilibria of CO2, CH4, N-2, O-2, and Ar on High Silica Zeolites. *J. Chem. Eng. Data* 56:4017-23
68. Combariza AF, Gomez DA, Sastre G. 2013. Simulating the properties of small pore silica zeolites using interatomic potentials. *Chem. Soc. Rev.* 42:114-27
69. Csicsery SM. 1984. SHAPE-SELECTIVE CATALYSIS IN ZEOLITES. *Zeolites* 4:202-13
70. Davis ME. 1993. NEW VISTAS IN ZEOLITE AND MOLECULAR-SIEVE CATALYSIS. *Accounts Chem. Res.* 26:111-5
71. Mabilia M, Pearlstein RA, Hopfinger AJ. 1987. MOLECULAR MODELING OF ZEOLITE STRUCTURE .1. PROPERTIES OF THE SODALITE CAGE. *Journal of the American Chemical Society* 109:7960-8
72. Mellot C, Lignieres J. 1996. Monte Carlo simulations of N-2 and O-2 adsorption in silicalite and CaLSX zeolites. *Mol. Simul.* 18:349-65
73. Papai I, Goursot A, Fajula F, Plee D, Weber J. 1995. Modeling of N2 and O2 Adsorption in Zeolites. *The Journal of Physical Chemistry* 99:12925-32
74. Pillai RS, Peter SA, Jasra RV. 2007. Correlation of sorption Behavior of nitrogen, oxygen, and argon with Ca2+ locations in zeolite A: A grand canonical Monte Carlo simulation study. *Langmuir* 23:8899-908
75. Siriwardane RV, Shen M-S, Fisher EP. 2003. Adsorption of CO2, N2, and O2 on Natural Zeolites. *Energy & Fuels* 17:571-6
76. van Donk S, Janssen AH, Bitter JH, de Jong KP. 2003. Generation, characterization, and impact of mesopores in zeolite catalysts. *Catal. Rev.-Sci. Eng.* 45:297-319
77. Yang L, Trafford K, Kresnawahjuesa O, Sepa J, Gorte RJ, White D. 2001. An examination of confinement effects in high-silica zeolites. *J. Phys. Chem. B* 105:1935-42
78. Zecchina A, Lamberti C, Bordiga S. 1998. Surface acidity and basicity: General concepts. *Catalysis Today* 41:169-77

79. Baerlocher C, McCusker LB. *Database of Zeolite Structures*. http://www.iza-structure.org/databases/
80. Kulprathipanja S. 2010. *Zeolites in Industrial Separation and Catalysis*. Wiley
81. Pedone A, Malavasi G, Menziani MC, Segre U, Musso F, et al. 2008. FFSiOH: a New Force Field for Silica Polymorphs and Their Hydroxylated Surfaces Based on Periodic B3LYP Calculations. *Chem. Mat.* 20:2522-31
82. Dick BG, Overhauser AW. 1958. Theory of the Dielectric Constants of Alkali Halide Crystals. *Physical Review* 112:90-103
83. Gale JD. 1998. Analytical Free Energy Minimization of Silica Polymorphs. *The Journal of Physical Chemistry B* 102:5423-31
84. Bushuev YG, Sastre G. 2009. Atomistic Simulations of Structural Defects and Water Occluded in SSZ-74 Zeolite. *The Journal of Physical Chemistry C* 113:10877-86
85. Mayo SL, Olafson BD, Goddard WA. 1990. DREIDING - A GENERIC FORCE-FIELD FOR MOLECULAR SIMULATIONS. *Journal of Physical Chemistry* 94:8897-909
86. Nicholas JB, Hopfinger AJ, Trouw FR, Iton LE. 1991. MOLECULAR MODELING OF ZEOLITE STRUCTURE .2. STRUCTURE AND DYNAMICS OF SILICA SODALITE AND SILICATE FORCE-FIELD. *Journal of the American Chemical Society* 113:4792-800
87. Cygan RT, Liang J-J, Kalinichev AG. 2004. Molecular Models of Hydroxide, Oxyhydroxide, and Clay Phases and the Development of a General Force Field. *The Journal of Physical Chemistry B* 108:1255-66
88. Buttefey S, Boutin A, Mellot-Draznieks C, Fuchs AH. 2001. A Simple Model for Predicting the Na+ Distribution in Anhydrous NaY and NaX Zeolites. *The Journal of Physical Chemistry B* 105:9569-75
89. Rappe AK, Casewit CJ, Colwell KS, Goddard WA, Skiff WM. 1992. UFF, A FULL PERIODIC-TABLE FORCE-FIELD FOR MOLECULAR MECHANICS AND MOLECULAR-DYNAMICS SIMULATIONS. *Journal of the American Chemical Society* 114:10024-35
90. Liu B, Smit B, Rey F, Valencia S, Calero S. 2008. A New United Atom Force Field for Adsorption of Alkenes in Zeolites. *The Journal of Physical Chemistry C* 112:2492-8
91. Bai P, Tsapatsis M, Siepmann JI. 2013. TraPPE-zeo: Transferable Potentials for Phase Equilibria Force Field for All-Silica Zeolites. *J. Phys. Chem. C* 117:24375-87
92. Lawler KV, Sharma A, Alagappan B, Forster PM. 2016. Assessing zeolite frameworks for noble gas separations through a joint experimental and computational approach. *Microporous and Mesoporous Materials* 222:104-12
93. vanKoningsveld H, Jansen JC, vanBekkum H. 1996. The location of p-dichlorobenzene in a single crystal of zeolite H-ZSM-5 at high sorbate loading. *Acta Crystallogr. Sect. B-Struct. Commun.* 52:140-4
94. van Koningsveld H, Jansen JC, van Bekkum H. 1990. The monoclinic framework structure of zeolite H-ZSM-5. Comparison with the orthorhombic framework of as-synthesized ZSM-5. *Zeolites* 10:235-42
95. Garcia-Perez E, Parra JB, Ania CO, Dubbeldam D, Vlugt TJH, et al. 2008. Unraveling the argon adsorption processes in MFI-type zeolite. *J. Phys. Chem. C* 112:9976-9
96. Dubbeldam D, Calero S, Ellis DE, Snurr RQ. 2016. RASPA: molecular simulation software for adsorption and diffusion in flexible nanoporous materials. *Mol. Simul.* 42:81-101
97. Dubbeldam D, Snurr RQ. 2007. Recent developments in the molecular modeling of diffusion in nanoporous materials. *Mol. Simul.* 33:305-25

98. Chempath S, Clark LA, Snurr RQ. 2003. Two general methods for grand canonical ensemble simulation of molecules with internal flexibility. *The Journal of Chemical Physics* 118:7635-43
99. Weitkamp J. 2000. Zeolites and catalysis. *Solid State Ion.* 131:175-88
100. Bare SR, Kelly SD, Sinkler W, Low JJ, Modica FS, et al. 2005. Uniform catalytic site in Sn-beta-zeolite determined using X-ray absorption fine structure. *Journal of the American Chemical Society* 127:12924-32
101. Haag WO. 1994. CATALYSIS BY ZEOLITES - SCIENCE AND TECHNOLOGY. In *Zeolites and Related Microporous Materials: State of the Art 1994*, ed. J Weitkamp, HG Karge, H Pfeifer, W Holderich, 84:1375-94. Amsterdam: Elsevier Science Bv. Number of 1375-94 pp.
102. Hamad S, Balestra SRG, Bueno-Perez R, Calero S, Ruiz-Salvador AR. 2015. Atomic charges for modeling metal-organic frameworks: Why and how. *J. Solid State Chem.* 223:144-51
103. Sastre G, Gale JD. 2001. ZeoTsites: a code for topological and crystallographic tetrahedral sites analysis in zeolites and zeotypes. *Microporous and Mesoporous Materials* 43:27-40
104. Sastre G, Corma A. 2006. Rings and strain in pure silica zeolites. *J. Phys. Chem. B* 110:17949-59
105. Kresse G. 1995. AB-INITIO MOLECULAR-DYNAMICS FOR LIQUID-METALS. *J. Non-Cryst. Solids* 193:222-9
106. Kresse G, Hafner J. 1994. AB-INITIO MOLECULAR-DYNAMICS SIMULATION OF THE LIQUID-METAL AMORPHOUS-SEMICONDUCTOR TRANSITION IN GERMANIUM. *Physical Review B* 49:14251-69
107. Kresse G, Furthmuller J. 1996. Efficient iterative schemes for ab initio total-energy calculations using a plane-wave basis set. *Physical Review B* 54:11169-86
108. Yang G, Pidko EA, Hensen EJM. 2013. Structure, Stability, and Lewis Acidity of Mono and Double Ti, Zr, and Sn Framework Substitutions in BEA Zeolites: A Periodic Density Functional Theory Study. *The Journal of Physical Chemistry C* 117:3976-86
109. Blochl PE. 1994. PROJECTOR AUGMENTED-WAVE METHOD. *Physical Review B* 50:17953-79
110. Kresse G, Joubert D. 1999. From ultrasoft pseudopotentials to the projector augmented-wave method. *Physical Review B* 59:1758-75
111. Vinet P, Smith JR, Ferrante J, Rose JH. 1987. Temperature effects on the universal equation of state of solids. *Physical Review B* 35:1945-53
112. Blöchl PE, Jepsen O, Andersen OK. 1994. Improved tetrahedron method for Brillouin-zone integrations. *Physical Review B* 49:16223-33
113. Limas NG, Manz TA. 2016. Introducing DDEC6 atomic population analysis: part 2. Computed results for a wide range of periodic and nonperiodic materials. *RSC Advances* 6:45727-47
114. Gupta A, Chempath S, Sanborn MJ, Clark LA, Snurr RQ. 2003. Object-oriented Programming Paradigms for Molecular Modeling. *Mol. Simul.* 29:29-46
115. Peng D, Robinson DB. 1976. A New Two-Constant Equation of State. *Industrial & Engineering Chemistry Fundamentals* 15:59-64
116. Allen MP, Tildesley DJ. 1987. *Computer simulation of liquids*. Oxford England New York: Clarendon Press;Oxford University Press

117. Frenkel D, Smit B. 2002. *Understanding molecular simulation : from algorithms to applications*. San Diego CA London: Academic Press
118. Fennell CJ, Gezelter JD. 2006. Is the Ewald summation still necessary? Pairwise alternatives to the accepted standard for long-range electrostatics. *J. Chem. Phys.* 124:12
119. Potoff JJ, Siepmann JI. 2001. Vapor–liquid equilibria of mixtures containing alkanes, carbon dioxide, and nitrogen. *AIChE Journal* 47:1676-82
120. Zhang L, Siepmann JI. 2006. Direct calculation of Henry's law constants from Gibbs ensemble Monte Carlo simulations: nitrogen, oxygen, carbon dioxide and methane in ethanol. *Theor. Chem. Acc.* 115:391-7
121. Qisheng H, Shouhua F, Ruren X. 1988. First syntheses of pentasil-type silica zeolites from non-aqueous systems. *Journal of the Chemical Society, Chemical Communications*:1486-7
122. King RSP, Dann SE, Elsegood MRJ, Kelly PF, Mortimer RJ. 2009. The Synthesis, Full Characterisation and Utilisation of Template-Free Silica Sodalite, a Novel Polymorph of Silica. *Chemistry – A European Journal* 15:5441-3
123. Hriljac JA. 2006. High-pressure synchrotron X-ray powder diffraction studies of zeolites. *Crystallography Reviews* 12:181-93
124. Jentoft FC. 2014. ADVANCES IN CATALYSIS VOLUME FIFTY SEVEN PREFACE. In *Advances in Catalysis, Vol 57*, ed. FC Jentoft, 57:IX-X. San Diego: Elsevier Academic Press Inc. Number of IX-X pp.
125. Gale JD, Rohl AL. 2003. The General Utility Lattice Program (GULP). *Mol. Simul.* 29:291-341
126. Barthomeuf D. 1987. ZEOLITE ACIDITY DEPENDENCE ON STRUCTURE AND CHEMICAL ENVIRONMENT - CORRELATIONS WITH CATALYSIS. *Materials Chemistry and Physics* 17:49-71
127. Zheng A, Chen L, Yang J, Zhang M, Su Y, et al. 2005. Combined DFT Theoretical Calculation and Solid-State NMR Studies of Al Substitution and Acid Sites in Zeolite MCM-22. *The Journal of Physical Chemistry B* 109:24273-9
128. Sastre G, Fornes V, Corma A. 2000. Preferential Siting of Bridging Hydroxyls and Their Different Acid Strengths in the Two-Channel System of MCM-22 Zeolite. *The Journal of Physical Chemistry B* 104:4349-54
129. Gale JD. 2006. A periodic density functional study of the location of titanium within TS-1. *Solid State Sci.* 8:234-40
130. Shetty S, Kulkarni BS, Kanhere DG, Goursot A, Pal S. 2008. A comparative study of structural, acidic and hydrophilic properties of Sn-BEA with Ti-BEA using periodic density functional theory. *J. Phys. Chem. B* 112:2573-9
131. Montejo-Valencia BD, Curet-Arana MC. 2015. DFT Study of the Lewis Acidities and Relative Hydrothermal Stabilities of BEC and BEA Zeolites Substituted with Ti, Sn, and Ge. *J. Phys. Chem. C* 119:4148-57
132. Sastre G, Vidal-Moya JA, Blasco T, Rius J, Jorda JL, et al. 2002. Preferential location of Ge atoms in polymorph C of beta zeolite (ITQ-17) and their structure-directing effect: A computational, XRD, and NMR spectroscopic study. *Angew. Chem.-Int. Edit.* 41:4722-6

133. Corma A, Navarro MT, Rey F, Rius J, Valencia S. 2001. Pure polymorph C of zeolite beta synthesized by using framework isomorphous substitution as a structure-directing mechanism. *Angew. Chem.-Int. Edit.* 40:2277-+
134. Nemeth L, Bare SR. 2014. Chapter One - Science and Technology of Framework Metal-Containing Zeotype Catalysts. In *Advances in Catalysis*, ed. CJ Friederike, Volume 57:1-97: Academic Press. Number of 1-97 pp.
135. van H. 1990. High-temperature (350 K) orthorhombic framework structure of zeolite H-ZSM-5. *Acta Crystallographica Section B* 46:731-5
136. van Koningsveld H, Tuinstra F, van Bekkum H, Jansen JC. 1989. The location of p-xylene in a single crystal of zeolite H-ZSM-5 with a new, sorbate-induced, orthorhombic framework symmetry. *Acta Crystallographica Section B* 45:423-31
137. Vankoningsveld H, Vanbekkum H, Jansen JC. 1987. ON THE LOCATION AND DISORDER OF THE TETRAPROPYLAMMONIUM (TPA) ION IN ZEOLITE ZSM-5 WITH IMPROVED FRAMEWORK ACCURACY. *Acta Crystallogr. Sect. B-Struct. Commun.* 43:127-32
138. Simperler A, Bell RG, Foster MD, Gray AE, Lewis DW, Anderson MW. 2004. Probing the Acid Strength of Brønsted Acidic Zeolites with Acetonitrile: An Atomistic and Quantum Chemical Study. *The Journal of Physical Chemistry B* 108:7152-61
139. Khaliullin RZ, Bell AT, Kazansky VB. 2001. An Experimental and Density Functional Theory Study of the Interactions of CH4 with H−ZSM-5. *The Journal of Physical Chemistry A* 105:10454-61
140. Zygmunt SA, Curtiss LA, Iton LE, Erhardt MK. 1996. Computational Studies of Water Adsorption in the Zeolite H-ZSM-5. *The Journal of Physical Chemistry* 100:6663-71
141. Brand HV, Curtiss LA, Iton LE. 1993. Ab initio molecular orbital cluster studies of the zeolite ZSM-5. 1. Proton affinities. *The Journal of Physical Chemistry* 97:12773-82
142. Sun KJ, Fan FT, Xia HA, Feng ZC, Li WX, Li C. 2008. Framework Fe Ions in Fe-ZSM-5 Zeolite Studied by UV Resonance Raman Spectroscopy and Density Functional Theory Calculations. *J. Phys. Chem. C* 112:16036-41
143. Pirc G, Stare J. 2008. Titanium Site Preference Problem in the TS-1 Zeolite Catalyst: A Periodic Hartree-Fock Study. *Acta Chim. Slov.* 55:951-9
144. Yuan SP, Si HZ, Fu AP, Chu TS, Tian FH, et al. 2011. Location of Si Vacancies and Ti(OSi)(4) and Ti(OSi)(3)OH Sites in the MFI Framework: A Large Cluster and Full Ab Initio Study. *J. Phys. Chem. A* 115:940-7
145. O'Malley PJ, Dwyer J. 1988. Ab-initio molecular orbital calculations on the siting of aluminium in the Theta-1 framework: Some general guidelines governing the site preferences of aluminium in zeolites. *Zeolites* 8:317-21
146. Sklenak S, Dedecek J, Li CB, Gao F, Jansang B, et al. 2008. ALUMINUM SITING IN THE ZSM-22 AND THETA-1 ZEOLITES REVISITED: A QM/MM STUDY. *Collect. Czech. Chem. Commun.* 73:909-20
147. Boronat M, Zicovich-Wilson CM, Viruela P, Corma A. 2001. Cluster and periodic calculations of the ethene protonation reaction catalyzed by theta-1 zeolite: Influence of method, model size, and structural constraints. *Chem.-Eur. J.* 7:1295-303
148. De Wispelaere K, Bailleul S, Van Speybroeck V. 2016. Towards molecular control of elementary reactions in zeolite catalysis by advanced molecular simulations mimicking operating conditions. *Catal. Sci. Technol.* 6:2686-705

149. Dixon DA, Gole JL. 1992. DESCRIPTION OF THE GROUND-STATE ELECTRONIC-STRUCTURES OF CU2O, CU2S, AG2O AND AG2S. *Chemical Physics Letters* 189:390-4
150. Weigend F, Ahlrichs R. 2005. Balanced basis sets of split valence, triple zeta valence and quadruple zeta valence quality for H to Rn: Design and assessment of accuracy. *Physical Chemistry Chemical Physics* 7:3297-305
151. Lawler KV, Hulvey Z, Forster PM. 2015. On the importance of a precise crystal structure for simulating gas adsorption in nanoporous materials. *Physical Chemistry Chemical Physics* 17:18904-7
152. Yang J, Ren Y, Tian AM, Sun HA. 2000. COMPASS force field for 14 inorganic molecules, He, Ne, Ar, Kr, Xe, H-2, O-2, N-2, NO, CO, CO2, NO2, CS2, and SO2, in liquid phases. *J. Phys. Chem. B* 104:4951-7

Curriculum Vitae

Jarod J. Wolffis

Email: jarod.wolffis@unlv.edu

Education

University of Nevada, Las Vegas
B.S., Chemistry, June 2013

Thesis Title:

Improved Partial Charge Models In Siliceous Zeolites For The Simulation Of Adsorption And Identification Of Catalytic Sites

Thesis Examination Committee:

Committee Chair: Paul Forster, Ph.D.

Committee Member: Kathleen Robins, Ph.D.

Committee Member: Keith Lawler, Ph.D.

Graduate College Faculty Representative: Carryn Warren Ph.D.